Sede Amministrativa: Università degli Studi di Padova

Dipartimento di Scienze Medico-Diagnostiche e Terapie Speciali

SCUOLA DI DOTTORATO DI RICERCA IN: SCIENZE MEDICHE, CLINICHE E SPERIMENTALI
INDIRIZZO: SCIENZE CARDIOVASCOLARI
CICLO XXI

DIFFERENTIATION BETWEEN HYPERTROPHIC CARDIOMYOPATHY AND HYPERTENSIVE LEFT VENTRICULAR HYPERTROPHY: THE ROLE OF STRAIN RATE IMAGING STUDY AND INTEGRATED BACKSCATTER ANALYSIS

Direttore della Scuola : Ch.mo Prof. Antonio Tiengo
Coordinatore d'indirizzo: Ch.mo Prof. Gaetano Thiene
Supervisore :Ch.mo Dott. Francesco Tona

Dottorando : Dott.ssa Silvia Orlando

SUMMARY

Background: To date, any non-invasive technique is satisfactory to differentiate Hypertrophic Cardiomyopathy (HCM) from hypertensive left ventricular hypertrophy (H-LVH). We hypothesized that in HCM the presence of local peculiar tissue abnormalities results in the significant impairment of the regional systolic deformation and myocardial reflectivity, even if global function appears normal.

Methods: Twenty non-obstructive HCM patients, 20 age- and gender-matched hypertensive patients (HTN) and 15 healthy volunteers (NTN) underwent grey-scale and tissue Doppler ultrasound imaging from three apical views (16 left ventricular segments model). Afterwards, high resolution deformation traces and integrated backscatter curves were analysed for each segment.

Results: HCM patients showed lower average values of systolic strain (Ssys), systolic strain rate (SR) and cyclic variation of integrated backscatter (CVIB) when compared to HTN or NTN, even if there was a substantial overlap between HCM segments and HTN segments. However, when identifying segments with quasi absent deformation (ND segments with Ssys>-5.68%), we found at least 2 ND segments in each HCM patient, heterogeneously distributed within the ventricle, while none of the HTN or NTN patient had one. Furthermore, in HCM, Ssys, SR and CVIB of the mid- and basal segments of the septum and lateral wall from 3 and 4 chamber views did not correlate with M-mode end-diastolic interventricular septum (IVS) and posterior wall (PW) thicknesses (linear regression analysis), demonstrating no differences in performance between asymmetric and concentric HCM LV pattern. Overall, HTN patients showed slightly but significantly reduced global Ssys, SR and CVIB when compared to NTN, with the most significant reduction in the basal septum. Moreover, post-systolic strain appeared a relevant phenomenon which may contribute to systolic and diastolic impairment in pathological left ventricular hypertrophy.

Additionally, a linear regression analysis revealed a significant correlation between Ssys and CVIB ($R=0.54$, $P<0.0001$).

Conclusions: Deformation and reflectivity analysis can easily discriminate HCM from H-LVH. In particular, HCM is uniquely characterized by the presence of non-deforming segments, distributed non-uniformly within the ventricle and independent on the degree or pattern of ventricular hypertrophy.

Key words: Hypertrophic Cardiomyopathy, hypertensive left ventricular hypertrophy, Strain Rate Imaging, Cyclic Variation of Integrated Backscatter.

RIASSUNTO

Premessa: Sino ad ora, nessuna tecnica diagnostica non invasiva appare soddisfacente nel differenziare la Miocardiopatia Ipertrofica (HCM) dalla Cardiopatia ipertensiva (H-LVH). Abbiamo ipotizzato che nella HCM la presenza di peculiari e localizzate alterazioni tessutali causi una significativa riduzione della deformazione sistolica regionale e della riflettività tessutale, nonostante la funzione sistolica globale possa apparire normale.

Metodi: Venti pazienti con HCM non ostruttiva, 20 pazienti ipertesi (HTN) e 15 controlli sani (NTN), tutti simili per età e sesso, sono stati sottoposti ad acquisizione ecocardiografica standard e mirata all'acquisizione dei segnali in radiofrequenza e dei segnali doppler tessutali dalle tre camere apicali, seguendo un modello ventricolare sinistro a 16 segmenti. In seguito, per ciascun segmento sono state ottenute curve di deformazione ad elevata risoluzione e curve di Integrated Backscatter.

Risultati: I pazienti HCM hanno presentato valori medi di strain sistolico (Ssys), strain rate sistolico (SR) e di variazioni cicliche dell'Integrated Backscatter (CVIB) significativamente ridotti rispetto ai soggetti ipertesi o normotesi, anche se si è evidenziata una rilevante sovrapposizione tra i valori dei segmenti HCM e dei segmenti HTN. Tuttavia, quando si sono identificati segmenti con deformazione quasi assente (segmenti ND con Ssys>-5.68%), si sono riscontrati almeno 2 segmenti ND in ciascun soggetto HCM, eterogeneamente distribuiti nel ventricolo sinistro, mentre nessun HTN o NTN ne possedeva alcuno. Inoltre, nei pazienti HCM, Ssys, SR e CVIB dei segmenti medio-basali del setto interventricolare e della parete posteriore non correlavano con i relativi spessori tele-diastolici rilevati in M-mode dalla parasternale asse-lungo (analisi di regressione lineare), dimostrando che non vi sono differenze nella performance cardiaca tra i pattern asimmetrico e concentrico di HCM. Nel complesso, i pazienti HTN hanno presentato valori di Ssys, SR e CVIB lievemente ma significativamente ridotti rispetto ai controlli, con le riduzioni più importanti a livello del setto basale. Inoltre, la presenza di strain post-sistolico è risultato essere un fenomeno rilevante che può contribuire alla disfunzione sistolica e diastolica nell'ipertrofia

ventricolare sinistra patologica. Oltretutto, un'analisi di regressione lineare ha evidenziato la correlazione tra Ssys e CVIB ($R=0.54$, $P<0.0001$).

Conclusioni: L'analisi della deformazione e delle riflettività tessutale può facilmente discriminare HCM da H-LVH. In particolare, HCM è caratterizzata in modo esclusivo dalla presenza di segmenti con deformazione quasi assente, distribuiti in modo non uniforme nel ventricolo sinistro ed indipendenti dal grado o dal pattern di ipertrofia ventricolare.

Parole chiave: Miocardiopatia Ipertrofica, Cardiopatia ipertensiva, analisi dello Strain Rate Imaging, Variazioni Cicliche dell'Integrated Backscatter.

CHAPTER 1

Myocardial Deformation Principles

The usual indices of global left ventricular (LV) function, such as ejection fraction and volumes, are load-dependent and standard volumetric approaches to their measurement may be influenced by image quality, technical considerations such as off-axis imaging and measurement error. Moreover, the assessment of regional function by visual valuation of wall motion and thickening requires extensive training and remain highly subjective.

Consequently, there is an increasing need for diagnostic modalities able to objectively quantify myocardial global and regional function.

In 1957 Satomura[1] described the first ultrasound system to estimate blood and myocardial velocities basing on continuous wave Doppler principles. Nevertheless, they do not give any information on where the detected velocities occur in the space in front of the transducer, i.e. they do not have spatial resolution. In order to solve this problem, pulsed wave Doppler system were developed in the late 1960's[2,3]. These systems allowed the estimation of velocities within a defined region. During the 1970's pulsed wave systems were further developed to make motion estimation faster and more reliable. In the early 1980's, further developments resulted in the introduction of systems enabling real-time velocity estimation across the whole two dimensional image[4]. In these systems, the velocity information was displayed as a colour-coded image superimposed on top of a grey-scale image. As such, they were referred to as colour flow mapping systems. Originally, they were used to image blood velocities by filtering out slow moving, relatively strongly reflecting structures (such as the myocardium). However, after an initial study by Isaaz[5], this technique was adapted by

McDicken in 1992 and further developed by Sutherland in order to enable the visualization of myocardial velocities[6,7]. Initial clinical studies have examined the potential diagnostic role of this technique in determining regional myocardial function from velocity data sets for a number of disease entities[8-13]. Although encouraging data were obtained, it was clear that the interrogation of regional myocardial velocities alone has two major drawbacks. Firstly, since the amplitude of the estimated velocity is dependent on the angle at which the region is imaged, accurate quantification of peak velocities can be difficult. Secondly, overall wall motion, rotation and contraction of adjacent myocardial segments will influence regional velocity estimates[14]. In order to overcome some of these problems, ultrasonic strain rate imaging, or in other words, rate of deformation imaging, has been developed by estimating spatial gradients in myocardial velocities. From strain rate curves, local strain (i.e. regional deformation curves) can be extracted, resulting in the concept or regional strain imaging[15].

The normal myocardial velocities examination

Currently, regional myocardial velocity profiles can be obtained in either Pulsed or Colour Doppler format[16] (figure 1.1).

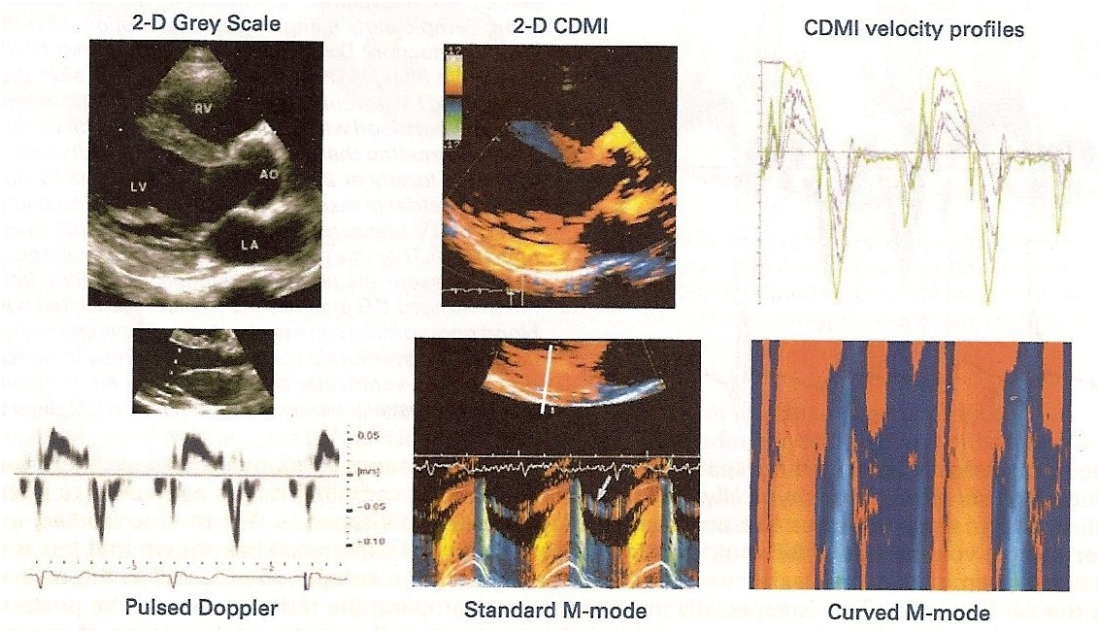

Fig 1.1: The modes in which regional myocardial velocity data can be acquired and displayed. Upper left: the underlying 2-dimensional (2-D) grey scale image. Lower left: the pulsed Doppler peak velocity waveform for radial motion (basal segment of the left ventricle (LV) posterior wall). Upper middle: the 2-D colour Doppler image. Lower middle: the standard colour M-mode of radial motion which can be post-processed to obtain the trans-myocardial velocity gradient. Upper right: a series of longitudinal regional velocity profiles extracted from a septal colour Doppler myocardial imaging (CDMI) data set. The highest is from the basal segment and the lowest from the upper part of the apical segment. Lower right: a curved M-mode data set obtained during post-processing of the same septal longitudinal velocity data set by drawing a free hand M-mode cursor from the apex (top of image) to the base of the septum (bottom of the image) (from 16,Sutherland GR et al. 2006).

Pulsed Doppler Myocardial Imaging

Pulsed Doppler interrogation measures the instantaneous peak velocities from the myocardium which passes through the sample volume during the cardiac cycle (figure 1.2).

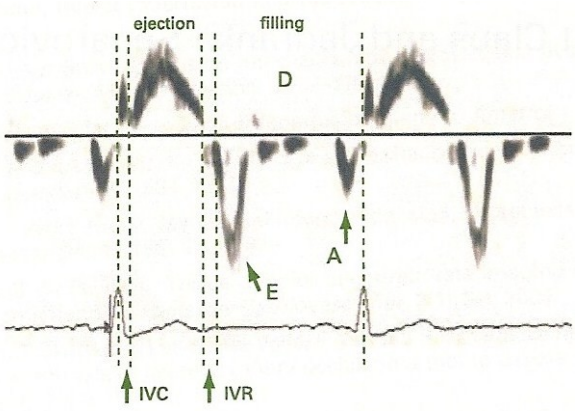

Fig 1.2: A typical Pulsed Doppler regional velocity wave-form and its subdivision into time periods related to mechanical events. The dotted lines mark the timing of the global event markers-aortic and mitral valve opening and closure. IVC=isovolumic contraction; IVR=isovolumic relaxation; E=rapid early filling; D=diastasis; A= regional motion due to filling following atrial contraction (from 16, Sutherland GR et al. 2006).

For routine studies, a pulsed Doppler sample volume size of 6-8 mm should be chosen. Clinical experience has shown that this is usually the best compromise between axial resolution and maintaining the sample volume within the myocardium during the cardiac cycle. The pulsed Doppler sample volume is best set within the centre of the region of myocardium to be studied. It is also important to ensure that motion in the segment to be interrogated is as parallel as possible to the insonating ultrasound beam. Normal myocardial velocities at rest seldom exceed 20 cm/sec and a velocity range of ± 24 cm/sec is usually appropriate. To exclude respiratory variation, data can be collected during a short breath hold[16].

Left ventricular fibre orientation and their thickening and shortening

In the subendo- and subepicardial layer, the principal fibre orientation is longitudinal. In the mid-myocardial layer, the fibres are mostly orientated in the circumferential direction (figure 1.3).

Fig 1.3: Fibre orientation in the left ventricle (from 16, Sutherland GR et al. 2006).

Thus long axis function is partly dependent on the subendocardial fibres and these are the fibres most susceptible to a reduction in coronary blood flow. In practise only longitudinal regional velocities can be obtained for every segment of the left and right ventricular walls. Measurement of radial function is limited to a few left ventricular segments. Attempts have also been made to measure circumferential function but to date this has proved to be of little clinical value (figure 1.4).

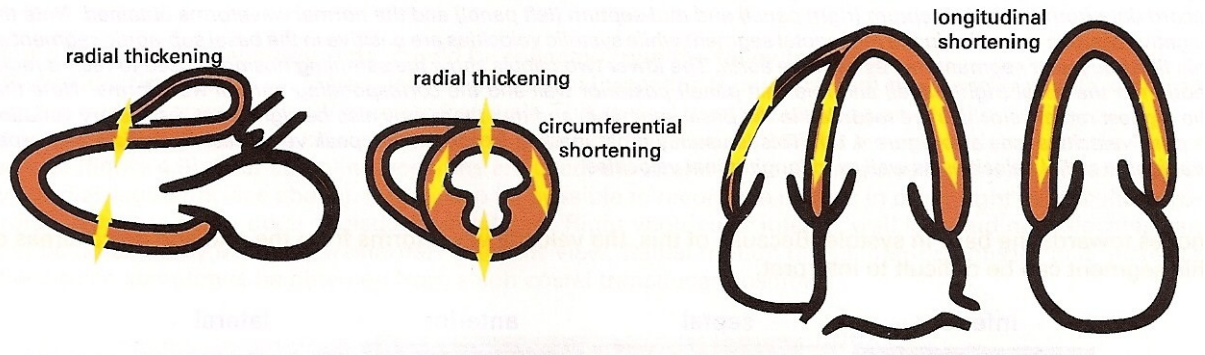

Fig 1.4: Radial thickening, circumferential and longitudinal left ventricular shortening (from 16, Sutherland GR et al. 2006).

Data acquisition

For regional radial motion data is recorded from a parasternal transducer position using either long or short axis views. For the interventricular septum, two sampling positions should be interrogated: the sub-aortic and mid-septal segments. For the LV infero-lateral wall, data should be recorded from the basal and mid wall segments (figure 1.5).

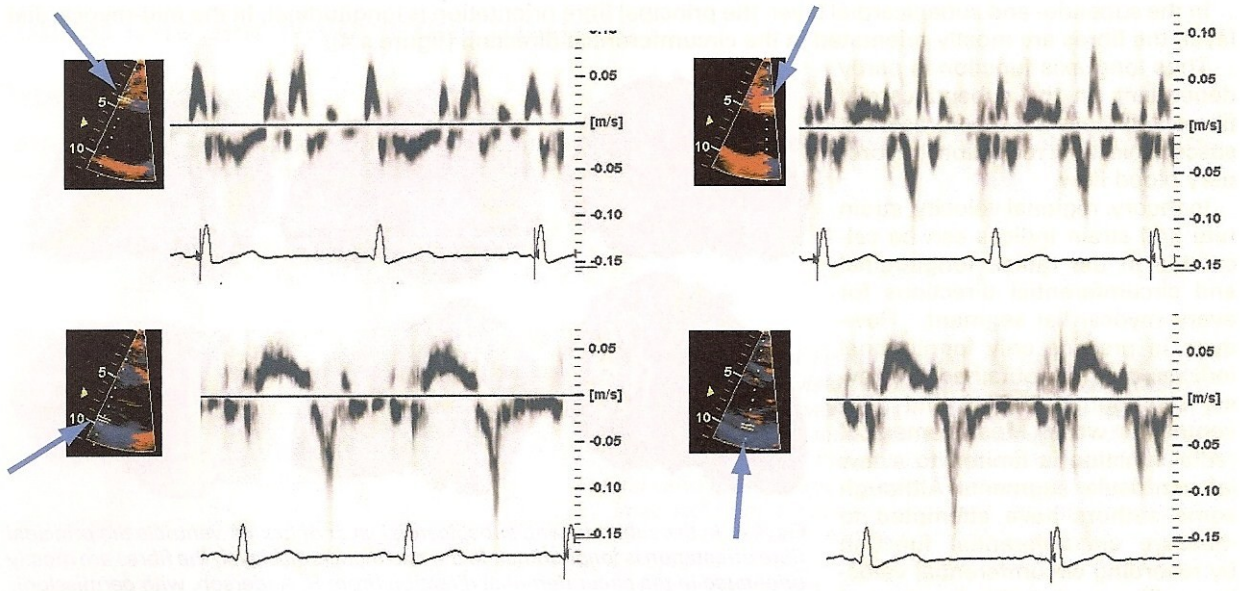

Fig 1.5: Pulsed Doppler evaluation of regional radial motion. The upper two panels show the sample positions used to record data from the basal septum (right panel) and mid-septum (left panel) and the normal waveforms obtained. The lower two panels show the sampling positions used to record radial motion in the basal (right panel) and mid (left panel) infero-lateral wall and the corresponding normal waveforms. Note that the highest radial velocities are recorded in the basal segments and that there may also be significant respiratory variation in peak velocities. There is a base-apex gradient in radial velocities as in longitudinal velocities (from 16, Sutherland GR et al. 2006).

For regional long axis motion, an apical transducer position is used. Studies obtain data from the apical two (inferior and anterior walls) and four (septal and lateral walls) chamber views and the apical long axis (infero-lateral wall and anterior septum) view. For each wall, the motion of the atrio-ventricular plane, the upper part of the basal segment, the upper part of the mid segment and the more basal part of the apical segment should be sample (figure 1.6). The latter is chosen as the sampling site for the very practical reason that the most apical part of the apical segment is either

stationary or moves towards the base in systole, consequently its velocity wave form could be difficult to interpret.

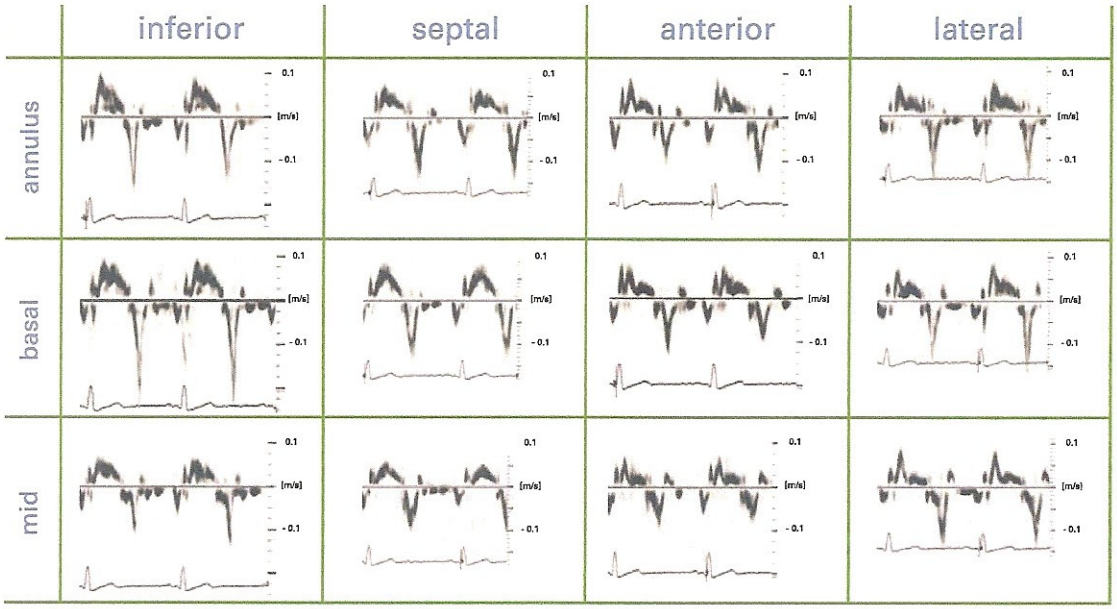

Figure 1.6: The typical variation in regional pulsed Doppler velocity profiles recorded from the fibrous ring, basal and mid-wall segments of each of the four walls of a normal left ventricle (from 16, Sutherland GR et al. 2006).

Note that the systolic velocity profiles in the septal and inferior walls are similar and differ markedly from the systolic velocity profiles in the anterior and lateral walls. Those in the septum and inferior wall tend to be mono-phasic while those in the anterior lateral and posterior walls tend to be bi-phasic. Subsequent regional deformation studies, based on strain imaging, have suggested that the early motion peak in the anterior, posterior and lateral walls is mostly due to overall heart motion rather than local myocardial shortening.

Moreover, the velocity profiles for radial and longitudinal motion can differ both during systole and diastole among different segments.

The relation between the velocities in early diastole and at atrial contraction have been shown to change with age in a manner similar to the mitral flow velocities, with a decrease in early diastole and increase at atrial contraction[17-22] (figure 1.7).

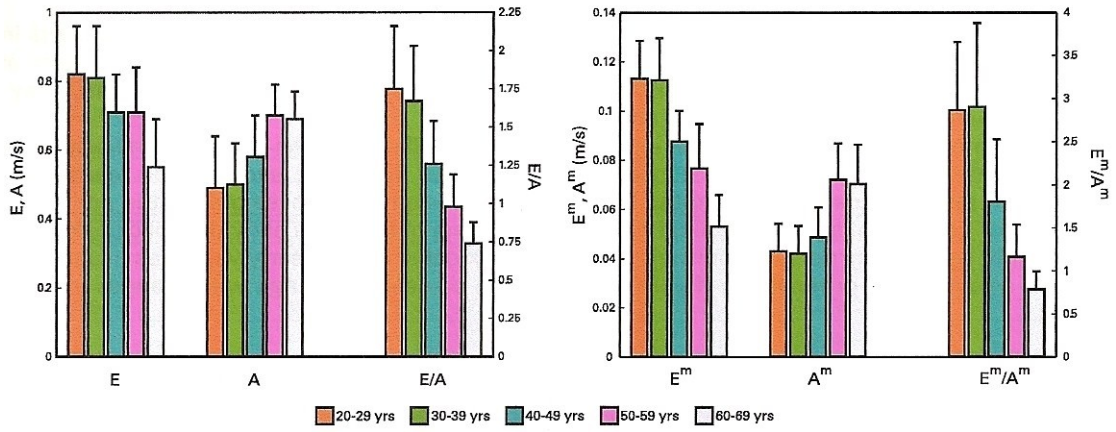

Figure 1.7: The typical age related changes in trans-mitral flow velocities in normal individuals (left). The peak velocity of early filling falls with age while the peak velocity of late filling increase. E=peak velocity early filling, A=peak velocity late filling, E/A=the ratio of early to late filling. The corresponding age related changes in myocardial velocities in normal individuals (right). The peak velocity of early filling falls with age while the peak velocity of late filling increases. E^m=peak velocity early filling, A^m =peak velocity late filling, E^m / A^m=the ratio of early to late filling (data from 18-Wilkenshoff UM et al. 2001-, image from 16- Sutherland GR et al. 2006-).

Normal myocardial velocity profiles

The normal radial systolic velocity curve obtained from the posterior wall has a rapid rate of rise, an early peak and a relatively slow deceleration to the zero line. Radial motion in the septal segments is much more complex because it is influenced by both left and right ventricular events; therefore, septal radial velocity waveforms are of limited value in assessing abnormal segmental function.

The marked differences in longitudinal systolic motion for each of the four walls has been well described. As seen in table 1.1 a higher peak velocity in the lateral, anterior and inferior wall than in the septum has been a consistent finding in many studies[19,23-26] . This may be related to the presence of relatively more longitudinal fibres in the free walls compared to the septum[25]. For both radial and longitudinal motion there is a base-to-apex gradient in peak systolic velocities with the highest velocities recorded at the base. The septum also differs from the free walls by showing more decrease in peak systolic velocity from the base to the mid-part of the ventricle[25,26]. The apex in most hearts in almost stationary. With increasing age a decrease in peak systolic longitudinal

velocities is seen[19,27]. Annular velocities are usually slightly higher than the velocities recorded from the basal myocardium [26,28] and show a similar decrease with age in the LV.

			4-chamber		2-chamber		3-chamber	
	N	Age	LV lat	septum	LV ant	LV inf	post	Sept
Edner-2000[19]	88	51 (20-81)	9,9±2,9	7,7±1,4				
Isaaz-1993[23]	17	31±13	10,3±1,8	8,7±1,4				
Pai-1998[24]	20	44±16	11,7±2,5	10,9±2,2	10,5±2,3	12,4±3,7		
Galiuto-1998[25]	27	24±10	10,3±1,9	8,1±0,8	10,3±1,6	9,6±0,9	9,9±1,3	7,5±1,3
Kukulski-2000[26]	25	33(16-68)	10,2±2,1	7,8±1,1	9,0±1,6	8,7±1,3		
Onose-1999[27]	80	45(15-78)<50					11,2±2,1	
		>50					7,9±1,9	

Table 1.1: Peak systolic velocities of longitudinal motion for the basal LV myocardial segments (cm/s).

Subsequently, in the isovolumic relaxation period a series of very rapid high velocity mono- or bi-phasic mechanical events occur which are mostly related to untwisting and global shape change.

Early diastolic motion represents the local interaction of early filling and the degree of relaxation in the segment interrogated. There is an apex-base gradient in early diastolic peak velocities for both radial and longitudinal motion. The timing of long axis early diastolic peak velocities also shows a slight base-apex delay. In normals, the base-apex delay in peak early velocities usually mirrors the base-apex delay in flow propagation.

During diastasis there is normally little segmental motion.

Late diastolic regional motion is passive and related to filling due to atrial contraction. There is also a base-apex time delay in the velocities caused by late filling. Both the peak velocity of myocardial motion during early filling and late filling can be markedly influenced by respiratory chances in normal individuals (fig 1.8).

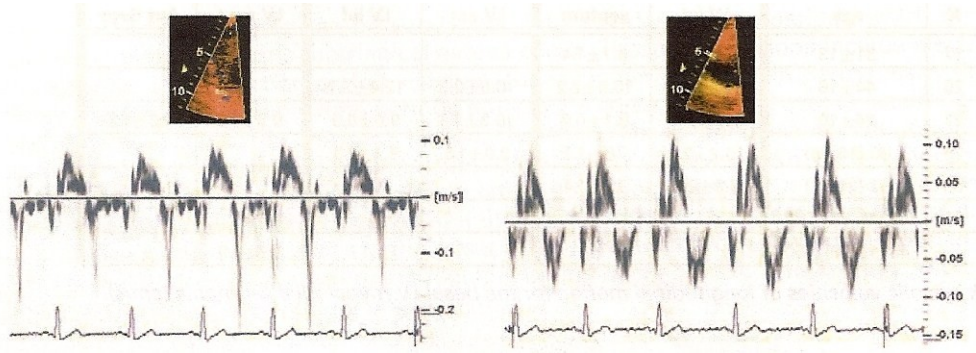

Fig 1.8: Marked respiratory variation in both the peak systolic velocity and the peak E wave velocity in the basal septal segment of the LV (left) and in the RV free wall (right). The variation is much more pronounced in the latter (from 16, Sutherland GR et al. 2006).

Table 1.2 sets out the values for early and late diastolic velocities obtained from studies in normal subjects. As for systolic velocities, there is a difference between the walls, with early diastolic velocities in the basal septum being lower than those in the free walls. In contrast, at atrial contraction, the higher peak velocities in the septum result in a lower E/A ratio for septal myocardial velocities. The lower early diastolic velocity in the septum is perhaps related to the presence of fewer longitudinal septal fibres compared to the free walls, while the higher septal velocity at atrial contraction might be related to the more medial direction of mitral inflow at atrial contraction compared to the more lateral jet direction during early diastole.

				4-chamber		2-chamber		3-chamber	
	N	Age		LV lat	septum	LV ant	LV inf	LV post	Ant Sept
Edner-2000[19]	88	51 (20-81)	E	12,8±4,3	9,7±2,8				
			A	9,2±2,9	9,2±2,3				
Yamada-1999[20]	80	52±18	E					12,1±2,0	9,8±2,2
			A					7,8±2,0	10,0±2,4
Isaaz-1993[23]	17	31±13	E	16,3±2,1	12,3±2,1				
			A	7,8±3,0	8,9±2,4				
Pai-1998[24]	20	44±16	E	16,7±4,3	12,1±2,6	12,9±4,9	16,0±4,5		
			A	11,7±2,8	12,6±2,3	11,7±5,2	13,0±3,5		
Galiuto-1998[25]	27	24±10	E	17,3±4,4	12,6±2,8	13,4±2,7	17,0±3,7	12,5±2,9	10,9±2,4
			A	6,9±1,6	7,4±2,2	6,2±2,0	8,0±1,8	7,2±1,8	6,5±1,7
Kukulski-2000[26]	25	33(16-68)	E	14,9±3,5	11,2±1,9	12,8±3,0	12,4±3,8		
			A	6,6±2,4	7,8±2,0	6,5±1,6	7,9±2,5		

Table 1.2: Peak diastolic velocities of longitudinal motion for the basal LV myocardial segments (cm/s). E=early diastole, A=atrial contraction.

For the right ventricle, both the systolic longitudinal annular and myocardial velocities are higher than those in the septum and free walls of the left ventricle[23,26,29], while early diastolic velocities can

be similar. Right ventricular myocardial velocities related to atrial contraction are similar or higher. All these velocities can be markedly influenced by respiration in normal individuals.

The timing of cardiac mechanical events was first based on high temporal resolution M-mode echocardiography. But if anatomical grey scale M-mode data is suboptimal, then blood pool Doppler data can be used to determine semilunar and atrioventricular opening and closure based on the timing of the valve clicks[16].

Colour Doppler myocardial imaging (CDMI)

Colour Doppler Myocardial velocity data may be acquired in two formats-either as an M-mode data set or as a real time 2-D data set (fig. 1.1).

In both, average mean velocity profiles from areas within the myocardium can be calculated. This resulted in the development of transmural myocardial gradient measurement as a new quantitative method to evaluate regional function, not influenced by either cardiac rotation or displacement (as were regional velocity profiles) and bringing to regional strain rate, later discussed.

The problem inherent in the use of a fixed M-mode approach to measuring transmural velocity gradients is that it only interrogates velocities along the M-mode scan line. Thus it can only be applied to radial function in the limited number of segments which can be insonated from the parasternal window.

A real time 2-D data set needs very high frame rates and it allows many post-processing possibilities[16].

Normal Regional Strain Rate/Strain Curves

As already said, the interrogation of regional myocardial velocities has some important problems correlated to the fact that they are influenced by overall heart motion, rotation and contraction of adjacent myocardial segments.

Consequently, strain rate imaging has been developed by estimating spatial gradients in myocardial velocities (fig 1.9).

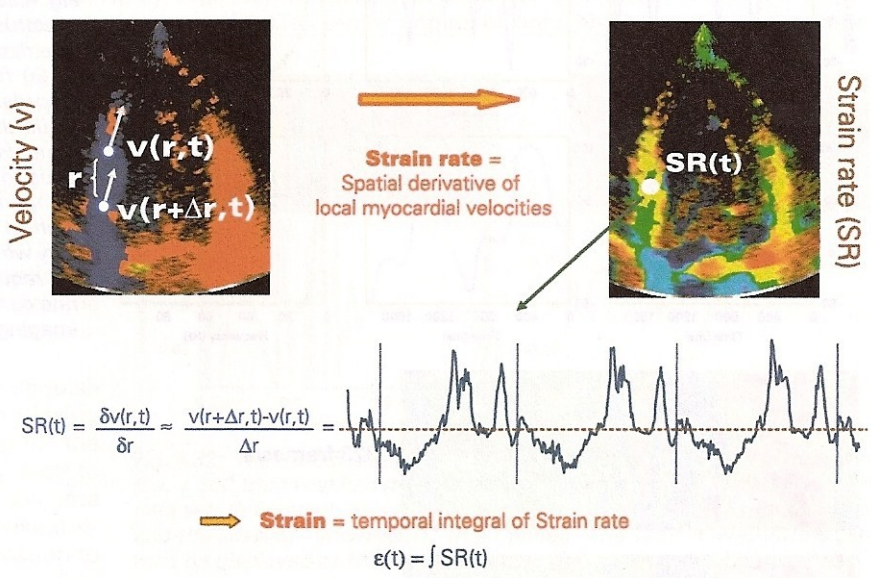

Fig 1.9: To derive Regional Strain Rate, velocity profiles from two adjacent regions (V(r) and V (r+Δ)) of interest, separated by a known distance (r) are tracked during the cardiac cycle (from 16, Sutherland GR et al. 2006).

Definitions and acquisition

Strain is defined as the deformation of an object, normalized to its original shape. In a one-dimensional object whose only possible deformation is lengthening or shortening, strain (ε) is the change in length relative to its initial length and it is expressed in percent[15,16,30,31] (fig 1.10).

$$\varepsilon = \frac{L - L_0}{L_0} = \frac{\Delta L}{L_0}$$

Fig 1.10: Strain of a one-dimensional object is limited to lengthening or shortening. Strain (ε) is the deformation of an object relative to its original shape: $\varepsilon=(L-L^0)/ L^0$; L=final length; L^0 =final length (from 30, Teske AJ et al. 2007).

Strain rate is the speed at which deformation (i.e. strain) occurs and it has the unit s^{-1}: SR: $[(L-L^0)/ L^0]/ \Delta t= (\Delta L/ L^0)/ \Delta t$, where Δt is the time gradient. It represent the difference of speed at the ends of an object whose original length is L^0, thus it is the spatial velocity gradient[15,16,30,31].

SR seems to be a correlate of rate of change in pressure (dP/dt), a parameter that is used to reflect contractility that is load-independent[32,33], whereas strain correlates to ejection fraction and it is then influenced by pre-load and after-load[33].

While regional strain rates measure the rate of local deformation, regional strain expresses the % deformation.

These deformation parameters are currently calculated from the local CDMI myocardial velocity profiles. For the processing of strain rate data, frame rate is even more important than it is for the acquisition of regional velocity profiles. Moreover, to allow the reliable calculation of regional deformation parameters, it is essential to have near optimal velocity curves on which to base the calculations. In fact, any random noise in the velocity data sets will be amplified in the computation of local strain rate. The strain rate curves should then be averaged for three consecutive cycles and median filtering algorithms applied to further reduce noise during post processing[16] (fig 1.11).

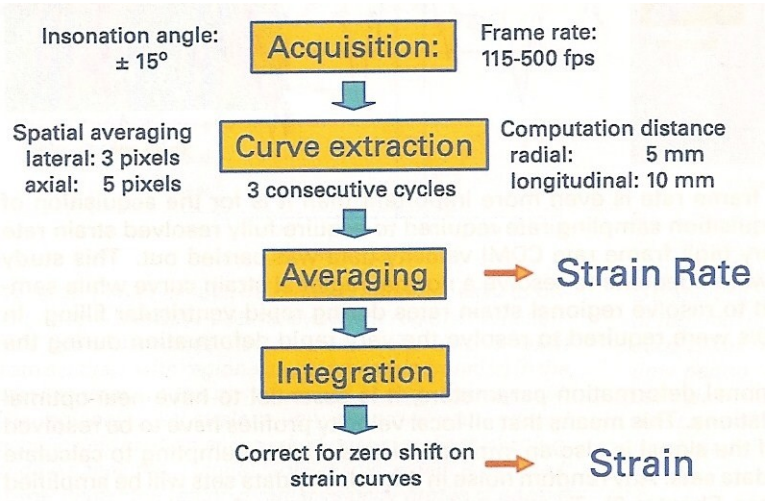

Fig 1.11: The methodology currently used in the University of Leuven to acquire and post-processing strain rate and strain data from high frame rate CDMI velocity data sets (from 16, Sutherland GR et al. 2006).

Therefore, strain rate is the primary parameter of deformation derived from tissue Doppler (figure 1.12) and Strain curves are derived from integration of the strain rate curves over time.

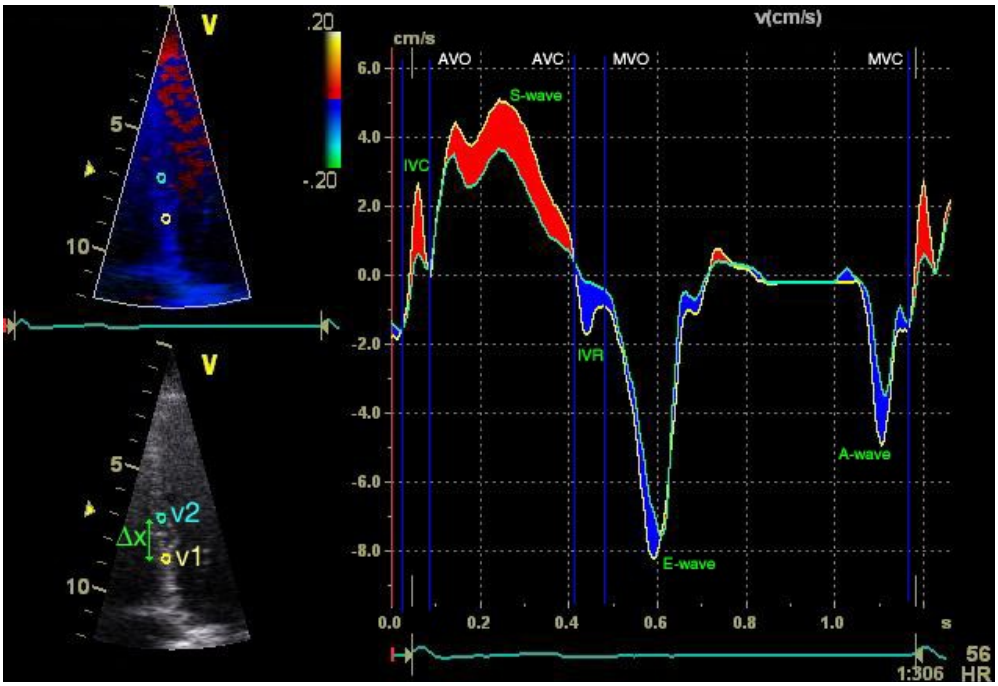

Fig 1.12: Calculation of Strain rate using the velocity gradient. Longitudinal velocities using two regions of interest (ROI) in the same recording. Y-axis represents velocity (cm/s), X-axis represents time (one cardiac cycle). IVC=isovolumic contraction; IVR=isovolumic relaxation. Calculation of SR can be derived from the spatial velocity gradient (Δv) at a defined distance (Δx). The red area indicates a negative Δv due to shortening, resulting in a negative SR and the blue area results in a positive SR (from 30, Teske AJ et al. 2007).

The process of integration itself has the beneficial effect of smoothing the strain curves, it acts as a type of low pass filter (compare figure 1.13 and 1.14).

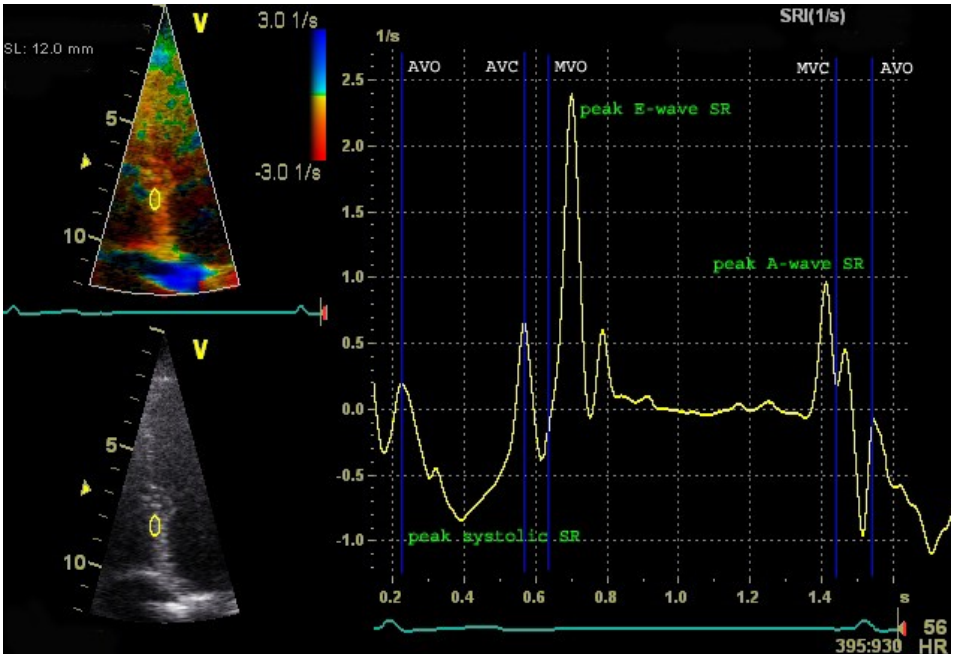

Fig 1.13: Example of longitudinal strain rate graph (Doppler derived). Y-axis represents strain rate (s^{-1}), X-axis represents time (one cardiac cycle). Note the negative SR during systole and the positive SR during the upstroke of the strain-curve during the E and A-wave. The SR is zero when no deformation occurs. Blue lines represent cardiac events: (MVC) mitral valve closure and (MVO) opening, (AVO) aortic valve opening and (AVC) closure (from 30, Teske AJ et al. 2007).

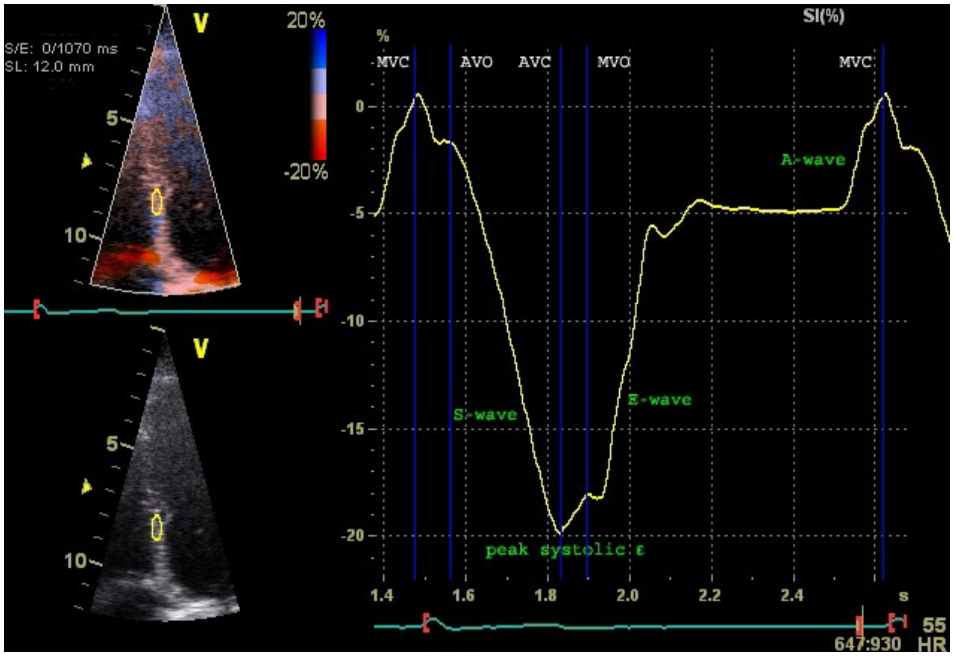

Fig 1.14: Example of longitudinal strain graph (Doppler derived) in the interventricular septum in a healthy person. Y-axis represents strain (%), X-axis represents time (one cardiac cycle). Blue lines represent cardiac events as in previous image (from 30, Teske AJ et al. 2007).

Each regional strain curve can be sub-divided into its component parts by the inclusion of timing data on global events. Ideally, the timing of aortic valve opening, aortic valve closure and mitral valve opening should all be imported[16] (fig 1.15).

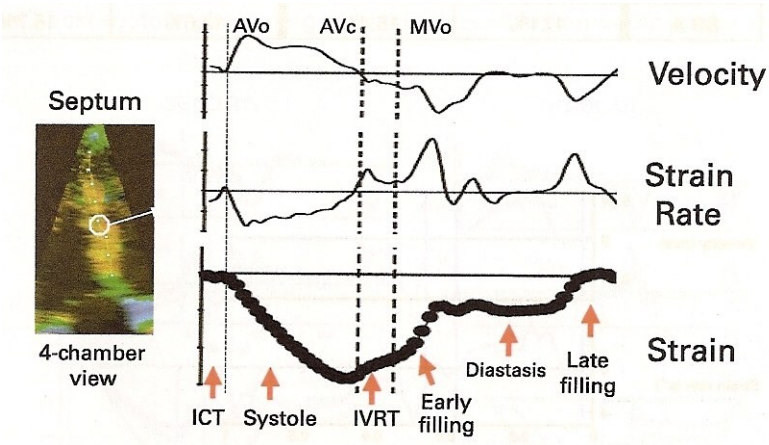

Fig 1.15: The incorporation of global event markers into the regional long axis velocity, strain rate and strain curves derived from the same mid-septal myocardial segment. This procedure allows the investigator to compare what is happening regionally with respect to global mechanical events (from 16, Sutherland GR et al. 2006).

Numerous measurement and calculations can be performed after the tracking of the ROI. These can be divided into parameters concerning the timing and/or the magnitude of strain and SR. the most relevant measurements are presented in figure 1.16. For shortening strains, the peak systolic strain value is defined as the lowest value between aortic valve opening and closure. Post-systolic strain is defined as myocardial deformation (shortening for longitudinal and lengthening for radial function) after the aortic valve closure (better described later on). For the SR trace, comparable parameters can be obtained as in the velocity trace; peak systolic, peak early and late diastolic SR and time to peak systolic SR (although the last measurement can be unreliable due to the noisy aspect of the SR curves)[30].

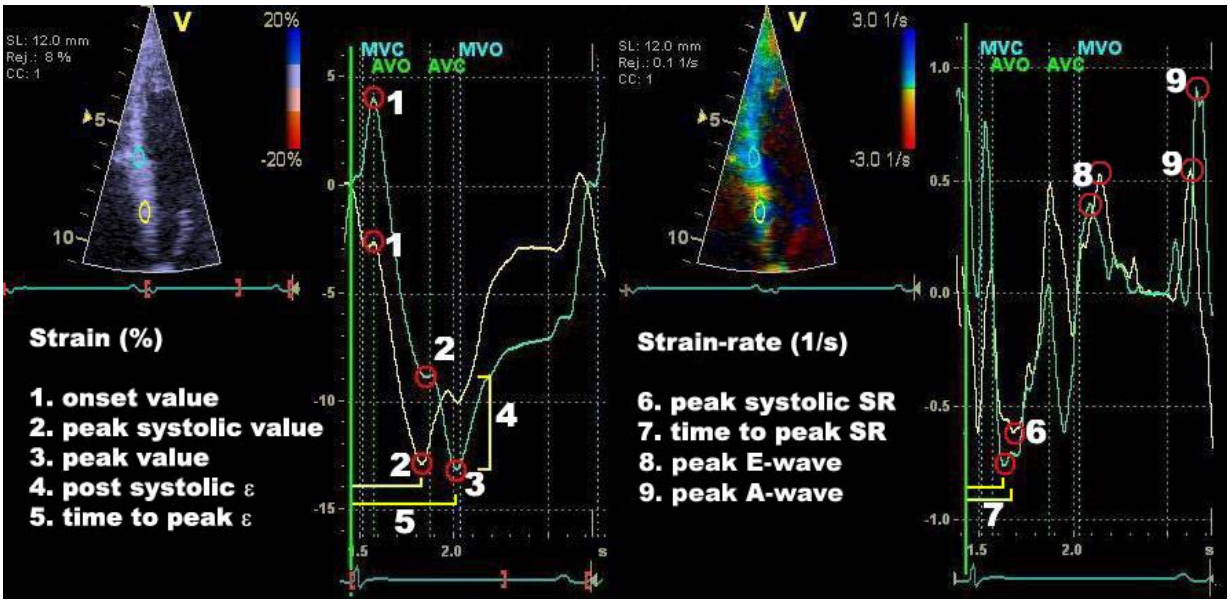

Fig 1.16: Strain and strain-rate parameters. Left: strain (ε) and right: strain-rate (SR) measurements of the basal and mid segment of the interventricular septum. Post-systolic strain (4) is defined as the amount of deformation after the AVC (value 3 minus value 2). In the yellow curve, the peak systolic value and the peak value are the same, while in the cyan curve these are two distinctive points (2 and 3). From this, the post-systolic index (PSI) can be calculated: (4)/(3)x100=PSI (%). The definition of the onset value (1) could also be defined at the onset of the QRS-complex for the yellow curve (from 30, Teske AJ et al. 2007).

Whereas there is a normal base-apex gradient in velocities, with the highest velocities at the cardiac base, there is a relatively homogeneous distribution of peak strain rate values within each of the left ventricular walls. Only the timing of peak strain rate may vary. The major differences between regional velocity and strain rate curves occurs during the isovolumic contraction and relaxation periods; in fact, in both these periods there may be relatively high velocities recorded but little change in regional strain rates.

Radial deformation can currently only be processed reliably for the mid and basal segments of the posterior wall.

The normal segmental velocity, strain rate and strain values for both radial and longitudinal function in a group of healthy 20-40 year olds[34] are set out in tables 1.3 and 1.4.

		Velocity (cm/s)	Strain rate (s^{-1})	Strain (%)
systole	LAX	4,31±1,30	3,03±0,76	46±12
	SAX	4,32±1,00	3,09±0,69	48±12
Diastole E	LAX	7,62±2,52	7,62±3,03	
	SAX	8,60±2,22	8,23±2,66	
Diastole A	LAX	1,94±1,12	1,82±0,89	
	SAX	1,85±0,89	2,03±0,97	

Table 1.3 : Normal radial peak velocity, strain rate and strain values from the postero-basal LV segment obtained from a group of 40 normal individuals (age 20-40 years) (data from 34, Kowalski M et al. 2001). LAX=long axis; SAX=short axis.

		Velocity (cm/s)	Strain rate (s^{-1})	Strain (%)
Apical 4CH Septum	basal	5,69±1,58	1,51±0,35	21±5
	mid	4,27±1,06	1,49±0,35	21±5
	apical	3,06±1,0	1,55±0,30	23±4
Apical 4CH lateral LV	basal	8,66±2,40	1,19±0,26	13±4
	mid	7,90±2,42	1,12±0,28	14±4
	apical	7,09±2,44	1,25±0,39	15±5
Apical 4CH lateral RV	basal	9,72±2,26	1,50±0,41	19±6
	mid	8,65±2,31	1,72±0,27	27±6
	apical	6,60±2,05	2,04±0,41	32±6
Apical 3CH infero-lateral LV	basal	6,39±1,08	1,17±0,33	15±5
	mid	5,42±1,21	1,23±0,33	16±5
	apical	4,17±1,43	1,24±0,31	18±5
Apical 2CH anterior LV	basal	7,73±1,97	1,50±0,44	17±6
	mid	6,28±2,19	1,45±0,54	17±6
	apical	4,80±2,46	1,51±0,48	18±6

Table 1.4: Normal longitudinal systolic peak velocity, strain rate and strain values for basal, mid and apical segments of the left ventricle (LV) and for the basal, mid and apical lateral wall of the right ventricle (RV). The data was obtained from 40 normal individuals (age 20-40 years) (data from 34, Kowalski M et al. 2001). 2CH=two chamber; 3CH= three chamber; 4CH=four chamber.

In normal individuals, peak systolic strain in the LV free wall segments is significantly higher in the radial direction compared to longitudinal peak systolic strain in the same segment.

As with regional strain rate profiles, longitudinal strain curves can be extracted for each of the three myocardial segments from each of the LV walls (fig 1.17).

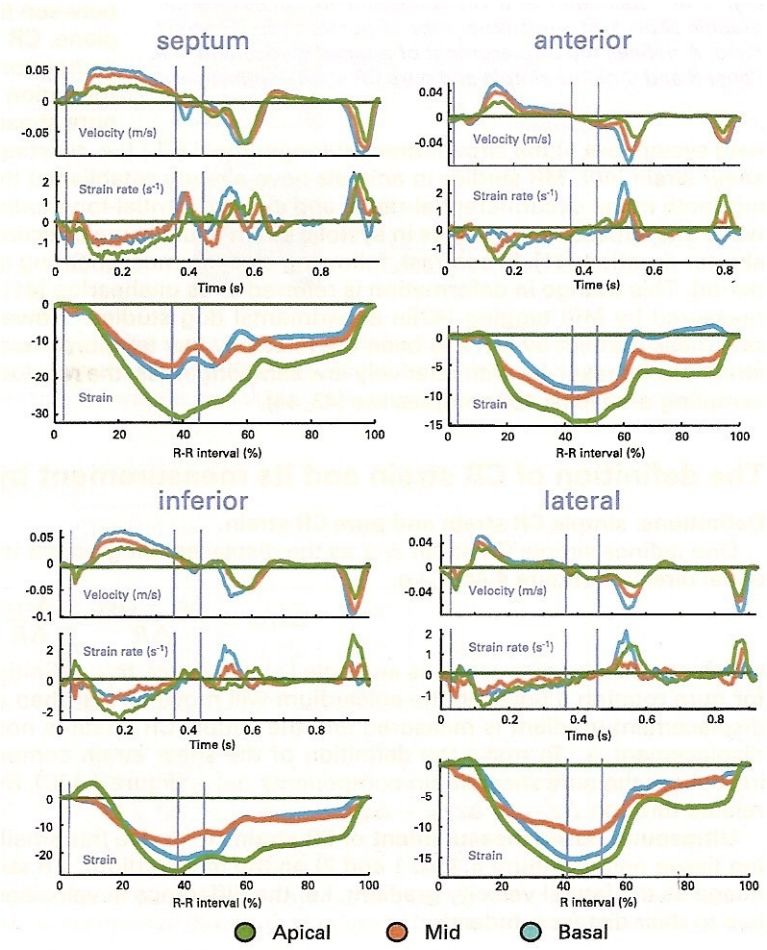

Fig 1.17: The regional long axis data sets from four walls which are now routinely acquired and post-processed for a complete left ventricular function study (from 16, Sutherland GR et al. 2006).

Longitudinal systolic peak strain is often (but not always) slightly higher in the mid wall segment in all four cardiac walls. Lower longitudinal peak systolic strain values can be obtained in basal segments, as data from the non-deforming atrioventricular ring can unwittingly be included in their estimation. For the apical segment, the angle of insonation versus direction of motion can also be a problem. Because of this, strain should only be calculated for the most basal part of the apical segment.

Regional systolic longitudinal shortening normally commences in mid wall segments by the time of aortic valve closure but may be delayed in basal segments. Here, peak shortening often occurs after aortic valve closure. Such “normal” post systolic shortening rarely occurs in apical and mid wall segments but is a common finding in basal segments. In normal ventricles, the amount of segmental

post-systolic shortening never exceeds 20% of peak systolic shortening and usually is less than 10%. The amount of this “normal” post-systolic shortening can be increased in normal hearts by an increase in both pre- and after-load[16].

Tissue Doppler-based strain limitations

The quality of strain rate curves may vary depending on the care used in obtaining the underlying velocity data. Optimizing the velocity signal should include avoidance of reverberation artefact (for example related to rib artefact) and insuring adequate frame rate(≥100 frames/s). It should be used harmonic imaging to improve the velocity signal. Moreover, it is important to track the sample throughout the cardiac cycle to ensure that the sample remains within the myocardium and to avoid cavity signal (i.e. blood-pool activity)[15]. Furthermore, use a narrow imaging sector enables a limited number of Doppler beams to be focused in a small area, optimizing spatial resolution.

Like all Doppler techniques, tissue velocity-based strain is sensitive to alignment and this implies that different vectors may be involved at each site[35]; it is therefore mandatory to align axis of movement with scan line and having an angle deviation below the 15 degrees for acceptable calculations. Anyway, being an unidirectional technique, even when tracking is used to try to maintain the sample volume within a segment of myocardium, it needs to be remembered that the myocardium undergoes a wringing, twisting motion so that the sample will inevitably move out of the scanning field in the course of the cardiac cycle. These considerations of through-plane motion may be particularly important when the myocardial function is non-uniform, as for example with an ischemic cardiomyopathy. Finally, angle changes with respiratory movement may contribute to drifting of the strain curve; this can be avoided by acquiring in end-expiration[16,31].

2D Echocardiography-based measurement of strain

A Doppler-independent technique for strain measurement would have attractions with respect to signal noise, angle dependency and the ability to monitor strain in two dimensions rather than one dimension. Recently, speckle tracking techniques have been used. These speckles are ultrasound reflectors within tissue, are highly reproducible and essentially behave like magnetic resonance tags. Shortening may be calculated by comparison of these speckles from frame to frame, although attention to technical detail is important, because comparisons at high frame rates are associated with high levels of noise, and comparisons at low frame rates risk loss of correlation because of excessive displacement of the speckles[31].

Unlike tissue Doppler strain, speckle tracking is an angle independent technique as the movement of speckles can be followed in any direction (fig. 1.18). For the apical views this implies that not only longitudinal but also transverse parameters can be calculated, which is not possible in TDI recordings. In short axis images both circumferential and radial parameters can be calculated for all myocardial segments. In addition to the circumferential deformation parameters, ventricular rotation and twist (additional parameters for LV function) can also be calculated using this technique[36,37].

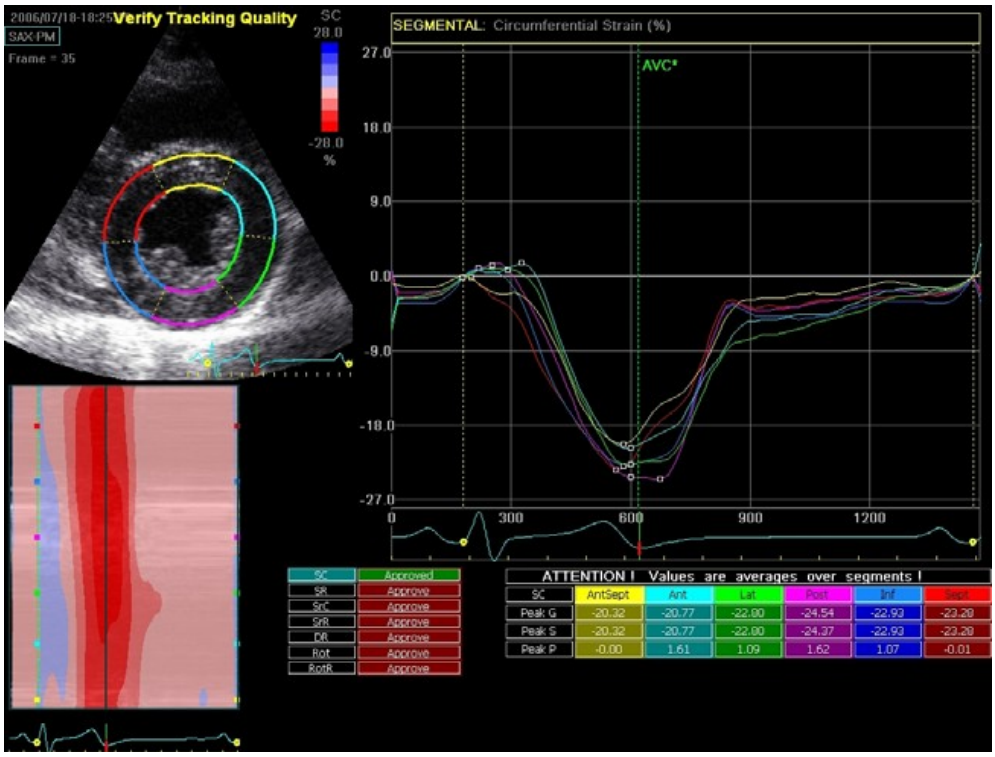

Fig 1.18: Results-screen of 2D strain echocardiography. Circumferential strain is calculated on a short axis recording at the level of the papillary muscle in a healthy individual. On the top left the short axis view with the ROI divided into six segments; top right: graphical representation of the selected parameter of all accepted segments; bottom right: peak values of all segments, these values are automatically calculated and can be manually adjusted in the graph if necessary; middle bottom: all available parameters (radial and circumferential strain and SR, radial displacement, rotation and rotation rate), if approved, these values are stored; bottom left: colour coded M-mode of the selected parameter (from 30, Teske AJ et al. 2007).

The initial experience with 2D strain methodologies suggests that they are robust, although the evidence base is limited and additional clinical assessment is required.

CHAPTER 2

Left Ventricular Hypertrophy

Left ventricular hypertrophy is defined a san increase in left ventricular mass, usually quantified by echocardiography or, more recently, by magnetic resonance imaging. According to Devereux and associates[38], the following equation provides a reasonable determination of LV mass in grams:

$1.04 [(LVEDD + PW + IVS)^3 - LVEDD^3] x 0.8 + 0.6$

Where LVEDD is the left ventricular end-diastolic diameter, PW is the posterior wall thickness, IVS is the interventricular septal thickness, 1.04 is the specific gravity of the myocardium and 0.8 is the correction factor. All measurements are made at end-diastole (at onset of the R wave) in centimetres and are derived from M-mode mid-ventricular long-axis parasternal view.

From Devereux's original study[39] of a racially mixed normotensive population, the suggested upper limits of normal were 134 g/m^2 for men and 110 g/m^2 for women. Epidemiological data from the mainly white population of Framingham[40] were used to define left ventricular hypertrophy as a left ventricular mass index (>131 g/m^2 for men and >100 g/m^2 for women).

More reliably, M-mode or two dimensional measurements of septum and posterior wall thicknesses in end-diastole can give an idea of normal and hypertrophied walls, according to age and sex[41, 42].

Left ventricular hypertrophy can be physiological in athletes as a result of intensive exercise training, or pathological in pressure overload (e.g. systemic hypertension, aortic stenosis), chronic volume overload (e.g. aortic regurgitation), or myocardial disease (e.g. hypertrophic cardiomyopathy, acromegaly). Pathological LV hypertrophy defined by echocardiography is an independent predictor of cardiovascular morbidity and mortality[43] and its regression is associated

with a reduction in cardiac failure and sudden death[44]. In fact, it is a maladaptive process. Although increased wall thickness tends to normalise wall stress, eventually this compensation is exhausted and there is contractile dysfunction of myocites, apoptosis and interstitial and perivascular fibrosis. These structural changes are localized mainly in the subendocardium and they precede and accompany the transition from compensated left ventricular hypertrophy to heart failure[45-47] . The major underlying stimulus appears to be progressive impairment of subendocardial perfusion, secondary to haemodynamic factors such as increased wall stress and intramyocardial pressure, and to microvascular disturbances associated with endothelial dysfunction and reduced coronary flow reserve. Subendocardial systolic dysfunction may remain clinically silent for many years if global systolic function is preserved. The earliest functional changes in left ventricular hypertrophy affect long-axis contraction and relaxation (considering that fibres in the subendocardium are aligned longitudinally from apex to base[48]) and these can be masked if at the same stage in the natural history there is a compensatory increase in radial function.

Discrimination between different types of hypertrophy is sometimes difficult by conventional echocardiographic methods, whereas Doppler myocardial imaging provides new criteria that can be used in difficult clinical cases. It also provides sensitive markers of early dysfunction regarding the subendocardial function that may be useful for monitoring regression of hypertrophy secondary to increased afterload and perhaps for estimating prognosis.

Hypertrophic Cardiomyopathy

Definition

Hypertrophic cardiomyopathy (HCM) is a complex and relatively common genetic cardiac disorder (about 1:500 in the general adult population). It affects men and women equally and occurs in many races and countries, although it appears to be under-diagnosed in women, minorities and under-served populations.

It is characterized by left ventricular hypertrophy (LVH) (typically asymmetric in distribution, and showing virtually any diffuse or segmental pattern of left ventricular (LV) wall thickening). Left ventricular wall thickening is associated with a non-dilated and hyperdynamic chamber (often with systolic cavity obliteration) in the absence of another cardiac or systemic disease (e.g., hypertension or aortic stenosis) capable of producing the magnitude of hypertrophy evident, and independent of whether or not LV outflow obstruction is present[49].

Genetics

Hypertrophic cardiomyopathy is inherited as a Mendelian autosomal dominant trait and roughly half of patients have another family member with HCM. It is caused by mutations in any one of 12 genes, each encoding protein components of the cardiac sarcomere composed of thick or thin filaments with contractile, structural, or regulatory functions[49-54]. Three of the HCM-causing mutant genes predominate in frequency—i.e., beta-myosin heavy chain (the first identified), myosin-binding protein C and cardiac troponin-T probably comprise more than one-half of the genotyped patients to date (figure 2.1). Seven other genes each account for fewer cases: regulatory and essential myosin light chains, titin, alpha-tropomyosin, alpha-actin, cardiac troponin-I, and alpha-

myosin heavy chain. This genetic diversity is compounded by intragenic heterogeneity, with about 400 mutations now identified. Many other mutations in previously identified genes (and even in additional genes, each probably accounting for a small proportion of familial HCM) undoubtedly remain to be identified. Phenotypic expression of HCM (i.e., LVH) is the product not only of the causal mutation, but also of modifier genes and environmental factors[55,56]. Even among families with the same mutation on a particular loci individuals vary with respect to phenotype and prognosis.

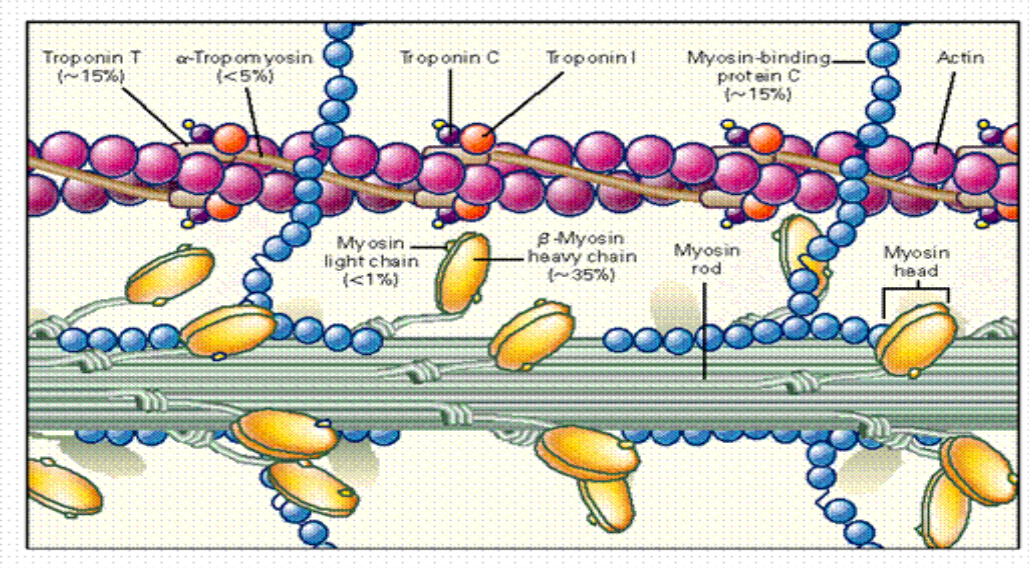

Fig 2.1: Sarcomeric mutations at the basis of HCM.

In a cohort of referred, unrelated patients with HCM, roughly 40% of patients with HCM were found to have sarcomeric mutations. In the remaining 60%, none of the known genotype abnormalities were found[57]. Younger age at diagnosis, marked wall thickness and a family history of HCM increase the frequency that a patient will be gene positive.

Laboratory DNA-analysis for mutant genes is the most definitive method for establishing the diagnosis of HCM. At present, however, there are several obstacles to the translation of genetic research into practical clinical applications and routine clinical strategy. These include the substantial genetic heterogeneity, the low frequency with which each causal mutation occurs in the general HCM population and the important methodological difficulties associated with identifying a

single disease-causing mutation among 12 different genes in view of the complex, time-consuming, and expensive laboratory techniques involved. Mutation analysis is presently confined to a few research-oriented laboratories.

Histopathology

On light microscopy individual myocyte hypertrophy is noted. Myocardial fiber disarray is the pathognomonic abnormality. In normals, myocytes are arranged in linear parallel arrays. In HCM with fiber disarray, myocytes form chaotic intersecting bundles (see figure 2.2). With electron microscopy, myofilament disarray is noted as well[58]. Although fiber disarray is noted in other diseases, the percentage of the myocardium occupied by disarray is higher in patients with HCM[59]. Nevertheless, its distribution is not related to the magnitude of LV wall thickness[60]. Fiber disarray is thought to predispose to electrical reentry and sudden death, as is particularly evident in the Troponin T disease[61]. Recently, cardiac diffusion MRI was used to image in vivo myocardial fiber architecture and it allowed correlating myocardial disarray in HCM with regional myocardial function[62].

Fibrosis is also a prominent feature on light microscopy (see figure 2.2). Interstitial and perivascular fibrosis may occupy as much as 17% of the myocardium in patients who die suddenly and its extent is not correlated with wall thicknesses or heart weight [63,64]. Fibrosis and hypertrophy decrease LV chamber compliance and cause diastolic dysfunction and exercise intolerance[65]. Fibrosis appears to predispose to complex ventricular arrhythmia[66].

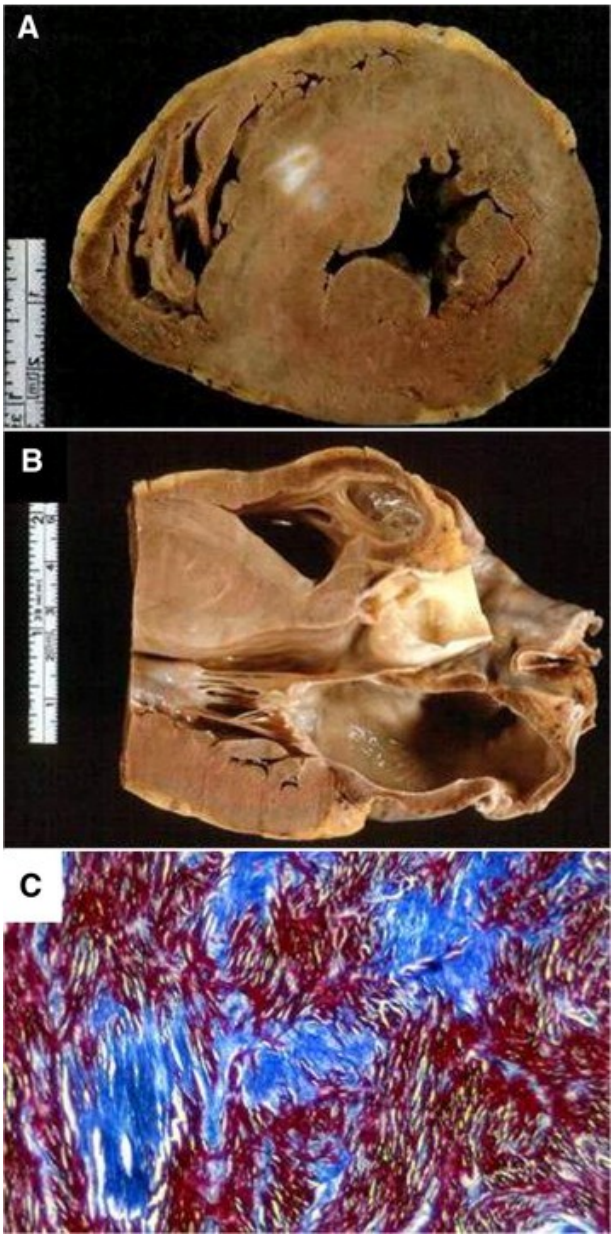

Fig 2.2: Sudden death due to hypertrophic cardiomyopathy. (A) Short axis section: note asymmetric septal hypertrophy with a large scar within. (B) Long-axis section with mid ventricular asymmetric septal hypertrophy. (C) Myocardial disarray and fibrosis (Azan stain) (from 71, Thiene G et al. 2009).

Recently, an MRI study has correlated fibrosis detected by delayed myocardial enhancement (DE) with regional left ventricular function, regardless of the degree of myocardial hypertrophy [67]. They distinguished the distribution of DE into an ill-defined patchy pattern and in a focal nodular pattern; the latter was particularly related with regional dysfunction (figure 2.3).

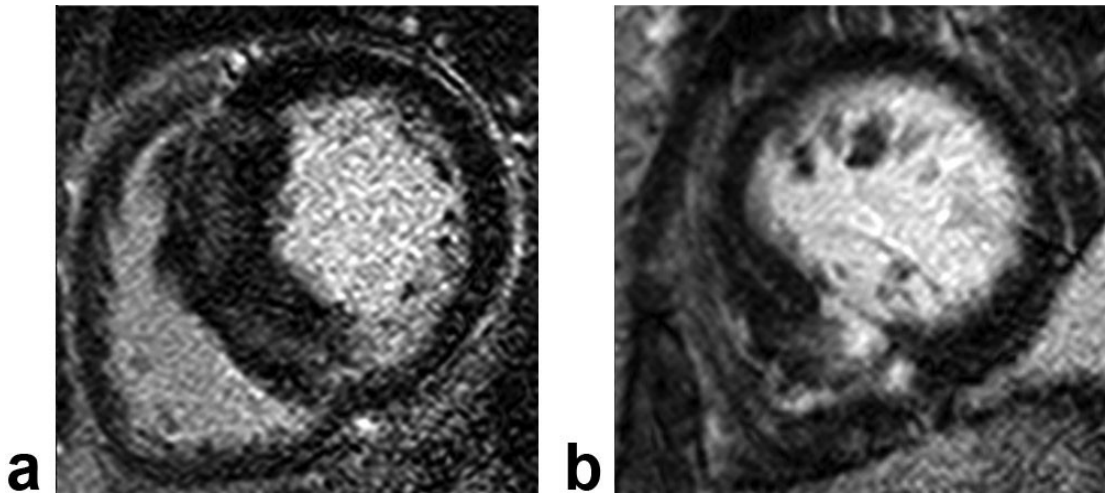

Fig 2.3: Patterns of delayed enhancement in patients with hypertrophic cardiomyopathy. **a:** ill-defined patchy enhancement. **b:** focal nodular enhancement (from 67, Kim YJ et al. 2008).

Although the epicardial coronary arteries are dilated, narrowings of the intramural penetrating coronary arteries are noted, due to arteriolar intimal and medial hyperplasia. These narrowings are thought to contribute to ischemia, well documented in HCM[68]. Figure 2.4 shows such narrowings in myectomy resections.

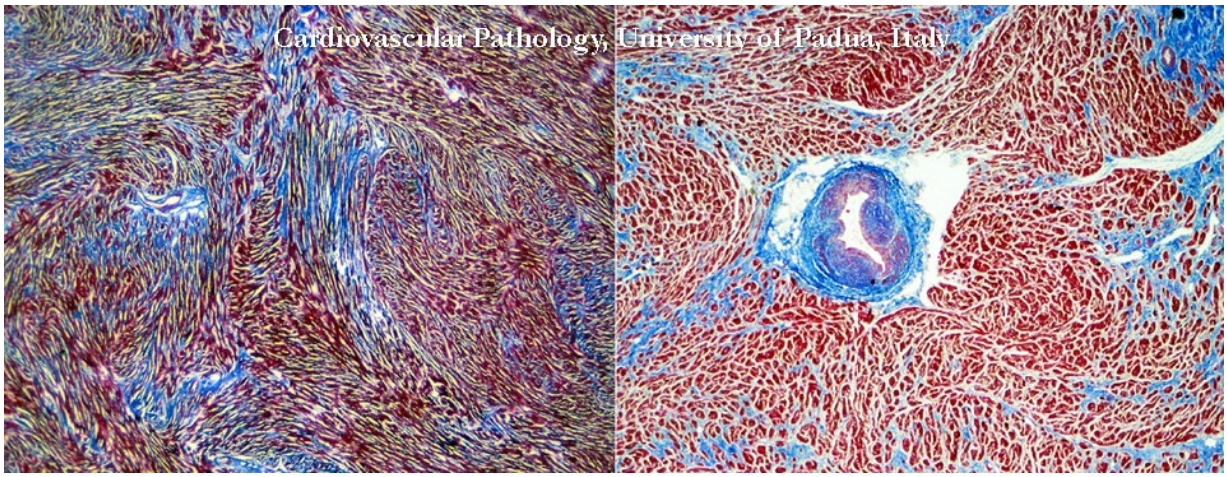

Fig 2.4: Histological features of hypertrophic cardiomyopathy. a) fascicular disarray of the myocardium; b) intramural small vessel disease with intimal dysplasia- Azan stain) (from 72, Basso C et al. 2010).

A recent Paduan study based on MRI[69] correlated focal tissue abnormalities with regional ischemia at various stages, i.e. the presence of patchy DE, edema and hypoperfusion with acute-subacute ischemic-phase parameters (chest pain or new onset of ST-segment depression), while extensive DE and perfusion defects in the absence of edema were significantly related to end-stage HCM (left ventricular ejection fraction<50%).

On the other hand, another possible ischemic mechanism may be involved with mortality in HCM, i.e. the presence of myocardial bridging of left anterior descending coronary artery. In fact, Basso et al[70] showed it is more common at necropsy in HCM hearts than in controls with or without LV hypertrophy, nevertheless without finding a systematic correlation with sudden death.

Clinical course

HCM shows a heterogeneous clinical course and expression and it may become phenotypicly evident at any ages.

Many people with hypertrophic cardiomyopathy do not have symptoms. However, if symptoms develop, initially they generally include dyspnea, angina, syncope or palpitations, all of these symptoms especially with exercise or exertion. Symptoms are more frequent in presence of obstruction of LV outflow, which may either be subaortic or mid-cavity in location. Subaortic obstruction is caused by systolic anterior motion (SAM) of the mitral valve leaflets and mid-systolic contact with the ventricular septum. SAM is probably attributable to a drag effect or possibly a Venturi phenomenon and is responsible not only for subaortic obstruction, but also the concomitant mitral regurgitation (usually mild-to moderate in degree) due to incomplete leaflet apposition, which is typically directed posteriorly into the left atrium. Occasionally (perhaps in 5% of cases), gradients and impeded outflow are caused predominately by muscular apposition in the mid-cavity region contact involving excessive mid-ventricular or papillary muscle hypertrophy and malalignment. Outflow obstruction is a strong, independent predictor of disease progression to

HCM-related death (relative risk vs. nonobstructed patients, 2.0), to severe symptoms of New York Heart Association (NYHA) class III or IV, and to death due specifically to heart failure and stroke (relative risk vs. nonobstructed patients, 4.4). Even if outflow obstruction is dynamic and therefore variable, it is reasonable to divide patients on the basis of the peak instantaneous gradient as assessed with continuous wave Doppler into an obstructive group (peak ≥30 mmHg under basal or provocable conditions) and a nonobstructive one (<30 mmHg under basal or provocable conditions)[49].

Moreover, HCM may develop important complications such as atrial fibrillation or heart failure.

Sudden death may occur from the onset of ventricular arrhythmias. Although it can occur in any age group, sudden death is most shocking when it happens to young adults or athletes. That was particularly studied in Padua university, finding that a certain number of cases of sudden death in the young (≤35 years) including athletes is caused by hypertrophic cardiomyopathy[71,72]. At necropsy analysis, pathologic findings of ischemic damage, either acute-subacute or in the form of fibrotic scars, support the clinical evidence that ischemia occurs in the natural history of HCM and may contribute to life-threatening electrical instability getting to sudden-death[73](figure 2.2 and 2.4). In the Paduan experience, HCM caused very few cases of sudden death among athletes while it was more frequent among non-athletes; in fact, HCM cases detected at preparticipation were disqualified and none of them died during a mean follow-up period of 8.2±5 years[74]. Thiene et al [75] stressed the effective role of the Italian protocol for prepartecipation screening in preventing sudden death in young athletes affected by HCM and in the last proposal for a common European protocol[76] was strongly suggested a complete athletes' screening including a 12-lead ECG in addition to history and physical examination.

Diagnosis

Laboratory DNA-analysis for mutant genes is the most definitive method for establishing the diagnosis of HCM.

At present, however, there are several obstacles to the translation of genetic research into practical clinical applications and routine clinical strategy. These include the substantial genetic heterogeneity, the low frequency with which each causal mutation occurs in the general HCM population, and the important methodological difficulties associated with identifying a single disease-causing mutation among 12 different genes in view of the complex, time-consuming, and expensive laboratory techniques involved. In fact, mutation analysis is presently confined to a few research-oriented laboratories.

On the other hand, myocardial biopsy is invasive with ethic considerations, expensive and anyway not so feasible in any hospitals.

Consequently, the clinical diagnosis of HCM is established most easily and reliably with two-dimensional echocardiography by demonstrating left ventricular hypertrophy (LVH) with maximal wall thickness greater than or equal to 15 mm [49]. The location of the abnormal hypertrophy is most often the anterior septum although the posterior septum and anterior wall are frequently hypertrophied as well[58,77]. Anyway, hypertrophy can occur in any segment. Consequently, it is possible to define the most common asymmetric pattern with the septal to posterior wall thickness ratio ≥1.3, and the less observed concentric pattern with this ratio<1.3 (figure 2.5).

Apical hypertrophy, that spares the basilar and mid segments, is a variant that occurs more frequently in East Asian patients with HCM. However, it is a relatively common variant in North American and European patients as well, occurring in 7%. This variant generally has a better prognosis (figure 2.5). Truly atypical HCM variants include thickening just of the lateral wall or posterior wall[58].

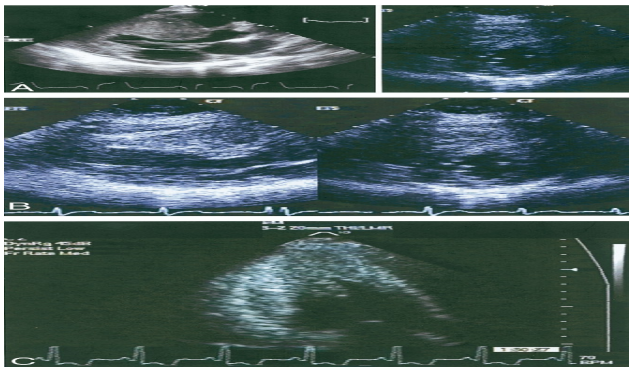

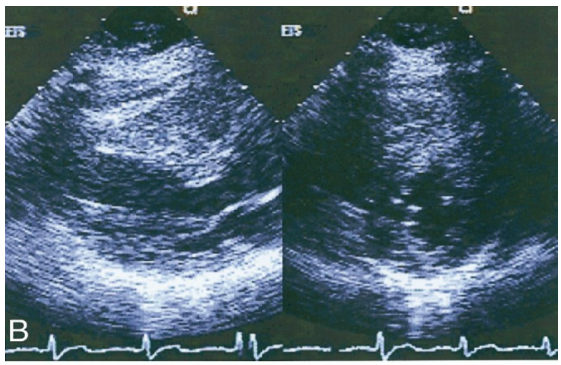

Fig 2.5: A) Asymmetric septal hypertrophy; B) concentric hypertrophy; C) apical hypertrophy (from 77, Nagueh SF et al. 2006).

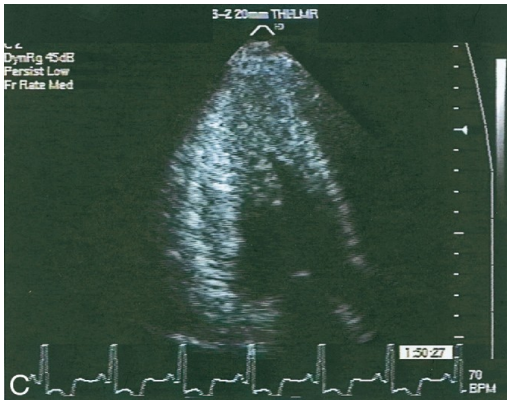

Recent studies have shown that MRI can be applied to measure LV dimensions, volumes, and EF with high reproducibility[78], including in patients with LVH. In HCM, MRI plays a major role in identifying the pattern and extent of hypertrophy, which can be more extensive than appreciated by echocardiography, particularly in the anterolateral free wall. This is also true with apical LVH. In addition, given its accuracy, this technique is useful for familial screening and genetic linkage studies. Moreover, with delayed enhancement it is possible to study the extent of fibrosis. In summary, cardiac MRI is considered a class I indication for patients with apical HCM and a class II indication for other phenotypic variants of HCM[78]. Nevertheless, MRI is expensive, not always available and not applicable to claustrophobic patients or with metallic devices.

In fact, echocardiography, widely available, non-invasive, of relatively low cost and with no contraindications (except sometimes for poor imaging quality) has proved over the years, to be the best technique to diagnose, evaluate, follow-up and guide the treatment of HCM.

Tissue Doppler Imaging in HCM

As previously mentioned, in pathological LVH interstitial fibrosis particularly involves the subendocardium[45-47,64], leading to an impairment of longitudinal shortening; in fact, subendocardial muscle bundles are oriented along the long axis of the left ventricle[48].

Consequently, in HCM myocardial longitudinal systolic velocities are reduced, with initially maintained or increased radial function as compensation mechanism. Obviously, also diastolic long-axis velocity parameters result impaired and correlated to LV diastolic pressure at catheterization. Systolic and diastolic asynchrony, i.e. differences among velocities of different LV regions, is also typical of HCM[79]. Vinereanu et al[80] found that systolic and diastolic velocities were similarly reduced in HCM and hypertensive LVH, but in HCM the heterogeneity of annular systolic velocities was more. Another study confirmed increased systolic heterogeneity in HCM, but also demonstrated lower systolic velocities, longer isovolumetric contraction, and prolonged pre-ejection times in HCM compared with hypertensive patients[81].Diastolic function was also more impaired in HCM, with lower velocities, higher heterogeneity and longer IVRT. Also Nunez et al[82] found more impaired systolic and diastolic velocities in HCM than in hypertensive LVH. Moreover, normal diastolic and systolic velocities can differentiate the athlete's heart from HCM[80,83] (figure 2.6) and in one study[80], the best differentiation of pathologic hypertrophy (either HCM or hypertensive LVH) from physiologic hypertrophy (in runners and weight-lifters) was provided by a mean systolic annular velocity < 9 cm/s. Individuals with HCM have lower systolic velocities even at annular sites contiguous to walls without hypertrophy.

Fig 2.6: Representative examples of Tissue Doppler traces of the velocities of lateral mitral annular motion in a patient with HCM (A), an athlete with physiologic LVH (B) and a normal subject (C). It is possible to observe lower systolic and early diastolic myocardial velocities, with a reversed myocardial E/A ratio, in the patient with HCM and supranormal velocities in the athlete's heart (from 79, Rajiv C et al. 2004).

Additionally, Nagueh et al[84] reported in a transgenic rabbit model of human that systolic and early diastolic velocities were significantly lower in the subjects with genetic HCM mutations, whether or not they had LVH. A lateral annular systolic velocity < 13 cm/s had excellent sensitivity and specificity for identifying subjects with mutations but no LVH.

Nevertheless, there are theoretical reasons why imaging of regional myocardial deformation may have several advantages over myocardial velocities for the diagnosis of regional function; in fact, overall wall motion, rotation and contraction of adjacent myocardial segments will influence regional velocity estimates[14]. Midseptal longitudinal strain was found markedly reduced or reversed in 31 patients with HCM[85] and in a child diagnosed with HCM, strain was absent in an isolated midventricular segment that was hypertrophied[86]. Moreover, patients with HCM were found to have more pathological post-systolic strain (PSS), i.e. deformation that occurs after aortic valve closure, when compared to normal subjects[87]. Another study[88] found a correlation between a strain pattern of double peak sign (the first in systole, the second in diastole, such as PSS) in pathological HLV and regional fibrosis detected by DE at MRI.

Moreover, Kato et al[89] observed that a systolic strain cut-off value -10.6% was associated with a sensitivity of 85.0%, specificity of 100%, and predictive accuracy of 91.2% for discrimination

between biopsy-proven HCM patients and hypertensive subjects. The combination of the end-diastolic interventricular thickness/end-diastolic posterior wall thickness ratio and systolic strain was able to discriminate HCM from hypertensive LVH with a predictive accuracy of 96.1%. Another study[90] based on 2-dimensional strain detected that radial and transverse strains were significantly higher in professional soccer players compared with normal subjects, whereas longitudinal strain was lower; compared with HCM patients, athletes had higher values for transverse, radial and circumferential strains (figure 2.7). Another 2-dimensional strain based study confirmed that, despite apparently normal left ventricular systolic function, all components of strain are significantly reduced in HCM compared to normal subject[91].

Furthermore, systolic and diastolic strain parameters were found to be impaired not only in hypertrophied but also in non-hypertrophied segments, although this is more evident in hypertrophied segments[92,93]. Velocity tissue Doppler[94,95] and RMN[96] studies confirmed the systolic and diastolic impairment also in non-hypertrophied segments in overt HCM and even in HCM mutations carriers without LV hypertrophy[84,97-99]. This is consistent with the previous findings that histological abnormalities are observed also in segments of the wall with normal or minimally hypertrophied thickness, even if they are more extensive in the hypertrophied septum[59-61,63,64,68].

Fig 2.7: Example of 2-dimensional strain curves obtained in athletes (A) and in patients with HCM (B) (from 90, Richand V et al. 2007).

Hypertensive heart disease

Hypertension is a major risk factor for cardiovascular morbidity and mortality. The presence of hypertension more than doubles the risk for coronary heart disease, including acute myocardial infarction and sudden death, and more than triples the risk of congestive heart failure as well as strokes. Patients with high blood pressure frequently have abnormalities of cardiac structure or function, including left ventricular hypertrophy, systolic and diastolic dysfunction and in extreme cases, overt heart failure. There may also be concomitant or related coronary heart disease and an increased risk of arrhythmias and sudden death[100].

In several epidemiological studies, left ventricular hypertrophy is an independent risk factor for cardiovascular morbidity and mortality[43,101,102]. This correlation between echocardiographically determined left ventricular mass and the development of cardiovascular disease appears to be without a critical mass, separating the sometimes postulated ‘compensatory’ from ‘pathological’ hypertrophy[101].

Histopathology

The progression from a structurally normal heart to left ventricular hypertrophy is not solely a consequence of increased afterload imposed by hypertension, with an increased total peripheral resistance. Many mechanisms are now known to be involved in the growth regulation of the heart, including neurogenic, humoral, autocrine, paracrine and possibly endocrine factors[100].

In fact, factors such as angiotensin II, endothelin-1 and aldosterone all have effects on fibroblast proliferation. Growth hormone, thyroxin, volume and pressure loading are other factors

contributing to myocyte proliferation and enlargement. The relative increase in fibroblastic activity that occurs in hypertensive heart disease may be an important factor in pathological rather than physiological left ventricular hypertrophy. Tanaka et al[64]found at necropsy cases that in hypertensive heart disease the percentage area of fibrosis was significantly greater than in normal hearts; furthermore, in the former condition the extent of fibrosis correlated with hearth weight, while in the latter one it did not. In hypertensive heart disease, the percentage area of fibrosis increased from the outer to the inner third of the left ventricular free wall, depending on the transmural gradient of tissue pressure and wall stress, as already told.

Coronary resistance vessels are also remodelled in hypertensive heart disease, with perivascular fibrosis of intramyocardial coronary arteries and arterioles, together with thickening of their media.

Since the left ventricular hypertrophy of hypertension is not only related to the amount of afterload but also to neurohormonal factors, its models differs from myocardial hypertrophy due to aortic stenosis. At the cellular level, the intraventricular pressure overload of hypertension as well as aortic stenosis results in myocytic hypertrophy and increased perimyocytic fibrosis. However, intramyocardial arteriole wall-thickening and enhanced perivascular fibrosis are distinctive features of hypertension, but are not seen in aortic stenosis[103].

Neurohormonal factors

Several growth factors have been implicated in initiating and maintaining myocardial hypertrophy[100]. In particular, the renin–angiotensin–aldosterone system is likely to have an important role in hypertensive heart disease, and both angiotensin-II and aldosterone are known to cause myocardial fibrosis.

An important role for the renin–angiotensin system is suggested by the impressive effect of angiotensin-converting enzyme (ACE) inhibitors, and more recently the angiotensin II receptor antagonists in causing regression of hypertensive left ventricular hypertrophy, and in preventing

remodelling and improving prognosis after myocardial infarction. Furthermore, there is a close correlation between circulating renin–angiotensin levels and left ventricular mass.

Experimental data also suggest that elevated levels of angiotensin II in the presence of systemic hypertension provoke predominantly left ventricular myocardial necrotic lesions.

There are synergistic effects of angiotensin II and aldosterone with regards to perivascular and interstitial fibrosis of the ventricle, but an angiotensin-independent effect of aldosterone on myocardial fibrosis in hypertension has been demonstrated in various animal models, as well as the protective effect of spironolactone.

The sympathetic activation present in hypertension contributes to the rise in blood pressure, but also seems to have adverse metabolic effects, such as insulin resistance, hyperinsulinaemia and hyperlipidaemia. There have been animal studies suggesting that sympathetic influences may exert cardiotrophic effects, thus favouring the development of myocardial hypertrophy.

Hypertension is commonly associated with the insulin resistance syndrome and diabetes. Indeed, insulin resistance has been identified as a blood pressure-independent determinant of left ventricular hypertrophy.

Other hormones probably correlated to left ventricular hypertrophy in hypertension are atrial and brain matriuretic peptides, growth hormones, endothelin, osteopontin, parathyroid hormones and thyroxin.

Geometry and remodelling

The prevalence of left ventricular hypertrophy has been shown to increase progressively with age and varies with ethnic group, sex and obesity[100]. African origin patients have a larger left ventricular mass than comparable white patients. In addition, left ventricular hypertrophy may also precede the development of hypertension. In general, women have a lower prevalence of left ventricular hypertrophy for a given level of blood pressure than men, even after their left ventricular mass has

been corrected for body surface area or body weight. However, this gender difference only appears to hold true for pre-menopausal women, raising the possibility of a preventive role of oestrogens in the pathogenesis of left ventricular hypertrophy.

In left ventricular hypertrophy, increased left ventricular wall thickness causes reduced ventricular compliance (that is, the ventricle is ‘stiffer’) together with the degree of diastolic dysfunction. This also increases left atrial filling pressure, resulting in atrial dilatation.

There are two common types of left ventricular hypertrophy[100]: concentric and eccentric. The widespread thickening of the left ventricular walls relative to the internal cavity is referred to as ‘concentric’ left ventricular hypertrophy (figure 2.8).

Fig 2.8: Transverse cross section of the heart in a patient with hypertensive heart disease: concentric left ventricular hypertrophy (from Cardiovascular Pathology, University of Padua, Italy).

Less common is the disproportionate (relative to the posterior wall) thickening of the intraventricular septum, referred to as asymmetrical or eccentric left ventricular hypertrophy. These different patterns of left ventricular hypertrophy have different features, haemodynamic relations, and prognostic implications. For example, concentric left ventricular hypertrophy is normally

associated with moderate to severe hypertension and is more common in the middle aged and elderly than in young patients. On the other hand, isolated septal hypertrophy has long been recognised as an early and frequent structural adaptation in hypertension.

Verdecchia et al[104] found a very high prevalence among untreated hypertensive subjects of asymmetric LV remodelling due to isolated septal thickening, especially in subjects with normal echocardiographic LV mass (figure 2.9). Other studies in large hypertensive populations confirmed the quite common eccentric pattern of myocardial hypertrophy[105,106].

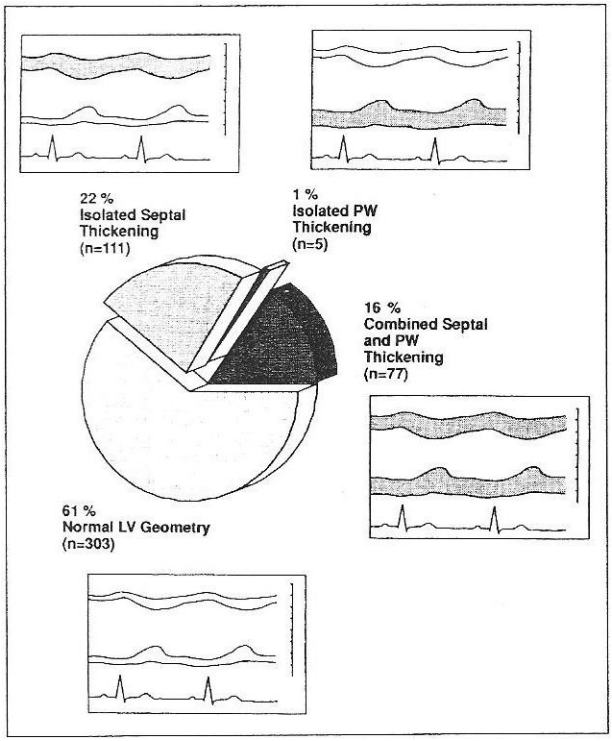

Fig 2.9: Distribution and schematic representation of the early structural changes in the left ventricle in 496 untraeated hypertensive subjects with normal left ventricular mass (from 104, Verdecchia P et al. 1994).

Hypertrophy could appear earlier and progress faster at the septal level than at the level of the posterior wall because of its larger bending radius compared with the posterior wall, leading to a greater tension during contraction wall, or owing to the addition of the right ventricular afterload or due to the septal over-reactivity to catecholamines[107-111].

Tissue Doppler Imaging in Hypertensive Heart Disease

In an experimental study (in rats), Derumeaux and collegues showed that the myocardial velocity gradient, i.e. the difference in velocities between the subendocardial and the subepicardial parts of LV wall, in systole is reduced in pressure-induced hypertrophy compared with control animals with physiological hypertrophy[112]. The ratio early-to-late diastolic gradients was also decreased. Reduced subendocardial function in pathological hypertrophy correlated with the degree of subendocardial interstitial fibrosis.

Vinereanu et al[80] demonstrated that systolic and early diastolic mitral annular velocities in hypertensive patients were significantly lower than in normal subjects; in the same study, systolic and diastolic velocities were found to be similarly reduced in HCM and hypertensive LVH, but in HCM the heterogeneity of annular systolic velocities was more, suggesting localized or patchy subendocardial dysfunction in the former condition and a diffuse subendocardial dysfunction in the latter one.

Patients with arterial hypertension but not left ventricular hypertrophy have been reported to have subendocardial diastolic disfunction, assessed by Doppler myocardial imaging of long-axis velocities, despite a normal E/A ratio; this was particularly evident at the basal septum when there was LV hypertrophy[113].

As for strain rate analysis, several studies have already demonstrated reduced deformation parameters in hypertensive heart disease. Yuda et al[114] observed decreased strain rate and peak systolic strain in hypertensive hypertrophied hearts not only with but also without abnormal LV filling when compared to normal hearts (figure 2.10). The systolic impairment was attributed to the increased fibrosis in the subendocardium, where myocardial fibres are mainly longitudinal oriented and so responsible for longitudinal shortening.

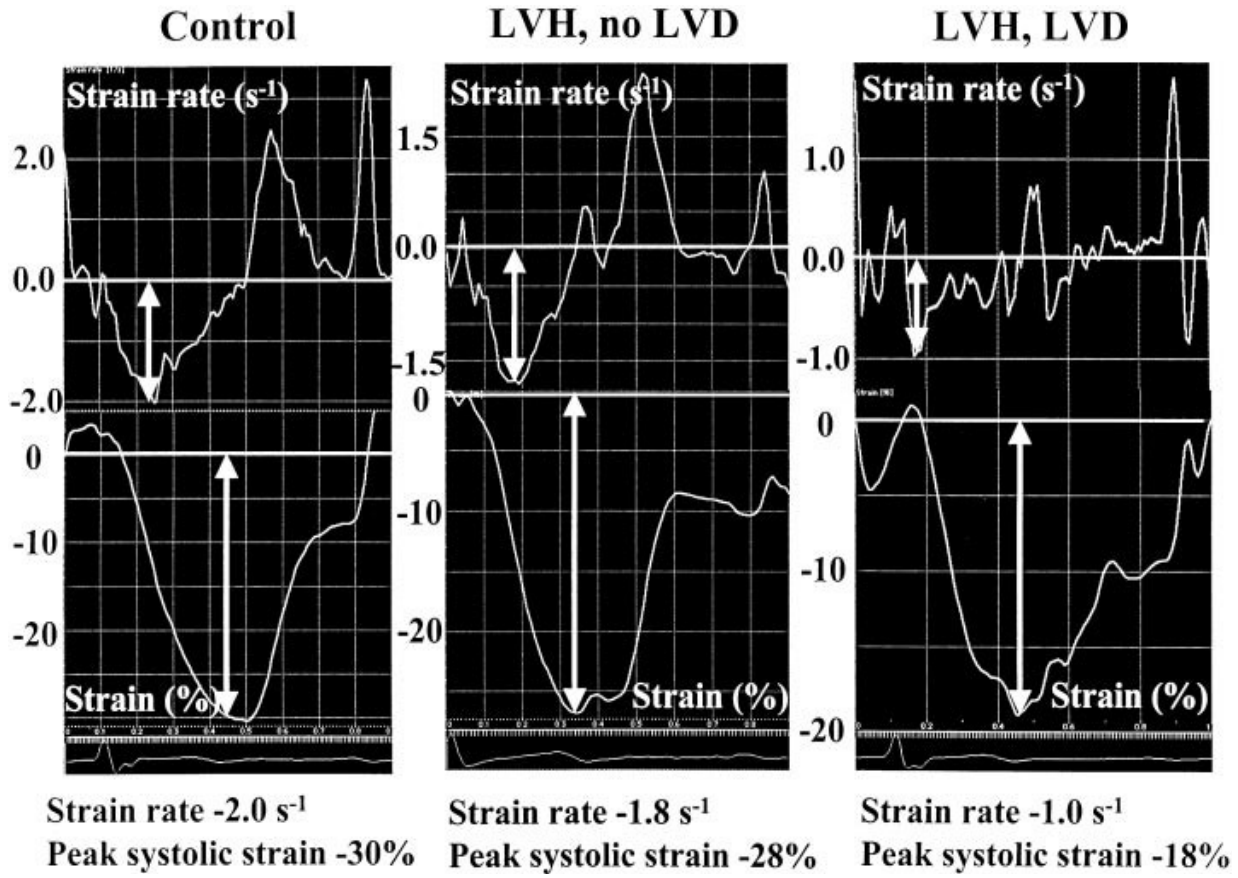

Fig 2.10: Representative strain rate (upper panels) and strain (lower panels) curves at mid septum in control patients (left) and in LVH patients without (middle) and with (right) abnormal LV filling (LVD) in the study 114, Yuda S et al. 2002.

Other studies confirmed lower systolic strain rate, peak systolic strain and peak early diastolic strain rate in hypertensive LV hypertrophy when compared to normal hearts[89,115] or physiologic cardiac hypertrophy (athlete's heart)[115]. The reduced systolic longitudinal deformation was found also in patients with hypertension who, earlier, were considered to have isolated diastolic dysfunction[116]. Furthermore, in a study in mild to moderate hypertension, prominent basal septal hypertrophy was observed and the peak systolic strain and strain rate were particularly reduced just in the basal septum[117].

CHAPTER 3

Integrated Backscatter and Left Ventricular Hypertrophy

Principles

The ultrasonic integrated backscatter (IB) technique is a useful noninvasive method for evaluation of the acoustic properties of tissue. As opposed to standard echocardiographic imaging with strong specular reflection occurring at tissue interfaces (such as epicardium and endocardium), ultrasonic IB signal is composed of low-amplitude, phase-sensitive, omnidirectional echoes arising from tissue heterogeneity within the myocardium. Thus, IB in extracted from raw, unprocessed radiofrequency data sets that are usually filtered to obtain the standard echocardiographic image. Integrated backscatter is calculated by integrating the power spectrum of the received signal (after compensation for the spectrum of the transmitted pulse) over the meaningful bandwidth of the transducer. This implies that IB is a measure of the mean reflected ultrasonic energy from a particular region of tissue[118].

Quantitative characterization of myocardial texture by analysis of ultrasonic reflectivity has been experimentally[119-122] and clinically[123,124] shown to correlate with the collagen content of the myocardial tissue. Nevertheless, the magnitude of IB depends on fundamental physical properties such as local elasticity, density and fiber geometry, which may be different between not only different areas of the interrogated myocardium but also among normal individuals[125]. Therefore, myocardial IB presents technical difficulties, the standardization among different patients is

problematic and it needs a calibration by the backscatter power of contiguous structures such as bloodstream or pericardium.

Madaras et al[126] first reported that the magnitude of IB measured from normal myocardium changed in a predictable manner during the cardiac cycle, with maximum values occurring at end diastole and minimum at end systole (figure 3.1).

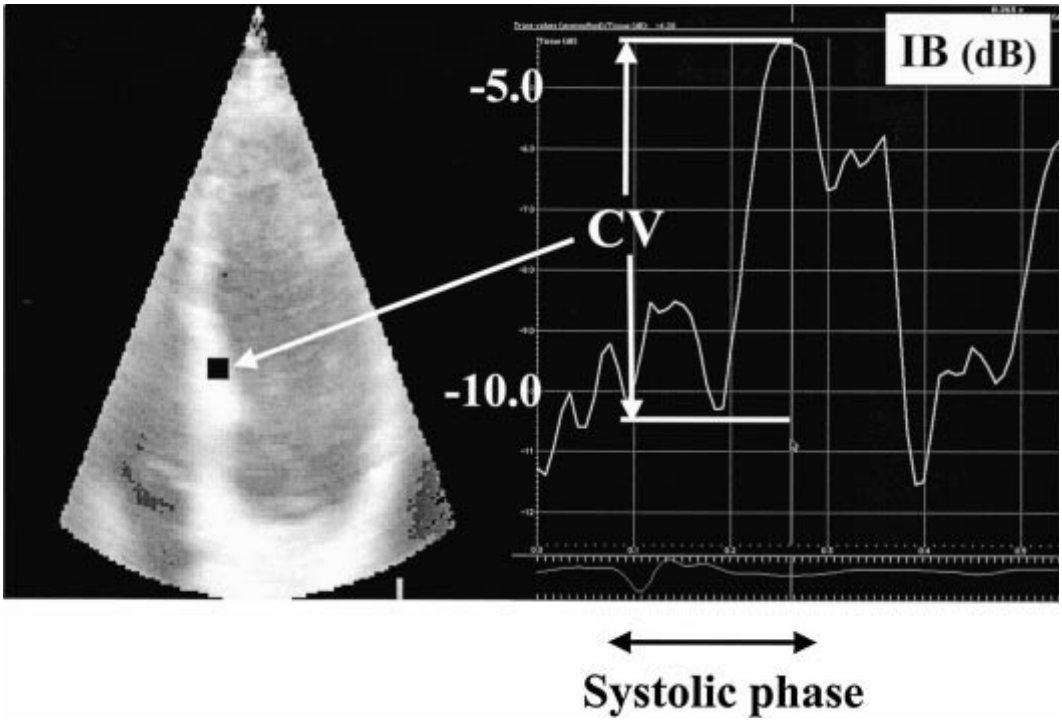

Fig 3.1: Representative mid-septal IB curve with measurement of CV (from 114, Yuda S et al. 2002).

Since then, this information has been confirmed in subjects with normal left ventricular function[127,128]. The mechanisms responsible for the cyclic variation of IB (CVIB) within the myocardium are still not clearly defined. Investigators have reported possible mechanisms that may influence this magnitude and variation. One such possible mechanism is a decrease in density and size of scatterers in the myocardium during systole[125]. It has also been shown that the magnitude of IB is dependent on the angle of the interrogating ultrasound beam with respect to the orientation of the myocardial fiber[129,130]. Lange et al[131] studied longitudinal IB from parasternal and apical echocardiographic views in normal subjects and he found that the same segments could present the

maximum value at end diastole when studied from the parasternal views but the maximum value in end systole when studied from the apical views. It seems likely that the source for the changes of the cyclic variation of IB measured from the myocardium during the cardiac cycle is due to two combined physiologic performances: first, because of the myocardial fiber contraction and changes in their orientation during this contraction and, second, because of the left ventricular rotation during the cardiac cycle.

CVIB analysis presents the advantage to be a relative value, being optimal to the comparison among different patients. Nevertheless its curves may be complex and they are easily studied by interventricular septum and posterior wall from parasternal view. A frame rate of at least 80 Hz would appear to be adequate to resolve the complexities of the IB curve at normal heart rates[118]. It has been shown that the CVIB is affected by regional myocardial performance [132,133], myocardial ischaemia [134-136] , orientation of the myocardial fibers and structural changes of the myocardium in cardiomyopathies[137-139], although the exact mechanisms responsible for CVIB are still unclear.

CVIB in pathological left ventricular hypertrophy

Previous studies on IB values in hypertensive patients showed a significant reduction of global CVIB when compared to normal subjects, dependently on LV mass and geometry [140, 141],on an abnormal LV filling [114, 142] or on the serum concentration of the carboxy-terminal propeptide of procollagen type I[143] or circulating aldosterone and immunoreactive endothelin[144].

In patients with hypertrophic cardiomyopathy, the degree of myocardial disarray, interstitial fibrosis and nonhomogeneity of myocyte size showed positive correlations with calibrated IB and negative correlations with CVIB[145]. Another study showed reduced CVIB in HCM carriers even in the absence of wall hypertrophy but at the time of appearance of ECG abnormalities[146].

A first study[138] tried to differentiate HCM from hypertensive heart disease and controls using parastenal CVIB, founding that there were any differences at the posterior wall level, while CVIB at the septum were significantly reduced in pathological left ventricular hypertrophy, but without differing the two pathological conditions.

Naito et al[137] tried to differentiate HCM from hypertensive LVH (H-LVH) on the basis of calibrated IB and CVIB, but the only difference was the greater transmural gradient of calibrated IB in patients with HCM than in normal subjects and in patients with H-LVH, in both the septum and posterior wall but mainly in the septum.

A following attempt[140] to distinguish HCM from H-LVH by IB measures showed just that the CVIB values in the subendocardium of the posterior wall of patients with H-LVH were reduced but not in patients with HCM (figure 3.2).

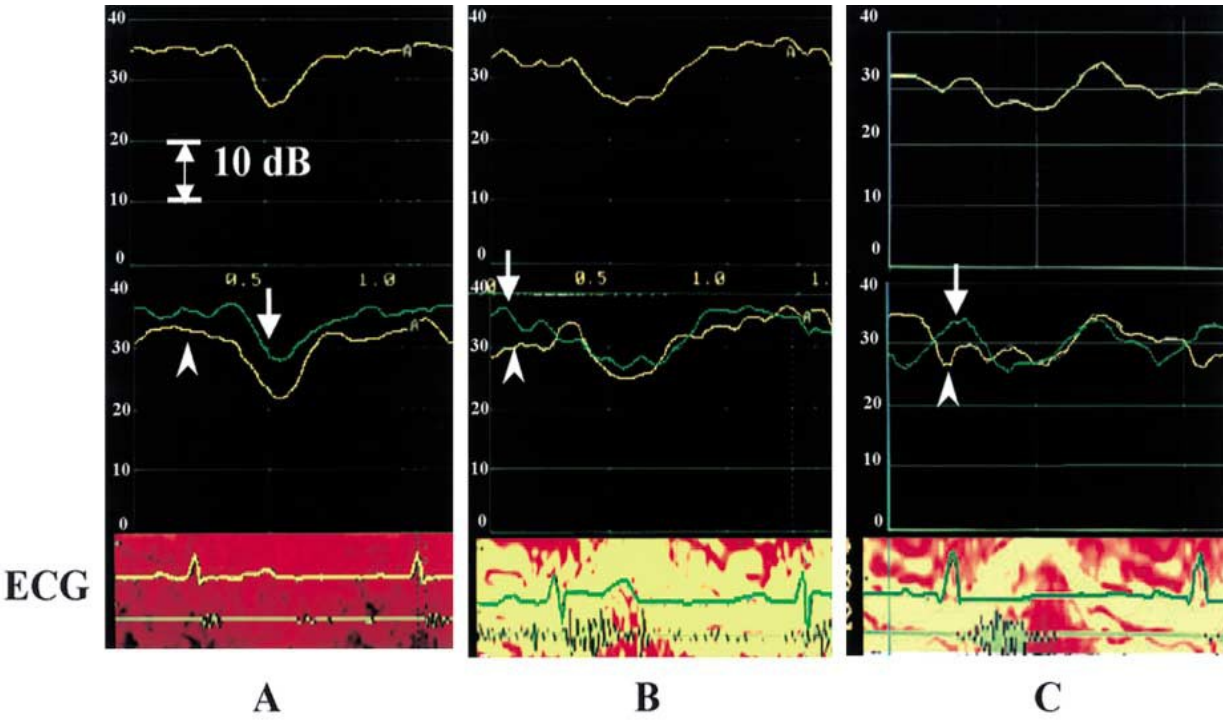

Fig 3.2: Representative curves of IB vs time for the entire region of interest (ROI) (upper), at the endocardial half (middle, arrow head) and the epicardial half (middle, arrow) of the ROI of the posterior wall in a normal subject (A), a patient wuitn hypertrophic cardiomyopathy (B) and a patient with hypertension (C) (from 140, Ueda K et al. 2002).

Nevertheless, all these studies used just parasternal CVIB, while, as already explained in Chapter 2, in pathological LVH the longitudinal function should be the most compromised, needing more exhaustive studies on longitudinal CVIB from apical views.

Relationship between strain and CVIB

Strain (-rate) imaging allows the quantitative assessment of regional myocardial deformation and CVIB describes changes in local reflectivity and thus tissue properties. It has been suggested that the peak systolic strain and CVIB are related in normals and in acute ischemia[147-149].

Rijsterborgh et al in their experimental studies into radial CVIB suggested that the most important factor determining local changes in CVIB was radial deformation. This correlated best with changes in unidimensional deformation as measured either by microcrystals or by M-mode echocardiography[150,151].

In another study, Bijnens et al[152] have compared normal changes in radial CVIB with radial two-dimensional strain calculated from an ultrasound radio-frequency data set and found an excellent correlation between the two. They concluded that a major determinant of CVIB would appear to be changes in local two-dimensional strain. This would explain both the transmural inheterogenicity of radial CVIB values across the septum and the posterior wall in normal myocardium and could explain the amplitude and timing changes in normal peak IB levels induced by acute ischemia. If this hypothesis is correct- and the signal processing involved in deriving regional strain values is currently much simpler than measuring CVIB and ultrasound-derived long axis strain values are relatively easy to obtain for long axis deformation for all left ventricle and right ventricle segments- it may be simpler and more robust to measure regional one or two-dimensional strain. However, further experimental and clinical studies are required to verify the correlation between local CVIB and strain over a range of myocardial pathologies.

CHAPTER 4

Objectives of the Original Study

In most cases, the diagnosis of hypertrophic cardiomyopathy (HCM) is based on conventional echocardiographic findings, with asymmetrical septal hypertrophy of the left ventricle (LV) being the most characteristic observation[49,58,77]; by contrast, hypertensive left ventricular hypertrophy (H-LVH) is usually characterized by symmetrical (concentric) hypertrophy of the LV[100]. However, there is substantial overlap in the extents of left ventricular hypertrophy (LVH) and asymmetrical septal hypertrophy between patients with HCM [49,58,77] and those with hypertensive left ventricular hypertrophy[100,104-111].

The development of quantitative echocardiographic techniques, such as strain rate (SR) imaging and integrated backscatter (IB), has enhanced our ability to assess myocardial function non-invasively and their application is therefore very promising to discriminate between different types of pathological LVH.

Previous Tissue Doppler Imaging (TDI) studies demonstrated lower systolic and diastolic mitral annular velocities in HCM compared to H-LVH, with a characteristic heterogeneity of values in the former condition explained with the heterogeneous distribution of tissue abnormalities, while in hypertensive heart disease the cardiac dysfunction appear more uniform, due most likely to the diffuse distribution of histological abnormalities[80-82]. On the other hand, overall wall motion, rotation and contraction of adjacent myocardial segments may influence TD velocities, while deformation parameters appear independent on these factors and therefore superior in studying myocardial abnormalities[15,16,30]. In Kato's study[89], systolic strain and peak early diastolic strain rate

were found to be lower in non obstructive HCM when compared to H-LVH, being a systolic strain value of 10.6% the optimal cut-off for the discrimination between the two conditions; moreover, the combination with the ratio between the septal and the posterior wall thicknesses, increased the predictive accuracy from 91.2 to 96.1% .

We hypothesized that HCM might be characterized by segments unable to deform, heterogeneously distributed in the LV, most likely due to the presence of local, non uniformly distributed, peculiar tissue abnormalities (consistent with myocardial disarray and interstitial fibrosis). In H-LVH, we expected a diffuse mild reduction of deformation, consistent with the fewer tissue alterations characteristic of the hypertensive heart disease. Furthermore, we sought to elucidate whether the phenomenon of post systolic strain could contribute to alter the regional myocardial function in pathological LVH. Moreover, because of the non predictable distribution of HCM tissue abnormalities, we tested the hypothesis that there were no relevant differences between the asymmetric and concentric HCM patterns.

Moreover, for the first time to differ HCM from H-LVH, Cyclic Variation of IB (CVIB) was analysed by the three apical views, which allow the assessment of longitudinal function. In fact, experimental and autopsy data demonstrated that pathological LV hypertrophy is associated with myocardial fibrosis, particularly in the subendocardium[45-47]. It is known that fibers in the subendocardium are aligned longitudinally, from apex to base, and responsible for long-axis dynamics[48]. Consequently, the study of the longitudinal function may be more truthful and exhaustive in explaining and differing between different types of pathological LV hypertrophy. Since it has been previously suggested that Strain and CVIB are related in normals and in acute ischaemia[147-152] but to date no clinical study has been conducted on the correlation between these parameters, we sought to elucidate whether there is a correlation between strain and CVIB in pathological LVH.

CHAPTER 5

Methods

Study group

In total 55 subjects who were referred to Echocardiographic Department of St George's Hospital (London) between May and December 2006 were included into the study. Out of whom 20 had echocardiographic features of HCM and 20 were non-treated, age- and gender-matched hypertensive subjects (HTN). In addition 15 normotensive healthy volunteers (NTN) were enrolled. The diagnosis of HCM was based on conventional echocardiographic demonstration of a non-dilated, hypertrophic LV in the absence of other causes as systemic hypertension or aortic stenosis which could lead to LVH. Furthermore patient with obstructive HCM (increased gradient across LV outflow tract above 30mmHg under resting and/or provocable conditions[49]) were excluded. Hypertensive subjects were recognised basing on office Blood Pressure (BP) measurements. BP was measured using an automatic oscillometric device (Omron HEM 705 CP, Omron Healthcare, UK). Three measurements were taken with the patient in a sitting position after 10 minutes of rest. A mean of three readings obtained at two minutes interval was calculated. Patients were diagnosed with hypertension if their systolic BP was ≥ 140mmHg and/or diastolic BP ≥ 90mmHg on more than three occasions and they were free of causes of secondary hypertension.

All studied patients exhibited normal sinus rhythm and had a normal LV performance as revealed by echocardiography. We excluded patients with diabetes, with coronary or valvular disease as determined by clinical assessment and standard echocardiography.

The study protocol was approved by the local Ethics Committee and an informed consent was obtained from each participant.

Echocardiographic acquisition

2-D Echo Imaging

A complete standard transthoracic ultrasound examination was performed in the left lateral recumbent position. This included the acquisition of complete grey scale imaging data sets and both colour and spectral Doppler flows as well as myocardial velocity data, using a GE Vivid 7 scanner. For each acquisition, three heart cycles were stored for post processing (EchoPac, GE and Speqle, Leuven). End-diastolic (EDD) and end-systolic dimensions (ESD) were assessed from the parasternal long axis view and fraction shortening (FS) was calculated. Moreover, the percent wall thickening of the interventricular septum (IVS) and of the posterior wall of the LV (LVPW) was calculated as (end-systolic wall thickness—end-diastolic wall thickeness)/(end-diastolic wall thickness)x100. Furthermore, we calculated the ratio IVS/LVPW in end-diastole. Among HCM patients, we distinguished between an asymmetric pattern (septal/posterior wall thickness ratio≥1.3 on M-mode) and a concentric one (septal/posterior thickness ratio<1.3). LV wall motion score index (WMSI) was performed by two independent observers in 16 segments (excluding the 17th segment by the 17 segments model[153] because of technical strain artefacts) in random order (1 = normal, 2 = hypokinetic, 3 = akinetic, 4 = dyskinetic, 5 = aneurysmal). All measurements were performed in accordance with the European Society of Echocardiography recommendations[42]. Heart rate was determined from the continuously recorded single channel ECG.

Colour Tissue Velocity Imaging

Doppler myocardial imaging velocity data were recorded using a narrow sector and optimal depth of imaging (frame rates of 200-300 Hz), using apical (long axis motion) views on the manner previously described (Chapter 1). For each acquisition, three complete heart cycles were stored in cineloop format for off-line post processing. To avoid any aliasing within the image and to simultaneously optimize velocity resolution, the pulse repetition frequency (PRF) was set as low as possible, just avoiding aliasing. Three consecutive cardiac cycles were averaged and total longitudinal peak systolic strain (Ssys), together with peak systolic strain rate (SR) were measured. End diastole (onset of isovolumic contraction) and end systole (aortic valve closure) were determined using transmitral and aortic Doppler profiles. For off-line analysis, dedicated software (Speqle, K.U.Leuven) was used to obtain the local velocity traces; LV was divided into 16 segments and the sample volume placed in the central part of the basal, mid and apical segment for each wall by the three apical views. Computational areas of 10 mm with a width of 1 mm (to avoid averaging different ultrasound beams) were used. Strain profiles were calculated by the integration of the Strain Rate over time. Post systolic strain (PSS) was defined if the peak strain existed beyond aortic valve closure (total strain minus systolic strain). The severity of PSS was assessed as post-systolic index [(PSS/whole strain amplitude)x100] (figure 1.16 Chapter 1).

IB Imaging

Integrated backscatter IB data were acquired by three apical views, maintaining constant the control settings of the imaging chain for all patients. The frame rates varied between 80 and 120 frames/s depending on the sector width. IB curves were obtained using an EchoPac workstation (GE). During analysis, the operator carefully adjusted the location of a fixed 9x9 pixel region of interest in the mid-myocardium in each frame to avoid inclusion of the specular reflections of the endocardium or the epicardium. The magnitude of the cyclic variation of IB (CVIB), determined as the difference

between the minimal and the maximal values in a cardiac cycle was measured by apical imaging of all 16 segments and calculated by averaging each segment.

Statistical Analysis

Data were analyzed with SPSS 13.0 (Chicago, SPSS, Inc., Chicago, IL). Results are expressed as mean ± standard deviation. Normality distribution was evaluated by Kolmogorov-Smirnov. Student's t-test, Mann-Whitney test and chi-square test were used as appropriate.

A cut-off point to identify quasi non-deforming segments (ND) was determined by subtracting 3 standard deviations from the mean Ssys from the HTN group. Using this approach we can assume that 99.9% of segments in the HTN group have a value of Ssys above this cut-off point, making the probability that a HTN patient has a segment with such low Ssys less than 0.1%. This also implies that this probability is even less for the NTN group.

Sensitivity (Se), specificity (Sp), positive (PPV) and negative predictive values (NPV) were determined according to standard definitions. Receiver operating characteristics (ROC) curve analysis was performed to test the predictive discrimination of patients with and without HCM. Linear regression analysis was used to find correlation between Ssys and CVIB and between M-mode IVS and LVPW and corresponding Ssys, SR and CVIB in 3 and 4 chamber views.

Intraobserver and interobserver reproducibility were evaluated by linear regression analysis and expressed as correlation of coefficients (r) and standard error of estimates (SEE), and by the intra-class correlation coefficient (ICC). Reproducibility is considered satisfactory if the ICC is between 0.81 and 1.0. A p value of <0.05 was considered to be significant.

CHAPTER 6

Results

Clinical characteristics and echocardiographic findings

The clinical characteristics and echocardiographic findings of all subjects included in the study are presented in Table 6.1. Neither systolic nor diastolic pressure differed significantly between NTN and HCM patients, while both groups had significantly lower blood pressure in comparison to the HTN group ($p<0.0001$ vs NTN or vs HCM). All three groups were age and gender matched.

M-mode LV cavity measurements showed that HCM patients had smaller ventricle (EDD and ESD, $p<0.01$ vs NTN; EDD and ESD, $p<0.05$ vs HTN). Global radial LV systolic function in our cohort of patients assessed by fractional shortening did not differ between the groups.

By contrast, HCM patients had significantly ($p<0.0001$) increased LV septum and posterior wall end-diastolic thicknesses when compared to NTN or to HTN patients. Also HTN group presented more thickened septum and posterior wall comparing to NTN group ($p<0.01$). The HCM patients showed lower IVS% thickening and LVPW% when compared to either NTN or HTN, while HTN presented only reduced IVS% thickening when compared to NTN. Moreover, the ratio IVSd/ LVPWd was significantly higher in HCM than in NTN or HTN but there was no difference between HTN and NTN. In 13/20 HCM patients, asymmetric septal hypertrophy (septal/free wall thickness ratio$\geq$1.3) was present on M-mode, while the other 7/20 patients had a ratio<1.3

(concentric HCM). The WMSI was significantly higher in HCM patients than in NTN or HTN patients ($p<0.0001$).

Table 6.1. Clinical Characteristics and Echocardiography findings of NTN, HTN and HCM patients.

	NTN n=15	**HTN n=20**	**HCM n=20**
Age (years)	52±12	52±8	52±18
Sex women	6	7	7
SBP mmHg	120±12	151±15**	125±10 §
DBP mmHg	76±9	92±11**	79±8 §
Echocardiography M-mode measurements			
LV EDD (cm)	4.7±0.5	4.5±0.7	4.0±0.6†#
LV ESD (cm)	2.7±0.4	2.7±0.5	2.4±0.4†#
FS (%)	41±6	40±6	41±7
IVSd (cm)	1.1±0.1	1.3±0.2**	2.0±0.5‡§
IVSs (cm)	1.5±0.1	1.8±0.2*	2.4±0.4‡§
IVS % thickening	45±5	38±9*	17±12‡§
LVPWd (cm)	1.0±0.2	1.2±0.2**	1.5±0.4‡#
LVPWs (cm)	1.5±0.2	1.8±0.2**	2.0±0.4‡
LVPW % thickening	46±5	45±10	31±14‡##
IVSd/ LVPWd	1.1±0.1	1.0±0.1	1.4±0.5†##
WMSI	1±0	1±0	1.87±0.91‡§

Values are mean ±SD; DBP, diastolic blood pressure; EDD, end-diastolic diameter; ESD, end-systolic diameter; FS, fraction of shortening; HCM, Hypertrophic cardiomyopathy patients; HTN, hypertensive subjects; IVS, interventricular septum; LVPW, left ventricle posterior wall; NTN, normotensive healthy volunteers; SBP, systolic blood pressure; WMSI, wall motion score index.

* P<0.01 when comparing HTN vs NTN;

** P<0.0001 when comparing HTN vs NTN;

† P<0.01 when comparing HCM vs NTN;

††P<0.001 when comparing HCM vs NTN;

‡ P<0.0001 when comparing HCM vs NTN;

# P<0.05 when comparing HCM vs HTN;

##P<0.001 when comparing HCM vs HTN;

§ P<0.0001 when comparing HCM vs HTN.

Strain and Strain Rate Imaging

Longitudinal peak systolic Strain

Table 6.2 presents the average regional longitudinal systolic strain for all three groups. Based on a 16 segments model, longitudinal peak systolic strain (Ssys) was calculated for the base, mid and apical segments in all three apical views. The quality of the acquired data allowed for the analysis of 920 (93%) segments (HCM: 354; HTN:310; NTN:256). HCM patients had globally reduced longitudinal Ssys ($p<0.0001$ vs NTN and HTN) (figure 6.1). This difference, although small, also remained significant between HTN and NTN patients (19.5±4.6 vs 21.0±4.7%; $p<0.05$). HCM had significantly decreased Ssys values in all segments when compared to HTN and NTN group, except for one segment (apical segment of infero-septum, not significant difference versus NTN). In comparison to NTN, our HTN group showed impaired Ssys in basal segments of infero- and antero-septum while all other segments did not differ significantly (figure 6.2).

Although Ssys was significantly lower in HCM compared to the others, there was still a large overlap for the individual patients (figure 6.3).

Figure 6.4 shows the distribution of the deformation of the individual segments. For the whole ventricle, HCM patients had a significantly lower mean Ssys (-10.1%) with greater SD (±7.2%). This significantly higher SD in HCM patients results from the coexistence of segments with significantly impaired deformation and segments with normal contraction.

The cut-off point for separating segments with quasi absent deformation (99.9% of HTN segments above the cut-off) was -5.68%. This cut-off allowed the identification of segments with extreme low deformation, referred to as non-deforming segments (ND). While these ND segments were not present in either the HTN or NTN group, we identified at least 2 of these segments in each

individual HCM patient. The lowest measured value of Ssys for NTN patients was -10.64% and for HTN patients -9.32%. In total we identified 113 ND in HCM patients (32% out of the total HCM analysed segments). The mean value of Ssys in the ND segments was -2.29±2.17% whereas it was -13.80±5.53% in the other HCM segments ($p<0.0001$). The location of the ND segments was distributed over the whole ventricle (Figure 6.5), but they were mostly found in the antero-septum (18.6%) and in the anterior wall (18.6%).

As for PSS, the number of segments with PSS accounted for 72.6% out of total HCM analyzed segments (257/354), 55.5% out of total HTN analyzed segments (172/310) and 33.2% out of total NTN analyzed segments (85/256).

HCM had a significant greater number of segments with PSS when compared to NTN ($p<0.0001$) or HTN ($p<0.0001$). Also HTN showed more PSS segments than in normal subjects ($p<0.0001$), mainly localized at the basal septum (figure 6.2). Moreover, HCM presented grater values of PSS index than in HTN (HCM 23.86±24.59%, HTN 7.71±9.30%, $p<0.0001$) or NTN (NTN 3.99±4.31%, $p<0.0001$). The difference in index PSS remains significant between HTN and NTN ($p=0.003$).

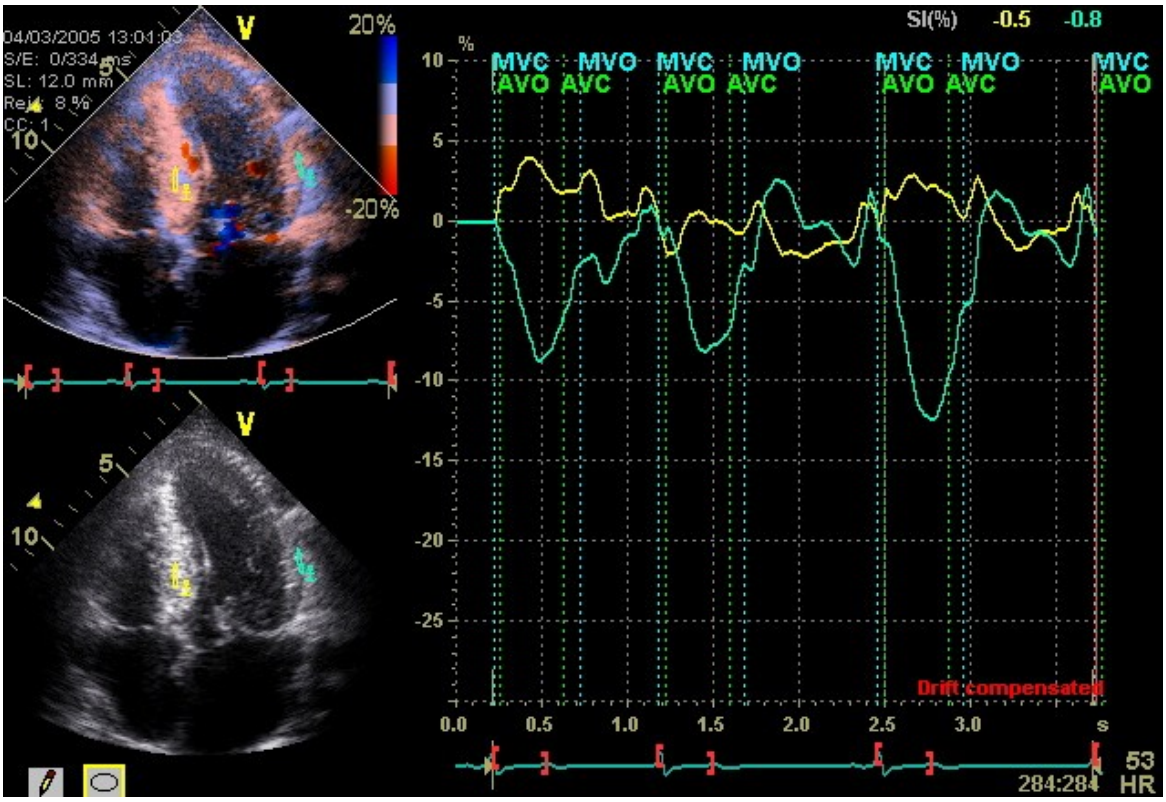

Fig 6.1: Ssys curves from the mid segment of the posterior septum (yellow line) and mid segment of antero-lateral wall (green line) in a HCM patient, showing clearly reduced Ssys values, even reversed at the septum.

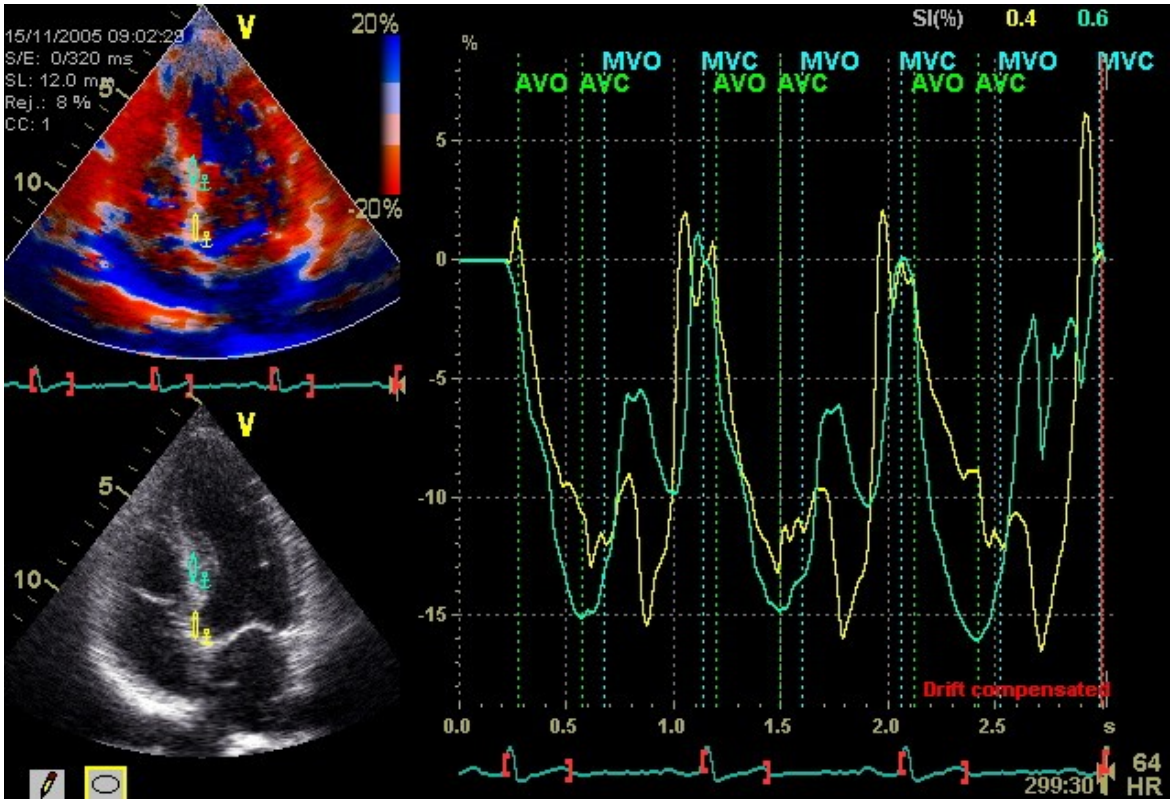

Fig 6.2: Ssys curves from the basal and mid segments of the posterior septum in a HTN patient, showing reduced Ssys with PSS in the basal septum (yellow line) and normal Ssys values (green line) in the mid septum.

Table 6.2. Systolic Strain in NTN, HTN and HCM.

		Ssys, %		
		NTN	**HTN**	**HCM**
Infero-Septum	Basal	-21.1±5.2	-16.2±3.9*	-9.8±6.6‡##
	Mid	-19.3±3.5	-20.6±4.9	-7.4±5.7‡§
	Apex	-17.6±5.1	-20.4±5.5	-12.9±9.3#
Antero-Lateral	Basal	-21.9±5.6	-20.4±4.6	-11.1±6.5‡§
	Mid	-20.9±3.4	-18.9±3.2	-10.8±5.7‡§
	Apex	-16.6±4.4	-14.2±3.1	-9.7±6.5††#
Anterior	Basal	-22.5±5.4	-20.6±4.3	-7.7±5.4‡§
	Mid	-19.8±4.4	-20.6±4.0	-11.6±8.0††§
	Apex	-17.4±5.1	-16.1±5.5	-10.0±6.4††#
Inferior	Basal	-21.3±4.5	-20.5±5.4	-13.0±6.2‡§
	Mid	-22.0±4.1	-19.4±3.4	-8.8±7.1‡§
	Apex	-21.4±5.9	-18.7±4.5	-9.4±7.2‡§
Antero-Septum	Basal	-20.9±3.5	-14.9±4.2***	-5.8±5.7‡§
	Mid	-21.9±3.3	-21.1±4.1	-10.8±9.4‡§
	Apex	-22.4±4.4	-21.6±3.4	-13.1±8.5††§
Infero-Lateral	Basal	-24.5±3.4	-22.4±3.1	-12.2±7.9‡§
	Mid	-23.7±3.6	-21.1±3.9	-9.6±6.3‡§
	Apex	-20.8±3.2	-20.9±3.0	-8.3±6.6‡§
	Global	-21.0±4.7	-19.5±4.6*	-10.1±7.2‡§

Values are mean±SD.

* P<0.05 when comparing HTN vs NTN.

** P≤0.001 when comparing HTN vs NTN

*** P<0.0001 when comparing HTN vs NTN.

† P<0.05 when comparing HCM vs NTN.

††P≤0.001 when comparing HCM vs NTN.

‡ P<0.0001 when comparing HCM vs NTN.

# P<0.05 when comparing HCM vs HTN.

##P≤0.001 when comparing HCM vs HTN.

§ P<0.0001 when comparing HCM vs HTN.

Fig 6.3: Longitudinal peak Systolic Strain of all segments included in the analysis of normotensive (NTN), hypertensive (HTN) and HCM patients.

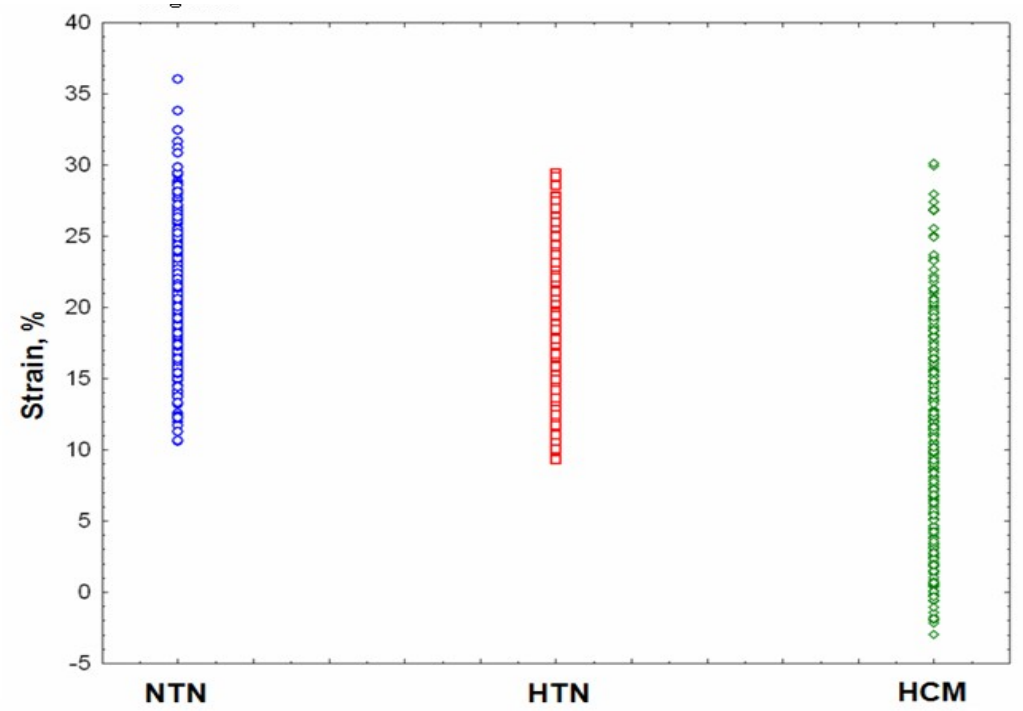

Fig 6.4: The distribution of Strain values in NTN (control group), HTN (hypertensive group) and HCM (hypertrophic cardiomyopathy group).

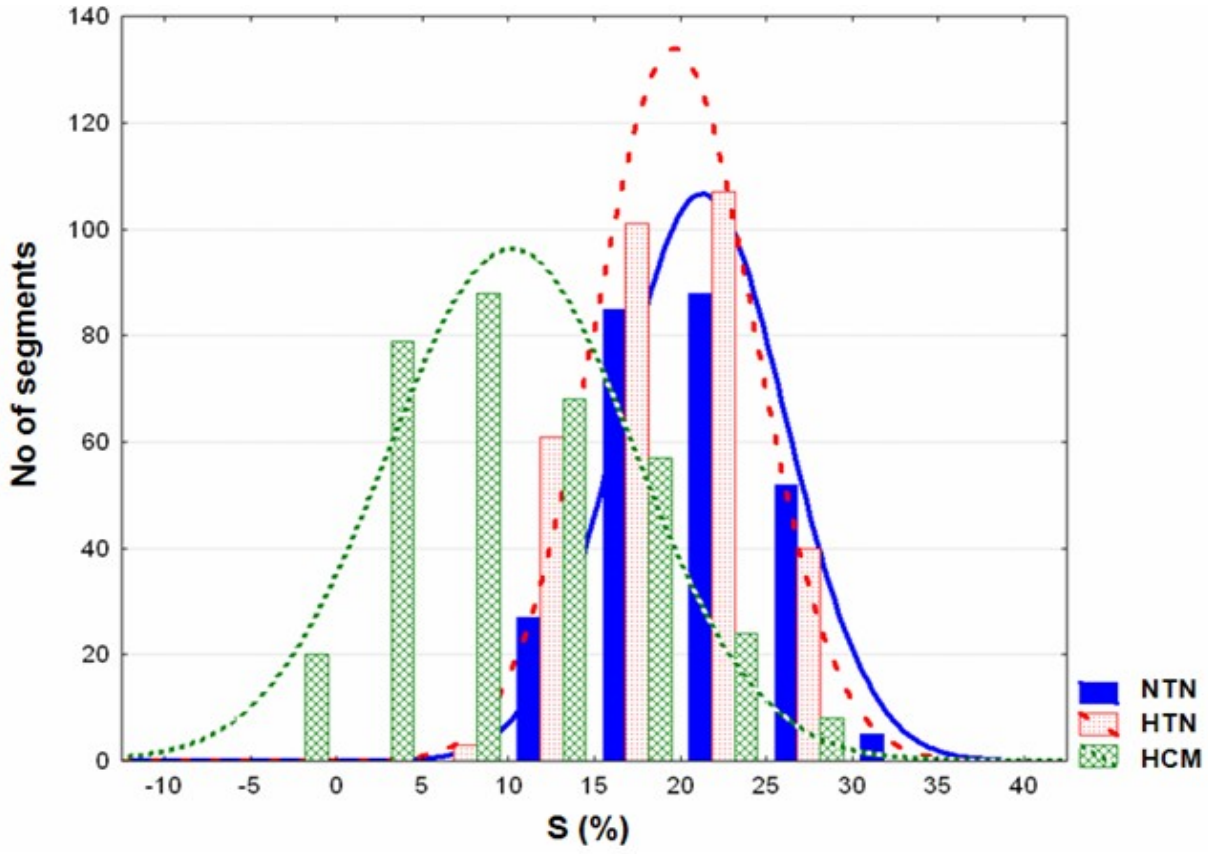

Fig 6.5. The location of non-deforming segments (ND) in the HCM group of patients.

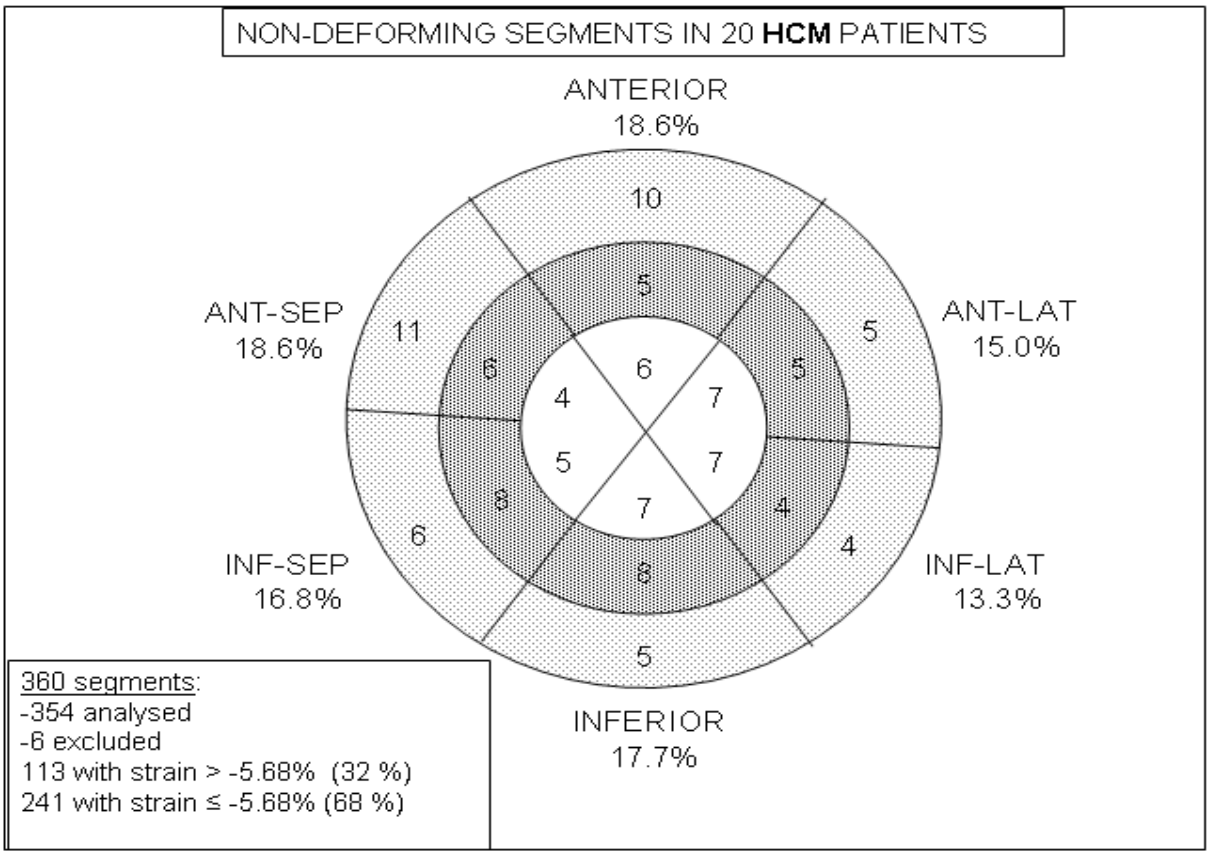

Longitudinal peak systolic Strain Rate

Regional longitudinal SR deformation for all three groups is shown in Table 6.3. Global longitudinal peak systolic SR values were significantly lower in HCM group compared to other groups. Also, SR values from each individual segment were significantly lower in HCM when compared to HTN or NTN group. Global peak systolic SR in HTN patients was slightly but significantly lower than in NTN subjects (-1.6±0.4 vs -1.7±0.4 s^{-1}). Similarly to strain findings, we observed a statistically significant reduction in longitudinal systolic SR in basal segments of infero- and antero-septum in HTN compared to NTN patients.

Table 6.3: Systolic Strain Rate in NTN, HTN and HCM.

		SR, s^{-1}		
		NTN	**HTN**	**HCM**
Infero-Septum	Basal	-1.8±0.4	-1.4±0.3**	-1.0±0.6‡#
	Mid	-1.6±0.5	-1.4±0.4	-0.8±0.5‡§
	Apex	-1.4±0.5	-1.5±0.4	-1.0±0.5†#
Antero-Lateral	Basal	-2.0±0.5	-1-8±0.4	-1.2±0.6‡§
	Mid	-1.8±0.4	-1.7±0.4	-1.0±0.4‡§
	Apex	-1.7±0.5	-1.6±0.4	-1.0±0.5‡##
Anterior	Basal	-1.8±0.5	-1.8±0.4	-1.0±0.4‡§
	Mid	-1.7±0.6	-1.6±0.4	-1.2±0.5†#
	Apex	-1.7±0.5	-1.4±0.3	-0.9±0.6††#
Inferior	Basal	-1.7±0.5	-1.5±0.4	-1.0±0.5‡##
	Mid	-1.7±0.4	-1.4±0.4	-0.9±0.6‡#
	Apex	-1.6±0.4	-1.5±0.3	-1.0±0.6††#
Antero-Septum	Basal	-1.8±0.4	-1.5±0.3*	-0.8±0.6‡§
	Mid	-1.8±0.3	-1.6±0.4	-1.0±0.6‡§
	Apex	-1.6±0.5	-1.6±0.4	-1.1±0.6†#
Infero-Lateral	Basal	-2.0±0.4	-2.0±0.3	-1.1±0.7‡§
	Mid	-1.9±0.4	-1.8±0.4	-0.9±0.6‡§
	Apex	-1.8±0.4	-1.8±0.3	-0.9±0.6‡§
	Global	-1.7±0.4	-1.6±0.4*	-1.0±0.6‡§

Values are mean ±SD; HCM, Hypertrophic cardiomyopathy patients; HTN, hypertensive subjects; NTN, normotensive healthy volunteers; SR, peak systolic strain rate.

P values as in table 2

Cyclic Variation of Integrated Backscatter

CVIB in NTN, HTN and HCM patients are presented in Table 6.4. The quality of the acquired data allowed for the analysis of 938 (95%) segments (HCM: 343; HTN; 355; NTN: 240). The mean values of CVIB in HCM patients were significantly reduced compared to other groups (5.6±2.7 dB vs 8.7±3.1 dB in HTN, p<0.0001; and vs 9.7±3.4 dB in NTN, p<0.0001) (figure 6.6). HCM showed significantly reduced CVIB in all individual segments when compared to both NTN and HTN. In HTN, a significantly lower magnitude of CVIB was observed in the basal LV septum compared to healthy volunteers (7.2±2.1 vs 9.5±1.4 dB in infero-septum, p<0.001; 8.9±2.6 vs 12.0±4.1 dB in antero-septum, p<0.05) (figure 6.7). The remaining segments did not differ significantly between NTN and HTN study groups.

Fig 6.6: CVIB curves from mid segment of posterior septum (yellow line) and mid segment of antero-lateral wall (green line) in a HCM patient, showing reduced CVIB values above all at the septum.

Fig 6.7: CVIB curves from mid (green line) and basal (yellow line) segments of the posterior septum of a HTN patient, showing more reduced CVIB values at the basal septum.

Table 6.4. Cyclic variation of integrated backscatter in NTN, HTN and HCM.

		Cyclic Variation, dB		
		NTN	**HTN**	**HCM**
Infero-Septum	Basal	9.5±1.4	7.2±2.1**	6.6±2.7††
	Mid	10.0±3.7	10.1±2.3	6.2±2.3†§
	Apex	9.3±3.3	8.4±2.9	5.4±2.6††#
Antero-Lateral	Basal	9.7±2.9	9.2±3.2	6.4±2.6†#
	Mid	10.2±3.3	8.4±2.2	6.3±1.9††#
	Apex	6.5±1.8	6.1±2.1	4.1±2.1†#
Anterior	Basal	10.1±3.4	9.4±3.2	6.0±2.8††##
	Mid	8.5±3.4	7.0±2.3	4.6±2.2††#
	Apex	7.9±4.6	5.7±2.3	4.0±2.1†#
Inferior	Basal	11.2±3.0	11.1±3.8	5.5±2.8‡§
	Mid	9.7±2.9	9.7±2.7	4.8±2.5‡§
	Apex	10.3±4.8	9.3±3.5	5.3±2.5‡§
Antero-Septum	Basal	12.0±4.1	8.9±2.6*	6.3±3.5‡#
	Mid	9.6±2.6	10.5±2.9	5.8±3.2††§
	Apex	8.7±2.6	7.3±2.1	5.4±2.9†#
Infero-Lateral	Basal	10.3±3.6	10.6±2.8	6.7±2.9††§
	Mid	10.6±2.8	9.1±2.5	6.2±2.6‡##
	Apex	8.4±2.5	7.8±2.9	4.3±1.9‡§
	Global	9.7±3.4	8.7±3.1*	5.6±2.7‡§

Values are mean ±SD; CVIB, cyclic variation of integrated backscatter; HCM, Hypertrophic cardiomyopathy patients; HTN, hypertensive subjects; NTN, normotensive healthy volunteers.

P values as in table 2

Discrimination of HCM from HTN patients

The presence of at least 1 non-deforming segment (with Ssys>-5.68%) in the whole ventricle discriminated HCM from HTN and NTN with a sensitivity of 100% and a specificity of 100%.

When not searching for non-deforming regions, but using the value of global average deformation, ROC analysis for discrimination between HCM and HTN showed the optimal cut-off value for global Ssys to be -16.9% (sensitivity 100%, specificity 95%); for systolic SR -1.32 s^{-1} (sensitivity 95%, specificity 100%) and for CVIB 7.4 dB (sensitivity 90%, specificity 85%). Using global Ssys, the NPV was 100%, the PPV 95% (OR=20, $p<0.0001$) and the accuracy 97%.

Relationship between Strain and CVIB

Figure 6.8 shows the relationship between Ssys and CVIB for all individual segments. Both CVIB and Ssys were significantly lower in HCM compared to other groups, although there was a marked overlap. A linear regression analysis revealed a significant correlation between Ssys and CVIB ($R=0.54$, $p<0.0001$).

Figure 6.9 shows examples of Ssys and CVIB traces from a HCM patient, indicating that the regional deformation is quasi absent in the septum whereas it is almost normal in the antero-lateral wall. CVIB and strain clearly follow a similar pattern.

Fig 6.8. Relationship between peak systolic strain and cyclic variation of integrated backscatter for all individual segments. NTN – control group; HTN – hypertensive group; ND-HCM- non-deforming segments of hypertrophic cardiomyopathy group with strain ≥-5.68%; HCM – remaining segments of HCM patients.

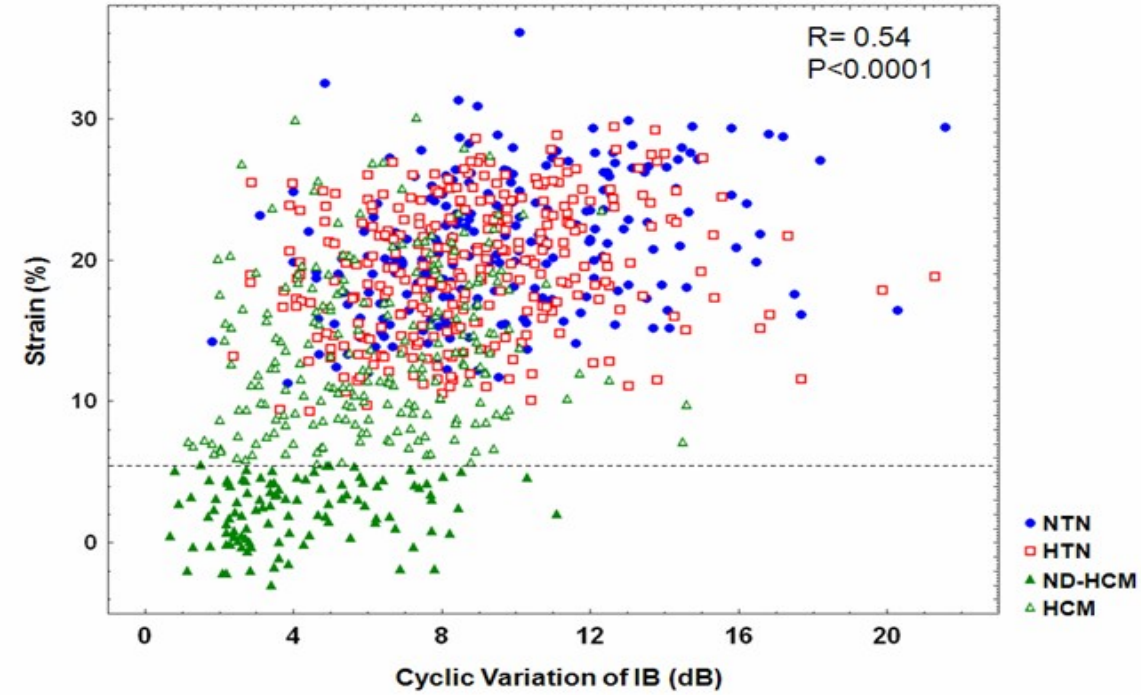

Fig 6.9. Example of strain (right upper graph) and CVIB curves (bottom right) of the mid segments of infero-septum and antero-lateral wall from the 4 chamber view in a HCM patient.

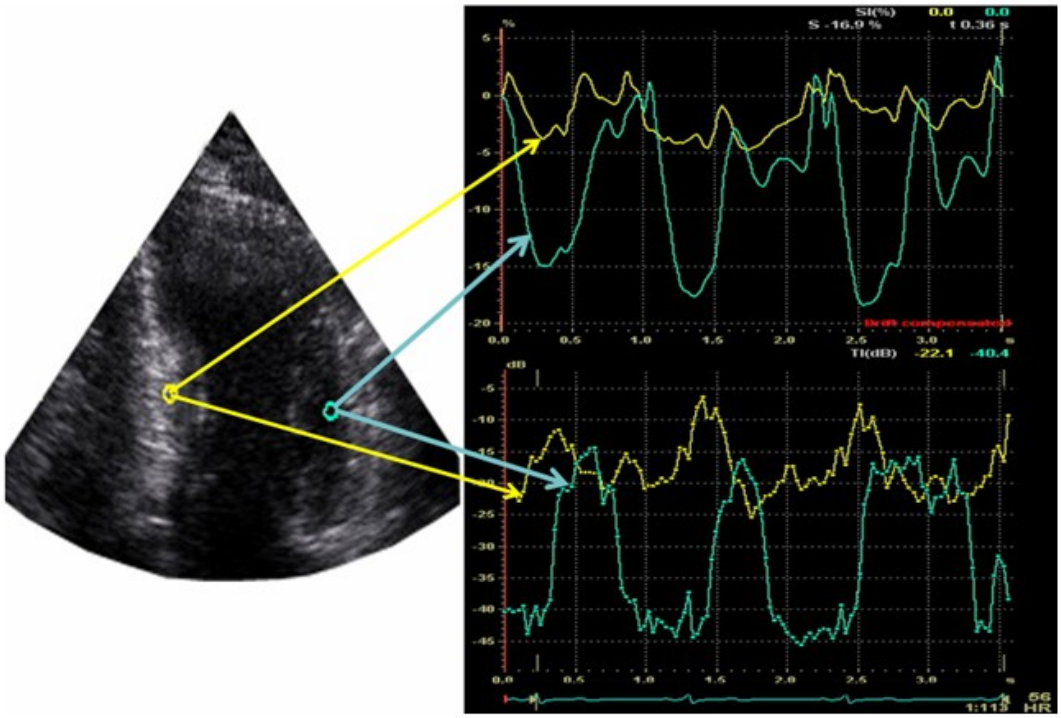

SR imaging and reflectivity in asymmetric and concentric HCM

Segmental comparison of Ssys between concentric and asymmetric HCM showed only a significant difference in the basal antero-septum (3-chamber view), with lower value in the concentric group (respectively -2.1% vs -7.6 %, *p* 0.21). SR was only significantly lower in the basal infero-septum (4-chamber view) in the concentric group (respectively -0.56 s^{-1} vs -1.20 s^{-1} , *p* 0.008). With regard to CVIB, there was no significant difference between asymmetric and concentric HCM patients. Furthermore, Ssys, SR and CVIB of the mid- and basal segments of the septum and lateral wall from 3 and 4 chamber views did not correlated with M-mode IVS and PW thicknesses (linear regression analysis).

Intraobserver and interobserver reproducibility

Intraobserver reproducibility was *r*=0.96, SEE=0.12; intraclass correlation coefficient was 0.986. Interobserver reproducibility was *r*=0.94, SEE=0.16; intraclass correlation coefficient was 0.966.

CHAPTER 7

Discussion

Strain to differentiate HCM from H-LVH

In this study, we have demonstrated that the detection of non-deforming regions, using ultrasonic strain (-rate) imaging allows for the easy and accurate discrimination between patients with hypertrophic cardiomyopathy and left ventricle hypertrophy due to hypertension.

As previously seen[85,86,89-93], we confirmed that HCM is associated with reduced overall and regional deformation when compared to HTN or NTN and we found that Ssys was the most sensitive and accurate index of differentiation between pathological H-LVH. Nevertheless, there was still a large overlap in the average values for the myocardial segments between individual patients. However, based on the assumption that HCM is intrinsically associated with heterogeneity in the location of pathological tissue segments[59-61,63,64], we hypothesised and confirmed that the presence (regardless of the location) of segments with quasi absent deformation is very specific and sensitive for HCM. Using the proposed cut-off point, we were able to identify at least two ND-segments in each HCM patient (mostly found in the anterior septum and in the anterior wall) whereas none of the segments in normal or hypertensive patients shows this absent deformation (although deformation can clearly be reduced).

The first studies demonstrating an impairment of systolic and diastolic functions in HCM were based on TDI velocities[79-84,94,95]. Some of these studies pointed out the heterogeneity of function in

HCM[80,81]; some others found impaired longitudinal systolic and diastolic parameters even in non hypertrophied segments in evident HCM[94,95] or in HCM mutations' carriers without macroscopic expression of the disease[97,98].

Afterwards, deformation studies based on Ultrasound Tissue Doppler[85,86,89,90] or speckle tracking[91] confirmed the idea that despite apparently normal left ventricular systolic function, all components of strain are significantly reduced in HCM when compared to normal subjects.

Kato et al.[11] demonstrated that Ssys and the IVST/PWT ratio are independent predictors for the discrimination of biopsy-proven HCM patients from H-LVH patients. ROC analysis identified the optimal cut-off value of Ssys for discrimination between HCM and H-LVH as -10.6%; this value was associated with a sensitivity, specificity, and predictive accuracy of 85.0, 100, and 91.2%, respectively. The combination of the IVST/PWT ratio and Ssys was able to discriminate HCM from H-LVH with a predictive accuracy of 96.1%. In this study, we find a corresponding value of -16.9% based on ROC analysis.

Some studies highlighted the presence of deformation abnormalities not only in hypertrophied but also in non-hypertrophied segments in HCM patients, although this is more evident in hypertrophied segments and to a higher extent in the interventricular septum[92,93], consistently with previous histological findings of heterogeneous alterations not correlated to the degree of LV hypertrophy[59-61,63,64]. Also in our study, ND segments were heterogeneously distributed into LV, even they were mostly found in the antero-septum (18.6%) and in the anterior wall (18.6%).

Even RMN studies confirmed the heterogeneity of function in HCM[96,154]. Using cardiac diffusion RMN, Tseng et al[62] were able to map myocardial disarray in vivo and to correlated it to both passive and active myocardial function. Kim et al[67] showed that there is a clear relationship between the presence of regional fibrosis, as detected with MRI delayed enhancement imaging and decreased regional (circumferential) strain. They also showed that the distribution of these regions is non-uniform throughout the ventricle.

Consistently with all these considerations, we could not find any differences in deformation or reflectivity between asymmetric or concentric HCM patterns. In fact, the segmental comparison showed just few and inconsistent differences and at Pearson correlation Ssys, SR and CVIB of the mid- and basal segments of the septum and lateral wall did not correlated with M-mode IVS and PW thicknesses. Indeed, the segmental performance does not correlate with the wall thickness but probably relates to tissue alterations (myofiber disarray and interstitial fibrosis), which are independent on the degree of hypertrophy.

Our findings confirm the previous studies in that deformation is abnormal in HCM and extends the knowledge about heterogeneity of the diseased segments by explicitly using the fact that abnormal regional histology is associated with the virtual absence of deformation, regardless of the presence of local hypertrophy and even if global systolic LV function appears normal.

The presence of any ND-segments is thus a very sensitive and specific characteristic of HCM which can be very easily identified using deformation imaging.

Strain in hypertensive heart disease

As for hypertensive patients, the finding of a reduced overall LV performance is consistent with previous studies. First studies demonstrating an impairment of diastolic and systolic functions were based on TDI velocities[80,112,113]. Vinereanu et al[80] demonstrated that systolic and early diastolic mitral annular velocities in hypertensive patients were significantly lower than in normal subjects; in the same study, systolic and diastolic velocities were found to be similarly reduced in HCM and hypertensive LVH, but in HCM the heterogeneity of annular systolic velocities was more, suggesting localized or patchy subendocardial dysfunction in the former condition and a diffuse subendocardial dysfunction in the latter one. In an experimental study (in rats), Derumeaux and collegues showed that the myocardial velocity gradient, i.e. the difference in velocities between the subendocardial and the subepicardial parts of LV wall, in systole is reduced in pressure-induced hypertrophy compared with control animals with physiological hypertrophy[112]. The ratio early-to-late diastolic gradients was also decreased. Reduced subendocardial function in pathological hypertrophy correlated with the degree of subendocardial interstitial fibrosis. This is consistent with previous histological findings regarding the presence of diffuse subendocardial fibrosis in pressure overload hypertrophy[45-47,64], affecting more longitudinal function considering that in the subendocardium fibers are mostly aligned longitudinally[48].

Also strain-based studies confirmed the idea of reduced diastolic and systolic functions when comparing hypertensive patients to normal subjects or athletes[89,114-116]. In particular, in the early stages of hypertension regional longitudinal peak systolic SR and peak systolic strain were found to be significantly reduced in the basal septum, where the hypertensive remodelling provoked a more prominent hypertrophy[117]. Other studies confirmed the quite common eccentric pattern of myocardial hypertrophy in hypertensive heart disease[104-106], having the isolated septal hypertrophy

been recognised as an early and frequent structural adaptation in hypertension. Hypertrophy could appear earlier and progress faster at the septal level than at the level of the posterior wall because of its larger bending radius compared with the posterior wall, leading to a greater tension during contraction wall, or owing to the addition of the right ventricular afterload or due to the septal over-reactivity to catecholamines[107-111].

Analysing the regional function, we confirmed that abnormal deformation is present in the basal septum, even if our hypertensive patients showed mildly hypertrophied septum and posterior wall. Probably this was the effect of the previously mentioned hemodynamic and humoral factors on basal septum, affecting in our cohort more the function than the geometry of hypertensive LVH. Probably, deformation parameters could be a more sensitive indicator of septal dysfunction than geometric pattern, but more studies are needed about this issue.

Nevertheless, while decreased deformation was diffuse, above all located in the basal septum, deformation was never as low as showing almost absence of deformation, as observed in HCM.

Post Systolic Strain

Post-systolic strain (PSS) is defined as myocardial deformation (shortening for longitudinal and lengthening for radial function) after the aortic valve closure. Despite much experimental work, the mechanism underlying PSS remain unclear. It might be a result of delayed active contraction after reduction of regional wall stress and relaxation of other adjacent LV segments, or delayed passive inward movement caused by adjacent normal contracting LV segments as the LV pressure rapidly decreases and the regional wall stress decreases. Whether PSS represent an active, passive or mixed process is still under investigation[155].

PSS has been more investigated in ischemic heart disease. Acute ischemia induces both maximal systolic thickening decrease and an abnormal thickening of the myocardium after aortic valve closure[156] (figure 7.1).

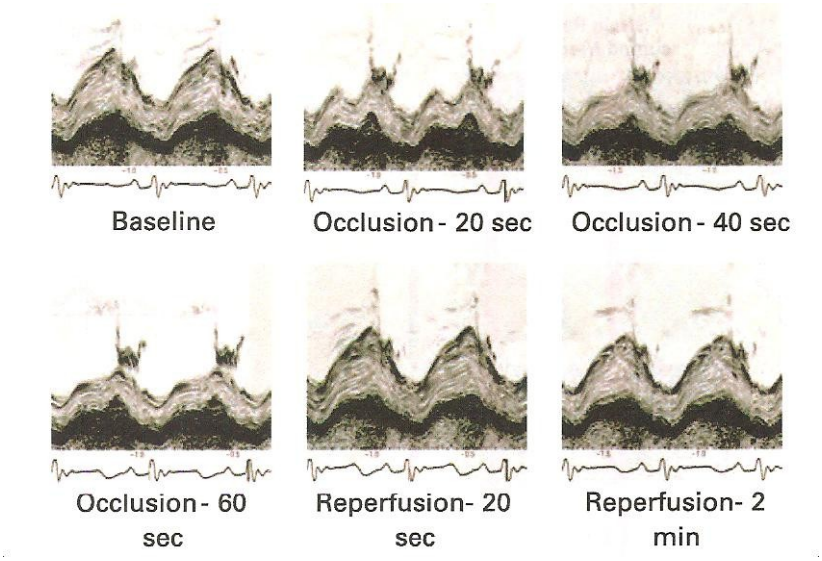

Fig 7.1: Typical M-mode images of changes in deformation induced during a short-lived experimental 60-second circumflex occlusion and response after 2 minutes of reperfusion. Such changes have also been shown to be consistent pattern in acute flow reduction/occlusion studies for patients undergoing percutaneous coronary angioplasty (from 156, Jamal F et al. 2001).

Stunned myocardium (i.e. post-ischemic myocardium with flow reserve) has an abnormal deformation pattern at rest that is similar to that of ischemic myocardium (i.e. myocardium with inadequate flow reserve). However during a low-dose (10-15 mcg/kg/min) dobutamine challenge, the response of stunned versus ischemic myocardium was completely different[157]. A "stunning" response is characterized by normalization of peak systolic strain rate and strain with an associate progressive decrease in PSS, whereas an ischemic response is characterized by a dose-dependent increase in PSS associated with either a reduction or no change in systolic strain rate or strain.

Preliminary clinical data suggest that the presence of PSS in the setting of coronary ischemia could predict functional recovery during and after recovery from ischemia[158].

Moreover, the differentiation of a transmural infarction from a nontransmural one can also be achieved by combining a baseline study with a low-dose dobutamine challenge; in the former condition there is no measurable systolic deformation or the presence of abnormal thinning/lengthening at rest with no inducible increase in thickening/shortening during test. Instead, during a low-dose dobutamine challenge, a partial-thickness infarct will exhibit an ischemic response, i.e. an increase in PSS associated with a reduction or no change in systolic strain[159].

A first index PSS, expressed as the ratio between PSS and the peak systolic strain, was first proposed by Kukulski et al[160] , but it has an important limitation when studying akinetic segments, with very low systolic strain. Voigt et al[161] have demonstrated that the ratio of PSS to regional maximal systolic strain has better specificity in addition to high sensitivity in defining dobutamine stress-induced ischemia with a cut-off of 35%.

However, small amplitudes of PSS are sometimes present in normal human myocardium[162] and it is clearly influenced by afterload and preload. Even in Voigt's study, PSS of small amplitude was found in two-fifths of all segments at baseline as well as non-ischemic segments. Effectively, we found in normal subjects that 33.2% out of total NTN analyzed segments had PSS of small amplitude (PSS index NTN 3.99±4.31%).

Moreover, PSS has been reported to occur in other clinical settings e.g. in left bundle branch block[163], syndrome x[164], aortic stenosis[165] and hypertrophic cardiomyopathy[87]. In fact, patients with HCM were found to have a greater number of segments with PSS, with a higher PSS index (calculated as the ratio of PSS to the maximum strain) when compared to normal subjects[87]. Another study[88] found a correlation between a strain pattern of double peak sign (the first in systole, the second in diastole, such as PSS) in pathological HLV and regional fibrosis detected by DE at MRI. We confirmed that in HCM there are many segments with PSS (72.6%), whose amplitude was remarkable (PSS index 23.86±24.59%). This might be due to typical LV asynchrony in HCM or to the presence of ischemic myocardium, already well documented in HCM[68-70]. Larger clinical trials are needed for defining its significance in HCM, nevertheless it is plausible that PSS may have etiologic contribution to systolic and diastolic dysfunctions.

Furthermore, since the main factors influencing regional myocardial deformation are intrinsic contractility, cavity pressure, segment interaction and tissue elasticity, it is comprehensible that PSS can occur also in the case of an increased afterload such as in hypertension. In fact, PSS will be present in all cases where there is an imbalance, at the moment the left ventricular pressure drops (i.e. at aortic valve closure), between deformation of contiguous segments, regardless whether this imbalance is caused by reduced contractility due to ischemia, due to high regional wall stress in some segments (mainly basal septum for larger bending radius and in the presence of increased afterload) or due to regionally delayed contraction[16]. It is a fact that we found more segments with PSS and with a higher PSS index in HTN patients than in normal subjects. Moreover, they were more localized at basal septum (where systolic strain resulted more impaired), demonstrating the higher wall stress at this level in systemic hypertension.

CVIB to differentiate HCM from H-LVH

We showed that regional longitudinal reflectivity (CVIB) can be used to discriminate HCM from H-LVH, with a magnitude of CVIB significantly smaller in patients with HCM compared to HTN and NTN (optimal cut-off value of 7.4 dB (sensitivity 90%, specificity 85%). Additionally, HTN had significantly lower global CVIB and regional basal septum CVIB when compared to NTN.

It has been shown that the CVIB is affected by regional myocardial performance[132, 133], myocardial ischaemia[134-136], orientation of the myocardial fibers and structural changes of the myocardium [137-139], although the exact mechanisms responsible for CVIB are still unclear. Previous studies on IB values in hypertensive patients showed a significant reduction of global CVIB when compared to normal subjects, related to LV mass and geometry[140, 141], on an abnormal LV filling[114, 142] or on humoral circulating factors (e.g. serum concentration of the carboxy-terminal propeptide of procollagen type I[143] or circulating aldosterone and immunoreactive endothelin[144]).

We confirm that the mean CVIB in hypertensive patients differs significantly from the ones in normal subjects. On the other hand, we found that hypertensive patients have lower CVIB in the basal septum, confirming the relation of regional reflectivity and deformation and the increased wall stress at this level.

In HCM, the degree of myocardial disarray, interstitial fibrosis and the nonhomogeneity of myocyte size showed positive correlations with calibrated IB and negative correlations with CVIB [145]. Another study showed reduced CVIB in HCM carriers even in the absence of wall hypertrophy but at the time of appearance of ECG abnormalities[146].

A first study[138] tried to differentiate HCM from hypertensive heart disease and controls using parasternal CVIB, founding that there were any differences at the posterior wall level, while CVIB at the septum were significantly reduced in pathological left ventricular hypertrophy, but without differing the two pathological conditions.

Naito et al. [137] tried to differentiate HCM from H-LVH on the basis of IB and the only difference was the greater transmural gradient of calibrated IB in patients with HCM than in normal subjects and in patients with H-LVH, in both the septum and posterior wall. Other attempts to distinguish HCM from H-LVH by IB measures showed just that the CVIB values in the subendocardium of the posterior wall of patients with H-LVH were reduced but not in patients with HCM[140]. Nevertheless, no studies were previously performed on IB values by the apical views to differentiate the various conditions of pathological myocardial hypertrophy, although many findings suggest that longitudinal function may be more affected than radial function[45-48,64].

Relationship between strain and CVIB

We also confirm that there is a significant correlation between strain and CVIB in pathological LVH. In fact, both Ssys and CVIB were significantly lower in HCM compared to both HTN and NTN, additionally in HTN they were reduced mildly but significantly as global value and both at the basal septum at the segmental comparison. A linear regression analysis revealed a significant correlation between Ssys and CVIB ($R=0.54$, $P<0.0001$).

It has been suggested that the peak systolic strain and CVIB are related in normals and in acute ischemia[147-149]. Rijsterborgh et al in their experimental studies into radial CVIB suggested that the most important factor determining local changes in CVIB was radial deformation. This correlated best with changes in unidimensional deformation as measured either by microcrystals or by M-mode echocardiography[150,151]. Bijnens et al[152] have compared normal changes in radial CVIB with radial two-dimensional strain calculated from an ultrasound radio-frequency data set and found an excellent correlation between the two. They concluded that a major determinant of CVIB would appear to be changes in local two-dimensional strain. If this is effectively the case, they conclude that may be simpler and more robust to measure regional one or two-dimensional strain, considering the difficult and time-consuming CVIB measurement. However, our study contributed to better understand the significance of CVIB, seeming to represent the regional myocardial performance, particularly impaired longitudinally in pathological left ventricular hypertrophy.

Clinical Implications

In most cases, the diagnosis of HCM is based on conventional echocardiographic findings; however, there is substantial overlap in the extents of LVH and asymmetrical septal hypertrophy between patients with HCM and those with H-LVH. Moreover, LVH results from multiple factors and about the 20% of HCM patients have hypertension. It is therefore clear that additional, quantitative techniques such as SR and IB imaging, might contribute to the ability to discriminate between different types of pathological LV hypertrophy.

In particular, the novel finding of the specific presence of non-deforming myocardial segments in HCM provides an easy and fast way to aid the diagnosis and differentiation of HCM from H-LVH. A correct diagnosis can lead to the most appropriate therapeutic options. Moreover, Ssys and CVIB may be useful clinical parameters for the follow-up of therapeutic effectiveness.

Study limitations

The diagnosis of HCM was based on conventional echocardiographic demonstration of a non-dilated hypertrophic LV in the absence of other cardiac or systemic diseases that might lead to LVH, but it was not confirmed by histology or genetics. Furthermore, we excluded patients with a history of coronary heart disease, but we did not confirm the absence of coronary heart disease by angiography.

Conclusions

In conclusion, deformation and reflectivity analysis are powerful non-invasive methods to easily discriminate patients with HCM from those with H-LVH. Besides overall reduced values, the presence of at least one non-deforming segment, irrespective of its location throughout the ventricle, is an effective and specific diagnostic finding for HCM. Probably they depend on the non predictable distribution of HCM peculiar tissue abnormalities throughout the left ventricle, which are independent on the degree of hypertrophy and therefore without making differences in performance between asymmetric and concentric HCM patterns. Furthermore, PSS contributes to cardiac impairment in HCM and hypertensive LVH. In this latter condition, the decrease of strain and the phenomenon of PSS are mainly present at the basal septum, indicating the greatest wall stress at this level in pressure overloaded LV.

Additionally, we found that deformation (Ssys) and reflectivity (CVIB) are significantly correlated in pathological left ventricular hypertrophy and in normal hearts and therefore they both seem to represent aspects of regional myocardial performance.

References

1. Satomura S. Ultrasonic doppler method for the inspection of cardiac functions. *J Acoust Soc Am* 1957;29:1181-1185.
2. Wells PNT. A range gated ultrasonic Doppler system. *Med Biol Eng* 1969;7:641-652.
3. Baker DW. Pulsed ultrasonic Doppler blood-flow sensing. *IEEE Trans Son Ultrason* 1970;SU-17:170-185.
4. Omoto R, Wokote Y, Takanoto, et al. The development of real-time two dimensional echocardiography and its clinical significance in acquired valvular diseases with special reference to the evaluation of valvular regurgitation. *Jap Heart J* 1984;25:325-340.
5. Isaaz K,Thompson A, Ethevenot G, et al. Doppler echocardiographic measurement of low velocity motion of the left ventricular posterior wall. *Am J Cardiol* 1989;64:66-75.
6. McDicken WM, Sutherland GR, Moran CM and Gordon LN. Colour Doppler velocity imaging of the myocardium. *Ultrasound Med Biol* 1992;18:651-654.
7. Sutherland GR, Stewart MJ, Groundstroem WE, Moran CM, Fleming A, Guell-Peris FJ, Riemersma RA, Fenn LN, Fox KAA and McDicken WN. Colour Doppler myocardial imaging: a new technique for the assessment of myocardial function. *J Am Soc Echocardiogr* 1994; 7:441-458.
8. Garcia MJ, Rodriguez L, Ares M, Griffin BP, Thomas JD, Klein AL. Differentiation of constrictive pericarditis from restrictive cardiomyopathy: assessment of left ventricular diastolic velocities in longitudinal axis by Doppler tissue imaging. *J Am Coll Cardiol* 1996;27:108-114.
9. Kats WE, Gulati VK, Mahler CM, Gorcsan J, III. Quantitative evaluation of the segmental left ventricular response to dobutamine stress by tissue Doppler echocardiography. *Am J Cardiol* 1997;79:1036-1042.

10. Severino S, Caso P, Galderisi M, De Simone L, Petrocelli A, De Divitiis O, Mininni N. Use of pulsed doppler tissue imaging to assess regional left ventricular diastolic dysfunction in hypertrophic cardiomyopathy. *Am J Cardiol* 1998;82:1394-1398.
11. Mankad S, Murali S, Kormos RL, Mandarino WA, Gorcsan J, III. Evaluation of the potential role of color-coded tissue Doppler echocardiography in the detection of allograft rejection in heart transplant recipients. *Am Heart J* 1999; 138:721-730.
12. Pasquet A, Armostrong G, Beachler MS, Lauer L, Marwick TH. Use of segmental tissue Doppler velocity to quantitate exercise echocardiography. *J Am Soc Echocardiogr* 1999;12:901-912.
13. Jamal F, Derumeaux G, Douillet R, Roussel C, Cribier A. Analyse et quantification de la contraction longitudinale ventriculaire gauche dans l'infarctus du myocarde: apport du Doppler tissuelaire myocardique. *Arch Maladies Coeur Vaisseaux* 1999;92:315-322.
14. Tsutsui H, Uematsu M, Shimizu H, Yamagishi M, Tanaka N, Matsuda H, Miyatake K. Comparative usefulness of myocardial velocity gradient in detecting ischemic myocardium by a dobutamine challenge. *J Am Coll Cardiol* 1998; 31:89-93.
15. D'hooge J, Heimdal A, Jamal F,Kukulski T, Bijnens B, Rademarkers F, Hatle L, Suetens P and Sutherland GR. Regional strain and strain rate measurement by cardiac ultrasound: principles, implementation and limitations. *Eur J Echocardiogr* 2000; 1:154-170.
16. Sutherland GR, Hatle L, Claus P, D'hooge J, Bijnens B. Doppler Myocardial Imaging, A textbook, BSWK, Hasselt, Belgium 2006.
17. Wilkenshoff UM, Sovany A, Kukulski T, Strotmann JM, Wranne B, Sutherland GR. When, where and to what extent does left ventricular regional function become abnormal with age in normal individuals. A colour Doppler Myocardial study. *Eur Heart J* 1998;19(Suppl):440.

18. Wilkenshoff UM, Hatle L, Wranne B, Sutherland GR. Age-dependent changes in regional diastolic function evaluated by color Doppler myocardial imaging: a comparison with pulsed Doppler indexes of global function. *J Am Soc Echocardiogr* 2001; 14:959-969.
19. Edner M, Jarnert C, Müller-Brunotte R,Malmqvist K, Ring M, Kjerr A-C, Lind L, Kahan T. Influence of age and cardiovascular factors on regional pulsed wave Doppler myocardial imaging indices. *Eur J Echocardiogr* 2000;1:87-95.
20. Yamada H, Oki T, Tabata T, Abe M, Onose Y, Wakatsuki T, Ito S. Effect of aging on diastolic left ventricular myocardial velocities measured by pulsed tissue Doppler imaging in healthy subjects. *J Am Soc Echocardiogr* 1999;12:574-581.
21. Henein M, Lindqvist P, Francis D, Mörner S, Waldenström A, Kazzan E. Tissue Doppler analysis of age-dependency in diastolic ventricular behaviour and filling. *Eur Heart J* 2002;23:162-171.
22. Tighe DA, Vinch CS, Hills JC, Meyer TE, Golderg RJ, Aurigemma GP. Influence of age on assessment of diastolic function by tissue Doppler imaging. *Am J Cardiol* 2003; 91:254-257.
23. Isaaz K, Munoz del Romeral L, Lee E, Shiller NB. Quantification of the motion of the cardiac base in normal subjects by doppler echocardiography. *J Am Soc Echocardiogr* 1993;6:166-176.
24. Pai RG and Gill KS. Amplitudes, durations and timings of apically directed left ventricular myocardial velocities:I. Their normal pattern and coupling to ventricular filling and ejection. *J Am Soc Echocardiogr* 1998;11(2):105-111.
25. Galiuto L, Ignone G, DeMaria AN. Contraction and relaxation velocities of the normal left ventricle using pulsed-wave tissue doppler echocardiography. *Am J Cardiol* 1998;812:609-614.
26. Kukulski T, Hubbert L, Arnold M, Wranne B, Hatle L, Sutherland GR. Normal regional right ventricular function and its change with age: a Doppler myocardial imaging study. *J Am Soc Echocardiogr* 2000;13:194-204.

27. Onose Y, Oki T, Mishiro Y, Yamada H, Abe M, Manabe K, Kageji Y, Tabata T, Wakatsuri T, Ito S. Influence of aging on systolic left ventricular wall motion velocities along the long and short axes in clinically normal patients determined by pulsed Doppler imaging. *J Am Soc Echocardiogr* 1999;12:921-926.
28. Oki T, Tabata T, Mishiro Y, Yamada H, Abe M, Onose Y, Wakatsuri T, Luchi A, Ito S. Pulsed Doppler imaging of left ventricular systolic and diastolic wall motion velocities to evaluate differences between long and short axes in healthy subjects. *J Am Soc Echocardiogr* 1999; 12:308-313.
29. Alam M, Wardell J, Anderson E, Samad BA, Nordlander R. Characteristics of mitral and tricuspid annular velocities determined by pulsed wave Doppler tissue imaging in healthy subjects. *J Am Soc Echocardiogr* 1999; 12:618-628.
30. Teske AJ, De Boeck BW, Melman PG, Sieswerda GT, Doevendans PA, Cramer MJ. Echocardiographic quantification of myocardial function using tissue deformation imaging, a guide to image acquisition and analysis using tissue Doppler and speckle tracking. *Cardiovasc Ultrasound* 2007 Aug 30;5:27. Review.
31. Marwick TH. Measurement of strain and strain rate by echocardiography. State-of the art paper. *J Am Coll Cardiol* 2006;47:1313-1327.
32. Greenberg NL, Firstenberg MS, Castro PL, Main M, Travaglini A, Odabashian JA, Drinko JK, Rodriguez LL, Thomas JD, Garcia MJ. Doppler-derived myocardial systolic strain rate is a strong index of left ventricular contractility. *Circulation* 2002;105:99-105.
33. Weidemann F, Jamal F, Sutherland GR, Claus P, Kowalski M, Hatle L, De Scheerder I, Bijnens B, Rademakers FE. Myocardial function defined by strain rate and strain during alterations in inotropic states and heart rate. *Am J Physiol Heart Circ Physiol* 2002;283:H792-H799.

34. Kowalski M, Kukulski T, Jamal F, D'hooge J, Weidemann F, Rademakers F, Bijnens B, Hatle L, Sutherland GR. Can natural strain and strain rate quantify regional myocardial deformation? A study in healthy subjects. *Ultrasound Med Biol* 2001;27(8):1087-1097.
35. Storaa C, Aberg P, Lind B, Brodin LA. Effect of angular error on tissue doppler velocities and strain. *Echocardiography* 2003;20:581-587.
36. Notomi Y, Lysyansky P, Setser RM, Shiota T, Popovic' ZB, Martin-Miklovic MG, Weaver JA, Oryszak SJ, Greenberg NL, White RD, Thomas JD. Measurement of ventricular torsion by two-dimensional ultrasound speckle tracking imaging. *J Am Coll Cardiol* 2005;45:2034-2041.
37. Helle-Valle T, Crosby J, Edvardsen T, Lyseggen E, Amundsen BH, Smith HJ, Rosen BD, Lima JAC, Torp H, Ihlen H, Smiseth OA. New noninvasive method for assessment of left ventricular rotation: speckle tracking echocardiography. *Circulation* 2005; 112:3149-3156.
38. Devereux RB, Alonso DR, Lutas ET, Gottlieb GJ, Campo E, Sachs I, Reichek N. Echocardiographic assessment of left ventricular hypertrophy: comparison to necropsy findings. *Am J Cardiol* 1986; 57: 450-458.
39. Devereux RB. Detection of left ventricular hypertrophy by M-mode echocardiography. Anatomic validation, standardization and comparison to other method. *Hypertension* 1987; 9: 119-126.
40. Savage D, Garisson RJ, Kannel WB. The spectrum of left ventricular hypertrophy in a general population sample: the Framingham study. *Circulation* 1987; 75 suppl I: I26-33.
41. Shub C, Klein AL, Zachariah PK, Bailey KR, Tajik AJ. Determination of left ventricular mass by echocardiography in a normal population: effect of age and sex in addition to body size. *Mayo Clin Proc* 1994;69:205-211.
42. Evangelista A, Flachskampf F, Lancellotti P, Badano L, Aguilar R, Monaghan M, Zamorano J, Nihoyannopoulos P on behalf of the European Association of Echocardiography. European Association of Echocardiography recommendations for

standardization of performance, digital storage and reporting of echocardiographic studies. *Eur J Echocardiogr* 2008 Jul; 9: 438-448.

43. Haider AW, Larson MG, Benjamin EJ, Levy D. Increased left ventricular mass and hypertrophy are associated with increased risk for sudden death. *J Am Coll Cardiol* 1998; 32:1454-1459.
44. Liao Y, Cooper RS, Durazo-Arvizu R, Mensah GA, Ghali KJ. Prediction of mortality by different methods of indexation for left ventricular mass. *J Am Coll Cardiol* 1997; 29:641-647.
45. Pick R, Janicki JS, Weber KT. Myocardial fibrosis in nonhuman primate with pressure overload hypertrophy. *Am J Pathol* 1989;135: 771–781.
46. Pearlman ES, Weber KT, Janicki JS, Pietra G, Fishman H. Muscle fiber orientation and connective tissue content in the hypertrophied human heart. *Lab Invest* 1982; 46:158-164.
47. Huysman JA, Vliegen HW, Van der Laarse A, Eulderink F. Changes in nonmyocite tissue composition associated with pressure overload of hypertrophic human hearts. *Pathol Res Pract* 1989; 184:577-581.
48. Greenbaum RA, Ho SY, Gibson DG, Becker AE, Anderson RH. Left ventricular fibre architecture in man. *Br Heart J* 1981;45:248 –263.
49. Maron BJ, McKenna WJ, Danielson GK, Kappenberger LJ, Kuhn HJ, Seidman CE, Shah PM, Spencer WH 3rd, Spirito P, Ten Cate FJ, Wigle ED; American College of Cardiology Foundation Task Force on Clinical Expert Consensus Documents; European Society of Cardiology Committee for Practice Guidelines. American College of Cardiology/European Society of Cardiology Clinical Expert Consensus Document on Hypertrophic Cardiomyopathy. A report of the American College of Cardiology Foundation Task force on Clinical Expert Consensus Documents and the European Society of Cardiology Committee for Practise Guidelines. *Eur Heart J*. 2003 Nov;24(21):1965-91.

50. Schwartz K, Carrier L, Guicheney P, Komajda M. Molecular basis of familial cardiomyopathies. *Circulation* 1995;91:532–40.

51. Niimura H, Bachinski LL, Sangwatanaroj S, Watkins H, Chudley AE, McKenna W, Kristinsson A, Roberts R, Sole M, Maron BJ, Seidman JG, Seidman CE Mutations in the gene for cardiac myosin-binding protein C and late-onset familial hypertrophic cardiomyopathy. *N Engl J Med* 1998;338:1248–57.

52. Watkins H, McKenna WJ, Thierfelder L, Suk HJ, Anan R, O'Donoghue A, Spirito P, Matsumori A, Moravec CS, Seidman JG, et al. Mutations in the genes for cardiac troponin T and alpha-tropomyosin in hypertrophic cardiomyopathy. *N Engl J Med* 1995;332:1058–64.

53. Charron P, Dubourg O, Desnos M, Bennaceur M, Carrier L, Camproux AC, Isnard R, Hagege A, Langlard JM, Bonne G, Richard P, Hainque B, Bouhour JB, Schwartz K, Komajda M et al. Clinical features and prognostic implications of familial hypertrophic cardiomyopathy related to the cardiac myosin-binding protein C gene. *Circulation* 1998; 97: 2230–6.

54. Maron BJ, Niimura H, Casey SA, Soper MK, Wright GB,Seidman JG, Seidman CE. Development of left ventricular hypertrophy in adults in hypertrophic cardiomyopathy caused by cardiac myosin-binding protein C gene mutations. *J Am Coll Cardiol* 2001;38:315–21.

55. Osterop AP, Kofflard MJ, Sandkuijl LA, ten Cate FJ, Krams R, Schalekamp MA, Danser AH. AT1 receptor A/C1166 polymorphism contributes to cardiac hypertrophy in subjects with hypertrophic cardiomyopathy. *Hypertension* 1998;32:825–30

56. Lechin M, Quinones MA, Omran A, Hill R, Yu QT, Rakowski H, Wigle D, Liew CC, Sole M, Roberts R, et al.. Angiotensin-I converting enzyme genotypes and left ventricular hypertrophy in patients with hypertrophic cardiomyopathy. *Circulation* 1995;92:1808–12.

57. Van Driest SL, Ommen SR, Tajik AJ, Gersh BJ, Ackerman MJ. Yield of genetic testing in hypertrophic cardiomyopathy. *Mayo Clin Proc* 2005 Jun;80(6):739-44.

58. Sherrid MV: Pathophysiology and treatment of hypertrophic cardiomyopathy. *Prog cardiovasc dis* 2006; 49(2):123-151.

59. Maron BJ, Anan TJ, Roberts WC: Quantitative analysis of the distribution of cardiac muscle cell disorganization in the left ventricular wall of patients with hypertrophic cardiomyopathy. *Circulation* 1981; 63:882-894.

60. Maron BJ, Wolfson JK, Roberts WC: Relation between extent of cardiac muscle cell disorganization and left ventricular wall thickness in hypertrophic cardiomyopathy. *Am J Cardiol* 1992; 70:785-790.

61. Varnava AM, Elliott PM, Baboonian C, Davison F, Davies MJ, McKenna WJ: Hypertrophic cardiomyopathy: histopathological features of sudden death in cardiac troponin T disease. *Circulation* 2001;104:1380-1384.

62. Tseng WYI, Dou J, Reese TG and Wedeen VJ: Imaging Myocardial fiber disarray and intramural strain hypokinesis in hypertrophic cardiomyopathy with MRI. *J Magn Reson Imaging.* 2006 Jan;23(1):1-8.

63. Shirani J, Pick R, Roberts WC, Maron BJ: Morphology and significance of the left ventricular collagen network in young patients with hypertrophic cardiomyopathy and sudden cardiac death. *J Am Coll Cardiol* 2000; 35:36- 44.

64. Tanaka M, Fujiwara H, Onodera T, Wu DJ, Hamashima Y, Kawai C: Quantitative analysis of myocardial fibrosis in normals, hypertensive hearts, and hypertrophic cardiomyopathy. *Br Heart J* 1986; 55:575-581.

65. Nihoyannopoulos P, Karatasakis G, Frenneaux M, McKenna WJ, Oakley CM: Diastolic function in hypertrophic cardiomyopathy: relation to exercise capacity. *J Am Coll Cardiol* 1992; 19:536- 540.

66. Varnava AM, Elliott PM, Mahon N, Davies MJ, McKenna WJ: Relation between myocyte disarray and outcome in hypertrophic cardiomyopathy. *Am J Cardiol* 2001;88:275-279.

67. Kim YJ, Choi BW, Hur J, Lee HJ, Seo JS, Kim TH, Choe KO, JW Ha: Delayed enhancement in hypertrophic cardiomyopathy: comparison with myocardial tagging MRI . *J Magn Reson Imaging* 2008 May;27(5):1054-60.
68. Maron BJ, Wolfson JK, Epstein SE, Roberts WC: Intramural (‘‘small vessel’’) coronary artery disease in hypertrophic cardiomyopathy. *J Am Coll Cardiol* 1986; 8:545-557.
69. Melacini P, Corbetti F, Calore C, Pescatore V, Smaniotto G, Pavei A, Bobbo F, Cacciavillani L, Iliceto S: Cardiovascular magnetic resonance signs of ischemia in hypertrophic cardiomyopathy. *Int J Cardiol* 2008 Aug 29;128(3):364-373.
70. Basso C, Thiene G, Mackey-Bojack S, Frigo AC, Corrado D, Maron BJ: Myocardial bridging, a frequent component of the hypertrophic cardiomyopathy phenotype, lacks systematic association with sudden cardiac death. *Eur Heart J* 2009 Jul; 30(13):1627-34.
71. Thiene G, Carturan E, Corrado D, Basso C. Prevention of sudden cardiac death in the young and in athletes: dream or reality? *Cardiovasc Pathol* 2009 Jun 15. [Epub ahead of print].
72. Basso C, Carturan E, Pilichou K, Corrado D, Thiene G. Sudden arrhythmic death and the cardiomyopathies: Molecular genetics and pathology. *Diagnostic Histopathology* 2010 (in press).
73. Basso C, Thiene G, Corrado D, Buja G, Melacini P, Nava A: Hypertrophic cardiomyopathy and sudden death in the young: pathologic evidence of myocardial ischemia. *Hum Pathol* 2000 Aug;31(8):988-998.
74. Corrado D, Basso C, Schiavon M, Thiene G: Screening for hypertrophic cardiomyopathy in young athletes. *N Eng J Med* 1998 Aug 6; 339(6):364-9.
75. Thiene G, Basso C, Corrado D: Is prevention of sudden death in young athlete feasible? *Cardiologia* 1999 Jun;44(6):497-505.
76. Pelliccia A, Fagard R, Bjørnstad HH, Anastassakis A, Arbustini E, Assanelli D, Biffi A, Borjesson M, Carrè F, Corrado D, Delise P, Dorwarth U, Hirth A, Heidbuchel H, Hoffmann E, Mellwig KP, Panhuyzen-Goedkoop N, Pisani A, Solberg EE, van-Buuren F, Vanhees L,

Blomstrom-Lundqvist C, Deligiannis A, Dugmore D, Glikson M, Hoff PI, Hoffmann A, Hoffmann E, Horstkotte D, Nordrehaug JE, Oudhof J, McKenna WJ, Penco M, Priori S, Reybrouck T, Senden J, Spataro A, Thiene G; Study Group of Sports Cardiology of the Working Group of Cardiac Rehabilitation and Exercise Physiology; Working Group of Myocardial and Pericardial Diseases of the European Society of Cardiology. Recommendations for competitive sports participation in athletes with cardiovascular disease: a consensus document from the Study Group of Sports Cardiology of the Working Group of Cardiac Rehabilitation and Exercise Physiology and the Working Group of Myocardial and Pericardial Diseases of the European Society of Cardiology. *Eur Heart J* 2005 Jul;26(14):1422-45.

77. Nagueh SF, Mahmarian JJ: Noninvasive cardiac imaging in patients with hypertrophic cardiomyopathy. *J Am Coll Cardiol* 2006;48:2410-22.
78. Pennell DJ, Sechtem UP, Higgins CB, Manning WJ, Pohost GM, Rademakers FE, van Rossum AC, Shaw LJ, Yucel EK; Society for Cardiovascular Magnetic resonance; Working Group on Cardiovascular Magnetic Resonance of the European Society of Cardiology: Clinical indications for cardiovascular magnetic resonance (CMR): Consensus Panel Report. *Eur Heart J* 2004;25:1940-1965.
79. Rajiv C, Vinereanu D, Fraser AG: Tissue Doppler imaging for the evaluation of patients with hypertrophic cardiomyopathy. *Curr Opin Cardiol* 2004;19:430-436.
80. Vinereanu D, Florescu N, Sculthorpe N, Tweddel AC, Stephens MR, Fraser AG: Differentiation between pathologic and physiologic left ventricular hypertrophy by tissue Doppler assessment of long-axis function in patients with hypertrophic cardiomyopathy or systemic hypertension and in athletes. *Am J Cardiol* 2001, 88:53–58.
81. Cardim N, Longo S, Ferreira T, Pereira A, Gouveia A, Reis RP, Correia JM: Tissue Doppler imaging assessment of long axis left ventricular function in hypertensive patients with

concentric left ventricular hypertrophy: differential diagnosis with hypertrophic cardiomyopathy. *Rev Port Cardiol* 2002, 21:709–740.

82. Nunez J, Zamorano JL, Perez De Isla L, Palomeque C, Almeria C, Rodrigo JL, Corteza J, Banchs J, Macaya C: Differences in regional systolic and diastolic function by Doppler tissue imaging in patients with hypertrophic cardiomyopathy and hypertrophy caused by hypertension. *J Am Soc Echocardiogr* 2004 Jul; 17(7):717-722.
83. Cardim N, Oliveira AG, Longo S, Ferreira T, Pereira A, Reis RP, Correia JM: Tissue Doppler imaging: regional myocardial function in hypertrophic cardiomyopathy and in athlete's heart. *J Am Soc Echocardiogr* 2003, 16:223–232.
84. Nagueh SF, Kopelen HA, Lim DS, Zoghbi WA, Quiñones MA, Roberts R, Marian AJ: Tissue Doppler imaging consistently detects myocardial contraction and relaxation abnormalities, irrespective of cardiac hypertrophy, in a transgenic rabbit model of human hypertrophic cardiomyopathy. *Circulation* 2000, 102:1346–1350
85. Yang H, Sun JP, Lever HM, Popovic ZB, Drinko JK, Greenberg NL, Shiota T, Thomas JD, Garcia MJ: Use of strain imaging in detecting segmental dysfunction in patients with hypertrophic cardiomyopathy. *J Am Soc Echocardiogr* 2003, 16:233–239.
86. Weidemann F, Mertens L, Gewillig M, Sutherland GR: Quantification of localised abnormal deformation in asymmetrical nonobstructive hypertrophic cardiomyopathy: a velocity, strain rate, and strain Doppler myocardial imaging study. *Pediatr Cardiol* 2001, 22:534–537.
87. Ito T, Suwa M, Tonari S, Okuda N, Kitaura Y: Regional postsystolic shortening in patients with hypertrophic cardiomyopathy: its incidence and characteristics assessed by strain imaging. *J Am Soc Echocardiogr* 2006 Aug;19(8):987-993.
88. Weidemann F, Niemann M, Herrmann S, Kung M, Störk S, Waller C, Beer M, Breuning F, Wanner C, Voelker W, Ertl G, Bijnens B, Strotmann JM: A new echocardiographic approach for the detection of non-ischaemic fibrosis in hypertrophic myocardium. *Eur Heart J* 2007 Dec;28(24):3020-6.

89. Kato TS, Noda A, Izawa H, Yamada A, Obata K, Nagata K, Iwase M, Murohara T, Yokota M: Discrimination of nonobstructive hypertrophic cardiomyopathy from hypertensive left ventricular hypertrophy on the basis of strain rate imaging by tissue Doppler ultrasonography. *Circulation* 2004 Dec 21;110(25):3808-14.
90. Richand V, Lafitte S, Reant P, Serri K, Lafitte M, Brette S, Kerouani A, Chalabi H, Dos Santos P, Douard H, Roudaut R: An ultrasound speckle tracking (two-dimensional strain) analysis of myocardial deformation in professional soccer players compared with healthy subjects and hypertrophic cardiomyopathy. *Am J Cardiol* 2007 Jul 1;100(1):128-32.
91. Serri K, Reant P, Lafitte M, Berhouet M, Le Bouffos V, Roudaut R, Lafitte S: Global and regional myocardial function quantification by two-dimensional strain: application in hypertrophic cardiomyopathy. *J Am Coll Cardiol* 2006 Mar 21;47(6):1175-81.
92. Runqing X, Xie M, Wang X, Lu Q: Assessment of regional myocardial function in patients with hypertrophic cardiomyopathy by tissue strain imaging. *J Huazhong Univ Sci Technolog Med Sci* 2006;26(3):334-7.
93. Liu Y, Deng Y, Li X, Chang Q, Lu Y, Li C: Assessment of left ventricular longitudinal regional myocardial systolic function by strain imaging echocardiography in patients with hypertrophic cardiomyopathy. *J Huazhong Univ Sci Technolog Med Sci* 2005;25(6):703-5.
94. Li X, Deng Y, Jang H: Left ventricular regional systolic function in patient with hypertrophic cardiomyopathy by quantitative tissue velocity imaging. *J Huazhong Univ Sci Technolog Med Sci* 2006;26(1):153-6.
95. Severino S, Caso P, Galderisi M, De Simone L, Petrocelli A, de Divitiis O, Mininni N: Use of pulsed Doppler tissue imaging to assess regional left ventricular diastolic dysfunction in hypertrophic cardiomyopathy. *Am J Cardiol* 1998 Dec 1;82(11):1394-8.
96. Mishiro Y, Oki T, Iuchi A, Tabata T, Yamada H, Abe M, Onose Y, Ito S, Nishitani H, Harada M, Taoka Y: Regional left ventricular myocardial contraction abnormalities and

asynchrony in patients with hypertrophic cardiomyopathy evaluated by magnetic resonance spatial modulation of magnetization myocardial tagging. *Jpn Circ J* 1999 Jun;63(6):442-6.

97. Ho CY, Sweitzer NK, McDonough B, Maron BJ, Casey SA, Seidman JG, Seidman CE, Solomon SD Assessment of diastolic function with Doppler tissue imaging to predict genotype in preclinical hypertrophic cardiomyopathy. *Circulation* 2002 Jun 25;105(25):2992-7.
98. Nagueh SF, McFalls J, Meyer D, Hill R, Zoghbi WA, Tam JW, Quiñones MA, Roberts R, Marian AJ Tissue Doppler imaging predicts the development of hypertrophic cardiomyopathy in subjects with subclinical disease. *Circulation* 2003 Jul 29;108(4):395-8.
99. Germans T, Wilde AA, Dijkmans PA, chai W, Kamp O, Pinto YM, Van Rossum C: Structural abnormalities of the inferoseptal left ventricular wall detected by cardiac magnetic resonance imaging in carriers of hypertrophic cardiomyopathy mutations. *J Am Coll Cardiol* 2006 Dec 19;48(12):2518-23.
100. Lip GYH, Felmeden DC, Li-Saw-Hee FL, Beevers DG: Hypertensive heart disease. A complex syndrome or a hypertensive "cardiomyopathy"? *Eur Heart J* 2000;21:1653-1665.
101. Levy D, Garrison RJ, Savage DD, Kannel WB, Castelli WP: Prognostic implications of echocardiographically determined left ventricular mass in the Framingham Heart Study. *N Engl J Med* 1990; 322: 1561–6.
102. Verdecchia P, Schillaci G, Borgioni C, Ciucci A, Gattobigio R, Zampi I, Santucci A, Santucci C, Reboldi G, Porcellati C: Prognostic value of left ventricular mass and geometry in systemic hypertension with left ventricular hypertrophy. *Am J Cardiol* 1996; 78: 197–202.
103. Schwartzkopff B, Frentzel H, Dieckerhoff J Betz P, Flasshove M, Schulte HD, Mundhenke M, Motz W, Strauer BE: Morphometric investigation of human myocardium in arterial hypertension and valvular aortic stenosis. *Eur Heart J* 1992; 13 (Suppl D): 17–23.

104. Verdecchia P, Porcellati C, Zampi I, Schillaci G, Gatteschi C, Battistelli M, Bartoccini C, Borgioni C, Ciucci A: Asymmetric left ventricular remodelling due to isolated septal thickening in patients with systemic hypertension and normal left ventricular masses. *Am J Cardiol* 1994;73:247-252.

105. Conrady AO, Rudomanov OG, Zaharov DV, Krutikov AN, Vahrameeva NV, Yakovleva OI, AlexeevaNP, Shlyakhto EV: Prevalence and determinants of left ventricular hypertrophy and remodelling patterns in hypertensive patients: the St. Petersburg study. *Blood Press* 2004;13(2):101-109.

106. Wachtell K, Bella JN,Liebson PR, Gerdts E, Dahlof B, Aalto T, Roman MJ, Papademetriou V,Ibsen H, Rokkedal J, Devereux RB: Impact of different partition values on prevalences of left ventricular hypertrophy and concentric geometry in a large hypertensive population: the LIFE study. *Hypertension* 2000 Jan;35(1Pt1):6-12.

107. Safar ME, Benessiano JR, Hornych AL: Asymmetrical septal hypertrophy and borderline hypertensione. *Int J Cardiol* 1982;2:103-105.

108. Corea L, Bentivoglio M,Verdecchia P, Motolese M: Left ventricular wall thickness and plasma catecholamines in borderline and stable essential hypertension. *Eur Heart J* 1982;3:164-170.

109. Niederle P, Widimsky J, Jandovà R, Ressi J, Grospic A: Echocardiographic assessment of the left ventricle in juvenile hypertension. *Int J Cardiol* 1982;2:91-101.

110. Corea L, Bentivoglio M, Verdecchia P, Motolese M: Plasma norepinephrine and left ventricular hypertrophy in systemic hypertension. *Am J Cardiol* 1984;53:1299-1303.

111. Burton AC: Physiology and biophysics of the circulation. Chicago: Year Book Medical Publishers, 1965:110-112.

112. Derumeaux G, Mulder P, Richard V, Chagraoui A, Nafeh C, Bauer F, Henry JP, Thuillez C: Tissue Doppler Imaging differentiates physiological from pathological pressure-overload left ventricular hypertrophy in rats. *Circulation* 2002; 105:1602-1608.

113. Galderisi M, Caso P, Severino S, Petrocelli A, De Simone L, Izzo A, Mininni N, De Divitiis O: Myocardial diastolic impairment caused by left ventricular hypertrophy involves basal septum more than other walls: analysis by pulsed Doppler tissue imaging. *J Hypertens* 1999 May;17(5):685-693.

114. Yuda S, Short L,Leano R,Marwick TH: Myocardial abnormalities in hypertensive patients with normal and abnormal left ventricular filling: a study of ultrasound tissue characterization and strain. *Clin Sci* 2002;103:283-293.

115. Saghir M, Areces M, Makan M: Strain rate imaging differentiates hypertensive cardiac hypertrophy from physiologic cardiac hypertrophy (athlete's heart). *J Am Soc Echocardiogr* 2007 Feb;20(2):151-7

116. Poulsen SH, Andersen NH, Ivarsen PI, Mogensen CE, Egeblad H: Doppler tissue imaging reveals systolic dysfunction in patients with hypertension and apparent "isolated" diastolic dysfunction. *J Am Soc Echocardiogr* 2003 Jul;16(7):724-31.

117. Baltabaeva A, Marciniak M, Bijnens B, Moggridge J, He FJ, Antonios TF, MacGregor GA, Sutherland GR: Regional left ventricular deformation and geometry analysis provides insight in myocardial remodelling in mild to moderate hypertension. *Eur J Echocardiogr* 2008 Jul;9(4):501-8.

118. D'hooge J, Bijnens B, Jamal F D'hooge J, Bijnens B, Jamal F, Pislaru C, Pislaru S, Thoen J, Suetens P, Van de Werf F, Angermann C, Rademakers FE, Herregods MC, Sutherland GR: High frame rate myocardial integrated backscatter. Does this change our understanding of this acoustic parameter? *Eur J Echocardiogr* 2000 Mar;1(1):32-41.

119. Mimbs JW, O'Donnell M, Bauwens D, Miller JG, Sobel BE. The dependence of ultrasonic attenuation and backscatter on collagen content in dog and rabbit hearts. *Circ Res* 1980;47:48–58.

120. Pérez JE, Barzilai B, Madaras EI, Glueck RM, Saffitz JE, Johnston P, Miller JG, Sobel BE. Applicability of ultrasonic tissue characterization for longitudinal assessment and

differentiation of calcification and fibrosis in cardiomyopathy. *J Am Coll Cardiol* 1984;4:88–95.

121. O'Donnell M, Mimbs JW, Miller JG. The relationship between collagen and ultrasonic backscatter in myocardial tissue. *J Acoust Soc Am* 198; 69:580–588.

122. Hoyt RM, Skorton DJ, Collins SM, Melton HE. Ultrasonic backscatter and collagen in normal ventricular myocardium. *Circulation* 1984;69: 775–782.

123. Picano E, Pelosi G, Marzilli M, Lattanzi F, Benassi A, Landini L, L'Abbate A. In vivo quantitative ultrasonic evaluation of myocardial fibrosis in humans. *Circulation* 1990;81:58–64.

124. Vered Z, Barzilai B, Mohr GA, Thomas LJ III, Genton R, Sobel BE, Shoup TA, Melton HE, Miller JG, Pérz JE. Quantitative ultrasonic tissue characterization with real-time integrated backscatter imaging in normal human subjects and in patients with dilated cardiomyopathy. *Circulation* 1987;76:1067–1073.

125. Skorton DJ, Miller]G, Wicklinc SA, Barzilai B, Collins SM, Perez JE. Ultrasonic characterization of cardiovascular tissue. In: Marcus ML, Schelbert HR, Skorton DJ, Wolf GL, eds. Cardiac imaging. Philadelphia: WB Saunders, 1991:538-56.

126. Madaras EI, Barzilai B, Perez JE, Sobel BE, Miller JG: Changes in myocardial backscatter throughout the cardiac cycle. *Ultrason Imaging* 1983;5:229-39.

127. Fitzgerald PJ, McDaniel MM, Rolett EL, James DH, Strohben JW. Two dimensional ultrasonic variation in myocardium during the cardiac cycle. *Ultrason Imaging* 1986;8:241-251.

128. Masuyama T, Nellessen U, Schnittger I, Tye TL, Haskell WL, Popp RL. Ultrasonic tissue characterization with a real time integrated backscatter imaging system in normal and aging human hearts. *J Am Coll Cardiol* 1989;14:1702-8.

129. Madaras EI, Perez JE, Sobel BE, Mottley JG, Miller JG. Anisotrophy of the ultrasonic backscatter myocardial tissue, II: measurements in vivo. *J Acoust Soc Am* 1988;83:762-9.

130. Wickline SA, Verdonk ED, Miller IG. Three-dimensional characterization of human ventricular myofiber architecture by ultrasonic backscatter. *I Clin Invest* 1991;88:438-46.

131. Lange A, Moran CM, Palka P, Fenn LN, Sutherland GR, McDicken WN: The variation of integrated backscatter in human hearts in differing ultrasonic transthoracic views. *J Am Soc Echocardiogr* 1995;8:830-8.

132. Wickline SA, Thomas LJ III, Miller JB, Sobel BE, Perez JE: The dependence of myocardial ultrasonic integrated backscatter on contractile performance. *Circulation* 1985;72:183-192.

133. Sagar KB, Pelc LE, Rhyne TL, Wann LS, Waltier DS: Influence of heart rate, preload, afterload, and inotropic state on myocardial ultrasonic backscatter. *Circulation* 1988; 77: 478 – 483.

134. Perez JE, Holland MR, Barzilai B et al. (1996) Ultrasonic characterization of cardiovascular tissue. In cardiac imaging: a comparison to Brawnwald's heart disease (Skorton DJ, Schelbert HR, Wolf JL and Brundage BH, eds) 2nd edn, pp 606-622, WB Sauders, Philadelphia.

135. Barzilai B, Madaras EI, Sobel BE, Miller JG, Perez JE. Effects of myocardial contraction on ultrasonic backscatter before and after ischemia. *Am J Physiol* 1984; 247: H478– H483.

136. Milunski MR, Mohr GA, Wear KA, Sobel BE, Miller JG, Wickline SA. Early identification with ultrasonic integrated backscatter of viable but stunned myocardium in dogs. *Circulation* 1989; 14: 462– 471.

137. Naito J, Masuyama T, Tanouchi J, Mano T, Kondo H, Yamamoto K, Nagano R, Hori M, Inoue M, Kamada T: Analysis of transmural trend of myocardial integrated ultrasound

backscatter for differentiation of hypertrophic cardiomyopathy and ventricular hypertrophy due to hypertension. *J Am Coll Cardiol* 1994;24:517-24.

138. Masuyama T, St Goar FG, Tye TL, Oppenheim G, Schnittger I, Popp RL. Ultrasonic tissue characterization of human hypertrophied hearts in vivo with cardiac cycle-dependent variation in integrated backscatter. *Circulation* 1989;80: 925– 934.

139. Bouki KP, Lange A, Palka P, Moran CM, Fenn LN, Wright RA, Fox KA, McDicken WN, Sutherland GR: Regional variations of ultrasonic integrated backscatter in normal and myopathic left ventricles. *Eur Heart J* 1996;17:1747-1755.

140. Ueda K, Murata K, Tanaka N, Tone T, Wada Y, Kimura K, Fujino T, Jinyao L, Matsuzaki M: Ultrasonic myocardial tissue characterization in patients with hypertrophic cardiomyopathy and pressure-overloaded hypertrophy by backscattered energy temporal analysis. *Circ J* 2002; 66:729-734.

141. Di Bello V, Giorgi D, Talini E, Dell' Omo G, Palagi C, Romano MF, Pedrinelli R, Mariani M. : Incremental value of ultrasonic tissue characterization (backscatter) in the evaluation of left ventricular myocardial structure and mechanics in essential arterial hypertension. *Circulation* 2003;107:74-80.

142. Maceira AM, Barba J, Beloqui O, Diez J: Ultrasonic backscatter and diastolic function in hypertensive patients. *Hypertension* 2002; 40:239-243.

143. Maceira AM, Barba J, Varo N, Beloqui O, Diez J: Ultrasonic backscatter and serum marker of cardiac fibrosis in hypertensive. *Hypertension* 2002;39:923-928.

144. Kozàkovà M, Buralli S, Palombo C, Bernini G, Moretti A, Favilla S, Taddei S, Salvetti A: Myocardial ultrasonic backscatter in Hypertension. Relation to aldosterone and endothelin. *Hypertension* 2003;41:230-236.

145. Mizuno R, Fujimoto S, Yamaji K, Yutani C, Hashimoto T, Nakamura S: Myocardial ultrasonic tissue characterization for estimating histological abnormalities in hypertrophic

cardiomyopathy: comparison with endomyocardial biopsy findings. *Cardiology* 2001;96(1):16-23.

146. Kaneda T, Shimizu M, Ino H, Yamaguchi M, Terai H, Fujino N, Nagata M, Sakata K, Mabuchi H: Changes in cardiac tissue characterization in carriers with gene mutations associated with hypertrophic cardiomyopathy. *Int J Cardiol* 2005;104:170-175.

147. D'hooge J, Turschner O, Dommke C, Claus P, Bijnens B, Thoen J, Van de Werf F, Sutherland GR, Suetens P: The Relationship between regional Integrated Backscatter levels and regional Strain in normal, acutely ischemic and reperfused myocardium in functional imaging and modelling of the heart; Lecture Notes in *Computer Science* 2674. Eds. Magnin IE, Montagnat J, Clarysse P, Nenonen J and Katila T. :278-286, 2003.

148. D'hooge J, Coenen S, Turschner O, Claus P, Mc Laughlin M, Mehwald P, Marciniak M, Dommke C, Bijnens B, Sutherland GR, Suetens P: The response of regional integrated backscatter levels and regional strain to inotropic stimulation and acute ischemia. In Proceedings of the *IEEE Ultrasonics Symposium*:614-617, 2004.

149. D'hooge J, Jamal F, Bijnens B, Thoen J, Van de Werf F, Suetens P, Sutherland GR: The relationship between regional integrated backscatter levels and regional strain. In *IEEE Ultrasonics Symposium*: 1325-1328, 1999.

150. Rijsterborgh H, Mastik F, Lancee CT, van der Steen AF, Sassen LM, Verdouw PD, Roelandt J, Bom N.: Ultrasonic myocardial integrated backscatter and myocardial wall thickness in animal experiments. *Ultrasound Med Biol* 1990;16:29-36.

151. Rijsterborgh H, Mastik F, Lancee CT, Sassen LM, Verdouw PD, Roelandt J, Bom N: The relative contributions of myocardial wall thikness and ischemia to ultrasonic myocardial integrated backscatter during experimental ischemia. *Ultrasound Med Biol* 1991;17(1):41-8.

152. Bijnens B, D'Hooge J, Sutherland GR, Herregods MC, Nuyts J, Suetens P, Van de Werf F: Robustness of integrated backscatter for myocardial tissue characterization. *Ultrasound Med Biol* 1999;25:95-103.

153. Cerqueira MD, Weissman NJ, Dilsizian V, Jacobs AK, Kaul S, Laskey WK, Pennell DJ, Rumberger JA, Ryan T, Verani MS; American Heart Association Writing Group on Myocardial Segmentation and Registration for Cardiac Imaging. Standardized myocardial segmentation and nomenclature for tomographic imaging of the heart: a statement for healthcare professionals from the Cardiac Imaging Committee of the Council on Clinical Cardiology of the American Heart Association. *Circulation* 2002;105: 539-42.

154. Kramer CM, Reichek N, Ferrari VA, Theobald T, Dawson J, Axel L: Regional heterogeneity of function in hypertrophic cardiomyopathy. *Circulation* 1994;90:186-194.

155. Skulstad H, Edvardsen T, Urheim S, Rabben SI, Stugaard M, Lyseggen E, Ihlen H, Smiseth OA: Postsystolic shortening in ischemic myocardium. Active contraction or passive recoil? *Circulation* 2002 Aug 6;106(6):718-24.

156. Jamal F,Szilard M, Kukulski T, Liu XS, D'hooge J, Bijnens B, Rademakers F, Hatle L, De Scheerder I, Sutherland GR: Changes in systolic and post-systolic thickening during acute coronary occlusion and reperfusion in closed-chest pigs. Implication for the assessment of regional myocardial function. *J Am Soc Echocardiogr* 2001; 14(7):691-697.

157. Jamal Jamal F, Strotmann J, Weidemann F, Kukulski T, D'hooge J, Bijnens B, Van de Werf F, De Scheerder I, Sutherland GR: Non-invasive quantification of contractile reserve of stunned myocardium by ultrasonic strain rate and strain. *Circulation* 2001 Aug 28;104(9):1059-65.

158. Hosokawa H, Sheehan FH, Suzuki T. Measurement of post-systolic shortening to assess viability and predict recovery of left ventricular function after acute myocardial infarction. *J Am Coll Cardiol* 2000; 35:1842-9.

159. Weidemann F, Dommke C, Bijnens B, Claus P, D'hooge J, Mertens P, Verbeken E, Maes A, Van de Werf F, De Scheerder I, Sutherland GR: Defining the transmurality of a chronic myocardial infarction by ultrasonic strain-rate imaging. Implication for identifying intramural viability. An experimental study. *Circulation* 2003;107:883-888.

160. Kukulski T, Jamal F, Herbots L, D'hooge J, Bijnens B, Hatle L, De Scheerder I, Sutherland GR: Identification of acutely ischemic myocardium using ultrasonic strain measurements: a clinical study in patients undergoing coronary angioplasty. *J Am Coll Cardiol* 2003;41:810-9.

161. Voigt JU, Exner B, Schmiedehausen K,Huchzermeyer C, Reulbach U, Nixdorff U,Platsch G, Kuwert T, Danile WG, Flachskampf FA: Strain-rate imaging during dobutamine stress echocardiography provides objective evidence of inducible ischemia. *Circulation* 2003;107:2120-2126.

162. Hammermeister KE, Gibson DG, Hughes D: Regional variation in the timing and extent of left ventricular wall motion in normal subjects. *Br Heart J* 1986; 56:226-35.

163. Grines CL, Bashore TM, Boudoulas H, Olson S, Shafer P, Wooley CF. Functional abnormalities in isolated left bundle branch block: the effect of interventricular asynchrony. *Circulation* 1989:79:845-53.

164. Henein MY, Rosano GM,Underwood R, Poole-Wilson PA, Gibson DG: Realtions between resting ventricular long axis function, the electrocardiogram and myocardial perfusion imaging in syndrome x. *Br Heart J* 1994;71:541-7.

165. Villari B, Vassalli G, Betocchi S, Briguori C, Chiarello M, Hess OM: Normalization of left ventricular nonuniformity late after valve replacement for aortic stenosis. *Am J Cardiol* 1996; 78:66-71.